Aus dem Exzellenzcluster Kardiopulmonales System

und dem Fachbereich Biologie und Chemie

der Justus-Liebig-Universität Gießen

# Amplified Canonical Transforming Growth Factor β Signaling via Heat Shock Protein 90 in Pulmonary Fibrosis

## Inauguraldissertation

zur

Erlangung des Grades

Doktor der Naturwissenschaften

- Dr. rer. nat. -

der naturwissenschaftlichen Fachbereiche

(Fachbereich 08 Biologie und Chemie)

der Justus-Liebig-Universität Gießen

vorgelegt von

MSc. Zaneta Natalia Sibinska

aus Slupsk, Polen

Gießen 2015

Dekan : Prof. Dr. Volker Wissemann
Institut für Botanik, FB 08
Justus-Liebig-Universität Gießen
Heinrich-Buff-Ring 38, 35392 Gießen

Erstgutachter: Prof. Dr. rer. nat. Michael Martin
Institut für Immunologie, FB 08
Justus-Liebig-Universität Gießen
BFS- Schubertstr. 81, 35392 Gießen

Zweitgutachter: Prof. Dr. rer. nat. Ralph Theo Schermuly
Exzellenzckuster Kardiopulmonales System (ECCPS)
Lungenzentrum der Universität Gießen (UGMLC)
Biomedizinisches Forschungszentrum (BFS)
Schubertstr. 81, 35392 Giessen

Die vorliegende Arbeit wurde im Rahmen der Graduiertenkollegs the Universities of Giessen and Marburg Lung Center (UGMLC) am Exzellenzcluster Kardiopulmonales System des Lungenzentrums der Justus-Liebig-Universität Gießen und dem Zentrum für Innere Medizin- Medizinische Klinik II/V in der Zeit von Oktober 2011 bis August 2015. Das Thema und das Labor wurden von Prof. Dr. rer. nat. Ralph Schermuly bereitgestellt, unter dessen Betreuung diese Arbeit entstand. Die Betreuung der Arbeit im Fachbereich 08 Biologie und Chemie erfolgte durch Prof. Dr. rer. nat. Michael Martin.

*For My Beloved Parents*

# TABLE OF CONTENTS

# 1. INTRODUCTION

## 1.1. Definition of idiopathic pulmonary fibrosis

Idiopathic pulmonary fibrosis (IPF) is the most common group of idiopathic interstitial pneumonias. According to the current definition, IPF is associated with a histological pattern of usual interstitial pneumonia (UIP). IPF is a chronic, irreversible, progressive and usually fatal disease of unknown etiology (King Jr et al., 2011) characterized by exertional dyspnea and cough (Selman et al., 2007).

## 1.2. Epidemiology of idiopathic pulmonary fibrosis

IPF is a rare disease with prevalence from 14 to 27.9 cases per 100,000 population in the USA or 1.25 to 23.4 cases per 100,000 population in Europe using narrow case definitions (Antoniou et al., 2013). IPF prevalence and incidence increase with age. IPF occurs in middle-aged and older people with the average age at diagnosis 66 years. Moreover, there is a higher predominance of the disease in males than in females (Nalysnyk et al., 2012). Particularly severe forms of pulmonary fibrosis have a mean mortality of 2-6 years after diagnosis (Wynn, 2011).

## 1.3. Risk factors of idiopathic pulmonary fibrosis

Although IPF is defined a disease of unknown etiology, several potential risk factors have been described over the last decades (Raghu et al., 2011).

### 1.3.1. Cigarette smoking

Smoking is strongly associated with both familial and sporadic IPF. It applies particularly to individuals with smoking history more than 20 pack-years (Iwai et al., 1994).

### 1.3.2. Environmental exposures

The onset and origin of IPF is not fully known (Fernandez and Eickelberg, 2012a). The most important environmental risk factors appear to be: smoking (ATS and ERS, 2002), exposure to metal and wood dust (ATS and ERS, 2000), pollutants, viral infections (Lasithiotaki et al., 2011) and ageing (Faner et al., 2012). Farming, raising birds, hair dressing, stone cutting/polishing, and exposure to livestock and to vegetable dust/animal dust have also been associated with IPF (Baumgartner et al., 1997).

### 1.3.3. Microbial agents

Viral infection, such as Epstein-Barr virus (EBV), human herpes virus 7 and 8, cytomegalovirus and hepatitis C virus (Wuyts et al., 2013), was proposed as initiator of IPF. EBV is the most studied virus in this context. EBV protein as well as DNA expression has been found in the lung tissue of patients with IPF. Further, a poor prognosis in patients with IPF was linked to the expression of EBV latent membrane protein-1 in alveolar epithelial cells (AECs) (Tsukamoto et al., 2000) and EBV-AEC interactions might be associated with fibrotic scars appearing during fibrosis (Fukuda et al., 2001). Despite of the extensive studies, one can hardly define the role of viral infection in IPF due to the variable confounding factors in the patients.

### 1.3.4. Gastroesophageal reflux (GER)

The prevalence of GER in IPF is estimated to be up to 90% (Raghu et al., 2006), and recent studies have demonstrated the association between acute exacerbations of IPF and GER. Considering the high prevalence of GER in normal population as well as patients with other advanced lung diseases, further studies are required to understand the role of GER in IPF.

### 1.3.5. Genetic predisposition

Most of DPLDs diseases are sporadic, however the examples of familial cases exist. Familial clustering of adult idiopathic interstitial pneumonias (IIP) suggests that genetic factors might play an important role in the disease development.

#### 1.3.5.1. Surfactant protein C (SP-C) gene

Some patients occur to have mutations in the gene of the surfactant protein C expressed by epithelial cells type II (Wuyts et al., 2013). Mutation in SP-C leads to incorrect protein folding and ER stress, and alveolar epithelial cell apoptosis accures. There are examples of familial occurrence in IPF, although most of these diseases are sporadic cases. Van Moorsel and colleagues reported that five out twenty unrelated patients with familial pulmonary fibrosis had the mutation of SP-C while this mutation was not present in sporadic disease (van Moorsel et al., 2010).

#### 1.3.5.2. Mucin 5B (MUC5B) gene

A polymorphism in the promoter region of mucin 5B gene has been found in familial cases as well as in idiopathic IPF (Seibold et al., 2011). Moreover, due to a common variant in the putative promoter of MUC5B, the expression of MUC5B was highly elevated in the lung of patients suffered from IPF when compared with healthy subjects (van Moorsel et al., 2010).

#### 1.3.5.3. ELMO domain containing 2 (ELMOD2) gene

ELMOD2 mRNA expression is significantly down-regulated in patients affected by IPF in comparison to healthy subjects. Further, ELMOD2 has been shown to be implicated in the regulation of interferon-related antiviral responses (Pulkkinen et al., 2010).

#### 1.3.5.4. Telomerase gene

Telomeres are a molecular cap of noncoding DNA which protect the chromosome ends against degradation. Telomeres become shorter during repeated cell division. A complex of proteins and RNA named telomerase is required in maintaining telomere length: the reverse transcriptase component (TERT) and the telomerase RNA template component (TERC) are key components of the telomerase complex. Mutations in TERC and TERT account for 8-15% of familial and 1-3% of sporadic cases. The short telomere length is more often found in IPF even in the absence of telomerase mutations (Spagnolo et al., 2012).

## 1.4. Classification of diffuse parenchymal lung diseases (DPLD) and diagnosis of interstitial lung fibrosis (IPF)

The idiopathic interstitial pneumonias (IIPs), also described as interstitial lung diseases, belong to DPLDs (Figure 1). The IIPs are characterized by heterogeneous group of nonneoplastic disorders resulting from damage to the lung parenchyma by different patterns of inflammation and fibrosis. The space between the epithelial and endothelial basement membranes is called the interstitium which is the primary site of injury in IIPs. However, these disorders often affect not only the interstitium, but also the peripheral airways, airspaces, as well as vessels along with their respective epithelial and endothelial linings (Raghu et al., 2011).

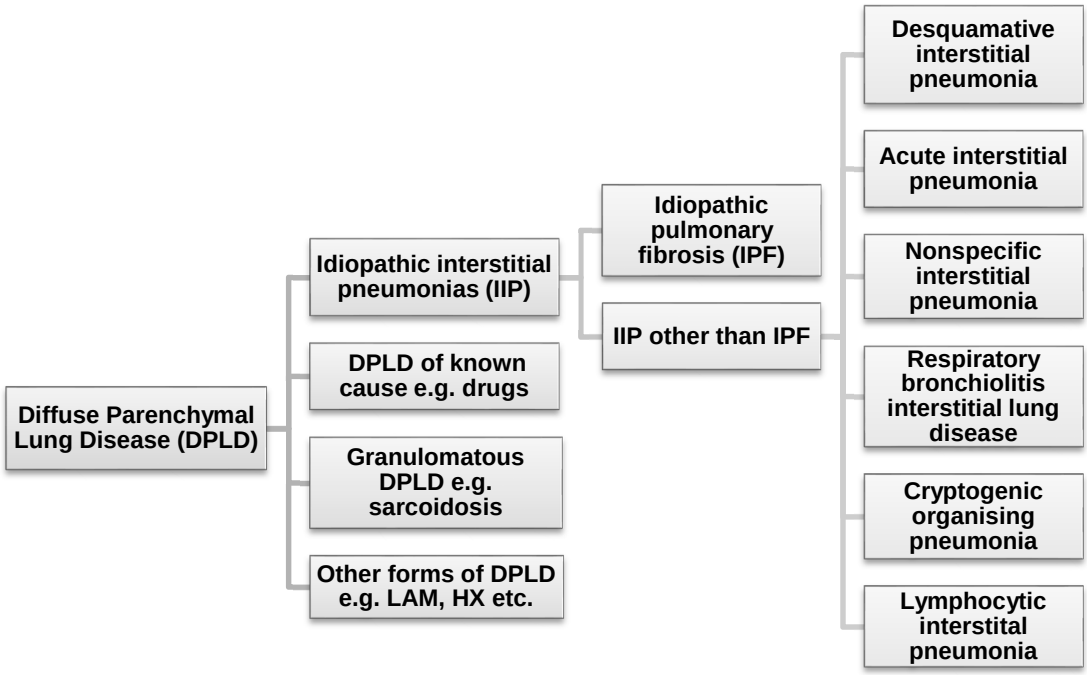


**Figure 1. Current classification of diffuse parenchyma lung diseases** (ATS and ERS, 2002)**.** DPLD: diffuse parenchymal lung disease; IIP: idiopathic interstitial pneumonias; LAM: lymphangioleiomyomatosis; HX: histiocytosis/histiocytosis.

### 1.5. Clinical, radiological and histological features of pulmonary fibrosis

To establish uniform definitions and criteria for the diagnosis of IPF, multidisciplinary approach is required, including the cooperation of clinicians, radiologists and pathologists (Flaherty et al., 2004). For the final diagnosis, a pattern of IIPs on high-resolution computed tomography (CT) or on lung tissue obtained by surgical lung biopsy is crucial (Travis et al., 2013). During the last 30 years the pathological description of IPF has been rearranged, and the most current classification was represented by American Thoracic Society and European Respiratory (Travis et al., 2013).

#### 1.5.1. Clinical characteristic of pulmonary fibrosis:

**1.** Gradual dyspnea, nonproductive cough (ATS and ERS, 2000).

**2.** Digital clubbing appears in 20 to 25% of patients (ATS and ERS, 2002).

**3.** A pattern of ventilatory defect with decreased DLCO and low resting $Pa_{O2}$ which drops during exercise (Pérez et al., 2010).

**4.** Classic clinical phenotype is slowly progressive in decrease of lung function and worsening dyspnea; some patients present a rapidly progressive disease (< 6 months

of symptoms before first presentation) and display shorter survival, mainly the men who smoke heavily cigarettes. A gene expression profile differs in these both groups, although the lung function, chest imaging and histology were similar (Ley et al., 2011).

**5.** There is increased level of neutrophils in bronchoalveolar lavage fluid (BALF). It also contains mild increase in percentage of eosinophils. Lymphocytosis is not a feature of UIP. Moreover, BALF cell count correlates with the severity of disease, however does not predicts prognosis (Wells et al., 1994).

### 1.5.2. Radiological characteristics of pulmonary fibrosis

1. On chest radiograph: the peripheral, reticular opacity appears, most visible at the basis, often associated with honeycombing. The chest radiography can occasionally be normal in IPF patients.
2. On computed tomography (CT): the abnormality in IPF patients is reticular opacity, often associated with traction bronchiectasis and little or no ground-glass opacifications; honeycombing is common. The distribution of UIP is noticed at the bases and periphery but often patchy (Figure 2a and 2b).
3. The architectural distortion is often prominent and lobar volume loss is observed in advanced fibrosis (King Jr et al., 2011).

### 1.5.3. Histologic characteristics of pulmonary fibrosis

1. There is temporal heterogeneous appearance with alternating zones of abnormal and healthy lung tissue (Figure 2c, asterisk).
2. Interstitial inflammation is mild and associated with hyperplasia of epithelial cells type II.
3. The temporal heterogeneity in the fibrotic zones is indicated by the presence of dense a cellular collagen and juxtaposed with fibroblastic foci of loose connective tissue (Figure 2c, arrows).
4. Fibroblast foci are small areas of active fibrosis present in the background of collagen deposition, and they reflect the temporal heterogeneity of the disease.
5. Area of honeycomb consist of cystic fibrotic airspaces (Figure 2d) are lined with bronchiolar epithelium and often filled by mucin and various number of inflammatory cell.
6. There is no single histological feature that can be correlated with the prognosis of IPF or the response to the treatment (Travis et al., 2013).

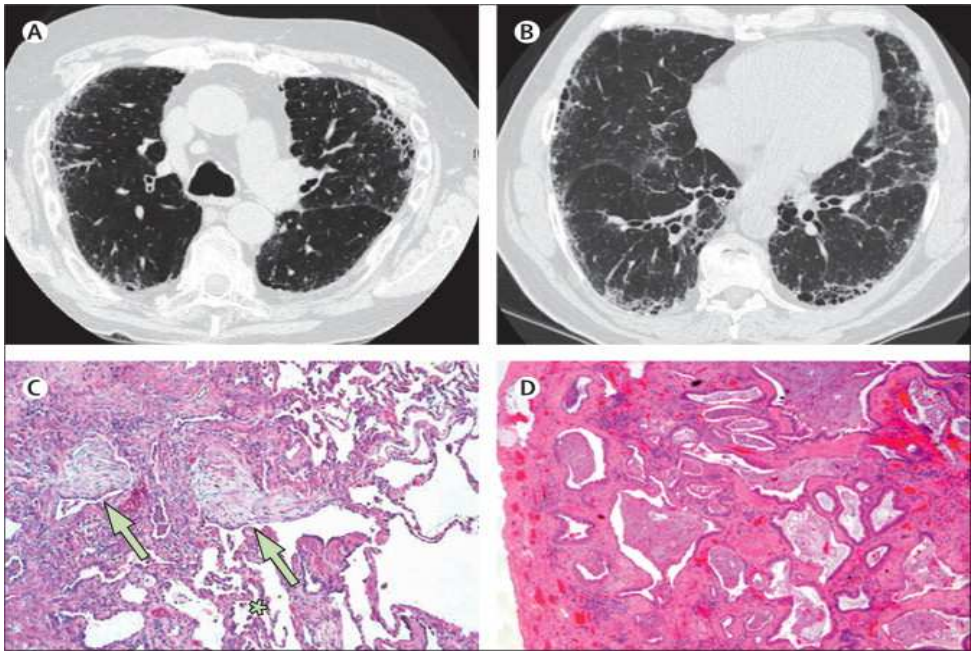


**Figure 2. The typical pattern of usual interstitial pneumonia (UIP) on high-resolution computed tomography (HRCT)** (King Jr et al., 2011)**.** There are zones of abnormal and healthy lung tissue (Figure 2c, asterisk), presence of dense cellular collagen and juxtaposed with fibroblastic foci of loose connective tissue (Figure 2c, arrows).

### 1.6. Pathogenic events initiate and promote pulmonary fibrosis

The precise mechanisms that drive the development of pulmonary fibrosis remain incompletely understood, however three broad areas such as inflammation, oxidative stress, coagulation disturbances (Figure 3) have been investigated. They may be responsible for altered lung fibroblast phenotype, apoptosis of epithelial cells and excessive production of ECM (Todd et al., 2012).

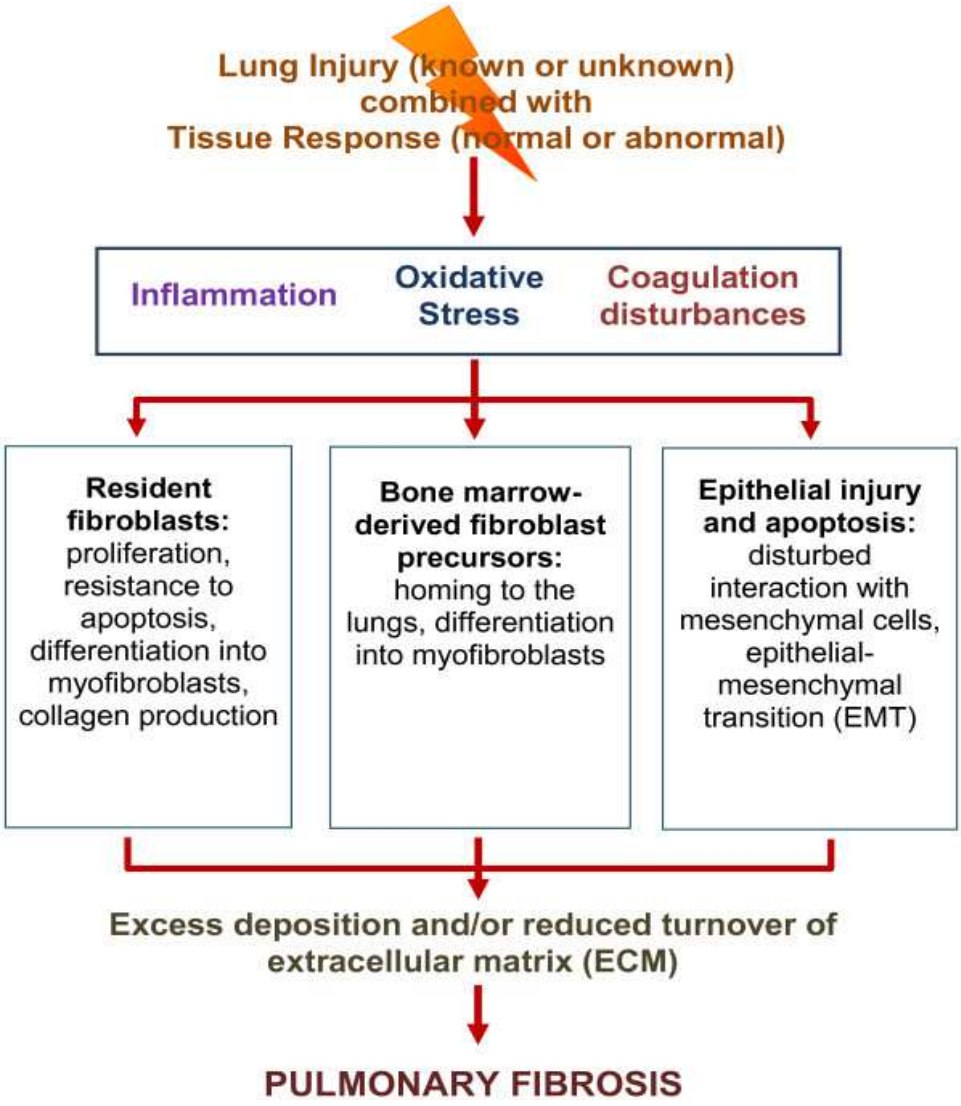


**Figure 3. Schematic diagram of three broad mechanisms that result in pulmonary fibrosis following lung injury** (Todd et al., 2012)**.**

### 1.6.1. Endoplasmic reticulum (ER) stress

Endoplasmic reticulum (ER) stress in alveolar epithelial cells is prominent in IPF. Not only does it cause alveolar epithelial cells apoptosis, it also serves as a fibrotic stimulus by promoting epithelial-mesenchymal transition (EMT) and inflammatory responses (Tanjore et al., 2013). ER stress is caused by events that disturb the processing and folding of proteins, which results in the accumulation of misfolded proteins in the ER and activation of the cellular response termed as unfolded protein response (UPR). Mammalian cells have three sensors of unfolded proteins: IRE1α (inositol requiring enzyme 1α), PERK (protein kinase RNA-like ER kinase), and ATF6 (activating transcription factor 6) which, when activated, initiate the UPR (Wolters et al., 2014). Many studies have shown that the markers of UPR activation, for example CHOP (CCAAT/enhancer-binding protein (C/EBP) homologous protein), p50ATF6 (the processed form of ATF6), BiP (binding immunoglobulin protein) and IRE1α, are increased in alveolar epithelial cells of IPF patients (Korfei et al., 2008). Many causes of ER stress were found in IPF patients. Expression of the G231V or F198S mutant of SP-A in epithelial cells causes the elevated level of BiP and XBP1s (Maitra et al., 2010). However, mutants SP-A and SP-C only present in 5% of IPF patients. There are other factors contributing to the ER stress. For example, herpesvirus protein expression was shown to co-localize with UPR markers, suggesting that ectopic production of viral proteins can activate the UPR (Lawson et al., 2008).

### 1.6.2. Oxidative stress

Oxidative stress is termed as imbalance in generating reactive oxygen species (ROS) in excess of a capacity to neutralize them. ROS overproduction may lead to oxidative stress that causes tissue injury. The key origins of oxidative stress in pulmonary fibrosis are environmental toxins, depletion of antioxidant defenses, mitochondria/ NADPH oxidase of inflammatory and lung target cells (Cheresh et al., 2013). This stress may initiate a tissue microenvironment which favors fibrosis against regeneration of lungs. This may be an important factor for fibroblast to develop resistance to apoptosis. Many papers demonstrated that myofibroblasts secrete hydrogen peroxide which can mediate fibrogenic effects and induce epithelial apoptosis (Waghray et al., 2005). Further, NADPH oxidase 4 is up-regulated in fibroblast foci from IPF patients. NADPH oxidase 4 is induced by TGF-β in mesenchymal cells isolated from IPF patients and is involved in ECM production, myofibroblast differentiation and contractility (Hecker et al., 2009).

### 1.6.3. Coagulation disturbance

Accumulating evidence has shown a disturbed coagulation cascade in patients with pulmonary fibrosis. The coagulation cascade plays a crucial role in inflammatory and tissue repair programs during wound healing in response to injuries. The cellular responses of the coagulation cascade are principally executed by several pro-coagulant proteinases such as tissue factor, factor XII or thrombin, all of which are elevated in bronchoalveolar lavage fluid (BALF) or alveolar epithelial cells (AECs) of IPF patients (Günther et al., 2000; Imokawa et al., 1997). Moreover, proteinase-activated receptor 1 and receptor 2 (PAR1 and PAR2) are activated in various lung cell types such as pulmonary epithelial cells, macrophages, and fibroblasts leading to activation and release of potent proinflammatory and profibrotic mediators (Wuyts et al., 2013; Wygrecka et al., 2011). On the other hand, the fibrinolytic activity was compromised by increased antifibrinolytic plasminogen activator inhibitors (PAIs) (Kotani et al., 1995).

### 1.6.4. Inflammation

#### 1.6.4.1. Pro arguments- pulmonary fibrosis is an inflammatory disease

The concept that dominated in the 1970s and 1980s described pulmonary fibrosis as ‘chronic inflammatory disease of the lung parenchymal’ and explained that chronic pulmonary inflammatory injures modulate fibrogenesis and lead to fibrotic scares. This paradigm was based on increased level of inflammatory cells from the BAL fluid of IPF patients when compared with healthy individuals (Homer et al., 2011). Considering the fact that numerous cytokines play a role in pulmonary fibrosis, and inflammatory cells, although not exclusively, are one of the major source of cytokines, inflammation is relevant to triggering the disease. Macrophages are involved in all stages of fibrosis. Studies showed that if macrophages were depleted during the early phase of fibrosis, scarring was reduced and the number of myofibroblasts was decreased. In contrast, if the macrophages were depleted during late-remodeling phase of fibrosis, the disease was not attenuated (Wynn and Barron, 2010). There are also studies showing that CD4+ lymphocyte- Th1 and Th2 play important role in the inflammatory phase of lung fibrosis (Todd et al., 2012).

#### 1.6.4.1.1. Lymphocytes

After injury, epithelial cells release IL-25 and IL-33 which can facilitate the development of profibrotic Th2 response. T cells also secrete IL-21 and IL-25 which promote Th2 differentiation (Fulkerson et al., 2006). However, Th2 cytokines can also trigger antifibrotic feedback. For instance, arginase-1 in M2 macrophages is activated by Th2 cytokines and the production of IL-13 and myofibroblasts differentiation is inhibited. IFN-γ, secreted by Th1 lymphocytes, suppresses collagen synthesis by fibroblasts and promotes the activation of M1 macrophages that promote ECM degradation (Ramalingam et al., 2008).

#### 1.6.4.1.2. Macrophages

M1 macrophages are induced by interferon gamma (IFN-γ) and identified by expression of interleukin IL-12, tumour necrosis factor (TNF) and C-X-C motif chemokine 10 (CXCL10). They are implicated in extracellular matrix (ECM) degradation, thus resolving fibrosis. M2 macrophages are induced by IL-4 and/or IL-13 and express IL-1 RII, mannose receptors, hemoglobin scavenger receptor CD163 and many others (Homer et al., 2011). They are involved in releasing EMC components and developing fibrosis.

### 1.6.4.2. Con arguments- pulmonary fibrosis is not an inflammatory disease

The concept seems to be currently challenged. The recent hypothesis presents that fibrosis results from repetitive epithelial injures and abnormal wound healing and it is rather an ‘epithelial-fibroblastic’ disease rather than an inflammatory disorder (Selman et al., 2001). First, inflammation is not essential for the development of fibrosis. For instance, IL-10 KO mice in silica-induced fibrosis, presented more severe lung inflammation but less fibrotic response in comparison to wild mice. Moreover, fibrosis develops without inflammatory phase when mice were exposed to 95% hyperoxia and lung explants were cultured in hyperoxic, blood-free environment. Moreover, fibroblasts proliferation and collagen deposition increased (Selman et al., 2001). Second, failure of anti-inflammatory therapies in disease outcome. There is not the recommendation for treatment with interferon gamma-1b because the drug did not improve survival for patients with IPF (King Jr et al., 2009). Third, there is the lack of correlation of inflammatory markers with progression of the disease. In various diffuse infiltrative diseases, the extent and severity of ground-glass opacities correlate with alveolitis.

However, in IPF they are not associated with the inflammatory response (Reynolds, 2005).

### 1.7. Cellular pathobiology

Myofibroblasts highly express α-smooth muscle actin (α-SMA) and secrete massive extracellular matrix (ECM) components such as collagen. In the wound remodeling phase, myofibroblasts initiate wound contraction, a process where the edges of the wound migrate toward the center, epithelial/endothelial cells divide and migrate over the temporary matrix to regenerate the damaged tissue. Fibrosis appears when the wound is severe, the tissue-damaging irritant persists for long time, or when the repair process becomes dysregulated (Wynn, 2011). Similarly to cancer, myofibroblasts can maintain their own growth by producing several cytokines such as TGF-β and losing the capability to produce the antifibrotic PGE2 (prostaglandin E2) (Moore et al., 2005). The origin of myofibroblasts remains unclear (Willis et al., 2005). There are three theories that seek to explain the origin of myofibroblasts: 1) activated resident lung fibroblasts, 2) epithelial cells via the process of epithelial-mesenchymal transition (EMT) or 3) bone marrow–derived fibrocytes (Figure 4).

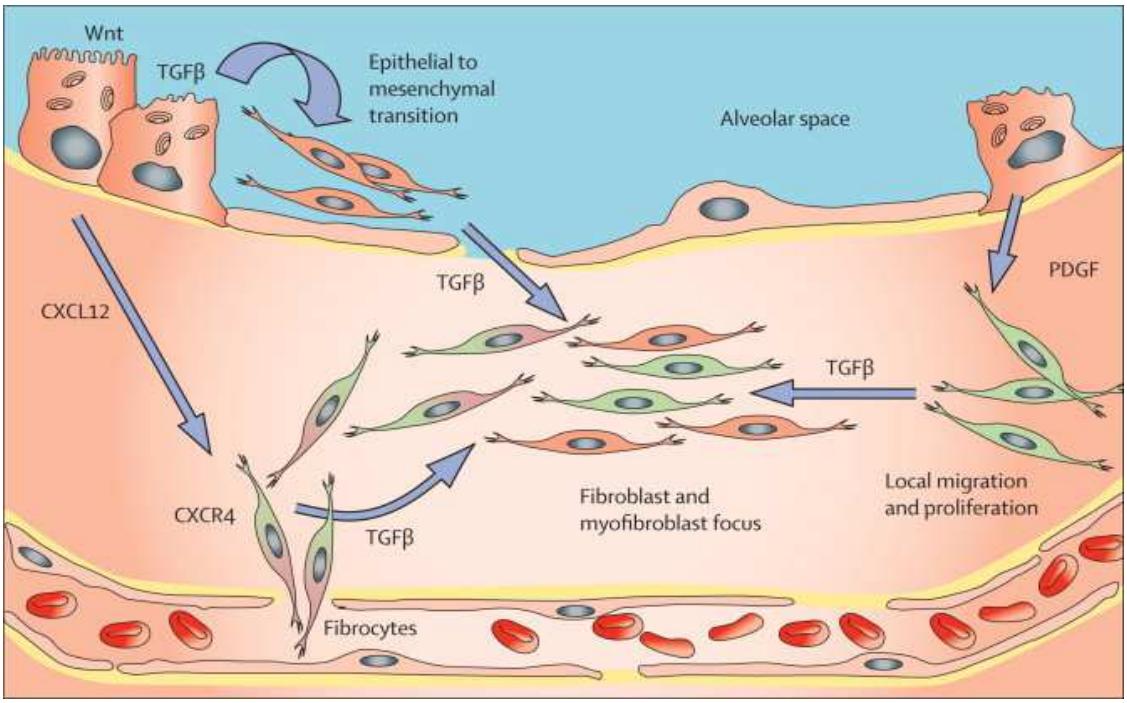


**Figure 4. Overview of the sources of recruitment of fibroblasts during the development of idiopathic pulmonary fibrosis** (King Jr et al., 2011).

### 1.7.1. Residental fibroblasts

The increased number of myofibroblasts in the subepithelial injured area and in the fibroblastic foci is caused by the fact that resting resident fibroblasts become activated, proliferate, and differentiate into highly contractile myofibroblasts in response to profibrotic growth factors, for instance transforming growth factor beta (TGF-β) or platelet-derived growth factors (PDGFs) (Fernandez and Eickelberg, 2012b). TGF-β promotes fibroblast and macrophage recruitment as well as fibroblast proliferation via PDGF expression. In these cells, TGF-β also stimulates expression of various proinflamatory and fibrogenic cytokines, such as TNF-a, PDGF, IL-1 or IL-13, thereby further enhancing and maintaining the fibrotic response (Fernandez and Eickelberg, 2012b).

### 1.7.2. Epithelial-mesenchymal transition (EMT)

EMT mostly known for its crucial role in tumor cell invasion and metastasis in many cancer diseases (Trovato-Salinaro et al., 2006). In the last decade, an increased number of studies indicate that alveolar epithelial cells undergo EMT under the profibrotic environment after the injury, and contribute to the myofibroblast population (Vancheri, 2012, (Willis et al., 2006) in the fibrotic lungs. More importantly, attenuated pulmonary fibrosis was observed in animal models by blocking the EMT process (Aoyagi-Ikeda et al., 2011). A few molecules have been suggested in the EMT process, with TGF-β and Wnt being highlighted. It has been shown that the epithelial cells stimulated with TGF-β or Wnt lose epithelial markers: cytokeratin and E-cadherin and express mesenchymal markers: vimentin, collagen type I and α-SMA (Lamouille et al., 2014); Vancheri et al., 2010).

### 1.7.3. Fibrocytes

Another important source of lung myofibroblast are bone marrow-derived mesenchymal progenitor cells called fibrocytes. They are the subpopulation of leukocytes expressing both haemopoietic (CD45, CD34) and mesenchymal (collagen I, fibronectin) cell markers (Strieter et al., 2009). Some studies have elucidated that fibrocytes account for 20% of cells which contribute to lung fibroblasts (Tanjore et al., 2009). Similar to resident fibroblasts and epithelial cells, fibrocytes respond to TGF-β–driven differentiation into myofibroblast through activation of Smad2/3, SAPK/JNK and MAPK signal transduction (Hong et al., 2007). In addition, the human fibrocytes express the chemokine receptor CXCR4 (chemokine (C-X-C motif) receptor 4), whereas epithelial

cells from the IPF patients upregulate CXCL12 (C-X-C motif chemokine 12), which probably induces the chemotactic gradient required for trafficking of CXCR4 positive fibrocytes (Andersson-Sjöland et al., 2008). This cooperation suggests that the CXCR4-CXCL12 biological axis is important for recruiting circulating fibocytes into lung during the pathogenesis of pulmonary fibrosis (Andersson-Sjöland et al., 2008).

### 1.8. Molecular pathobiology of interstitial lung fibrosis (IPF)

There is a multiple-pathway mechanism that plays the role in the pathogenesis of IPF. A range of molecular abnormalities that can result in fibrosis are well characterized. The TGF-β signaling pathway is the best known in pulmonary fibrosis, however, there is not only one pathway that is implicated in the development of IPF (Figure 5).

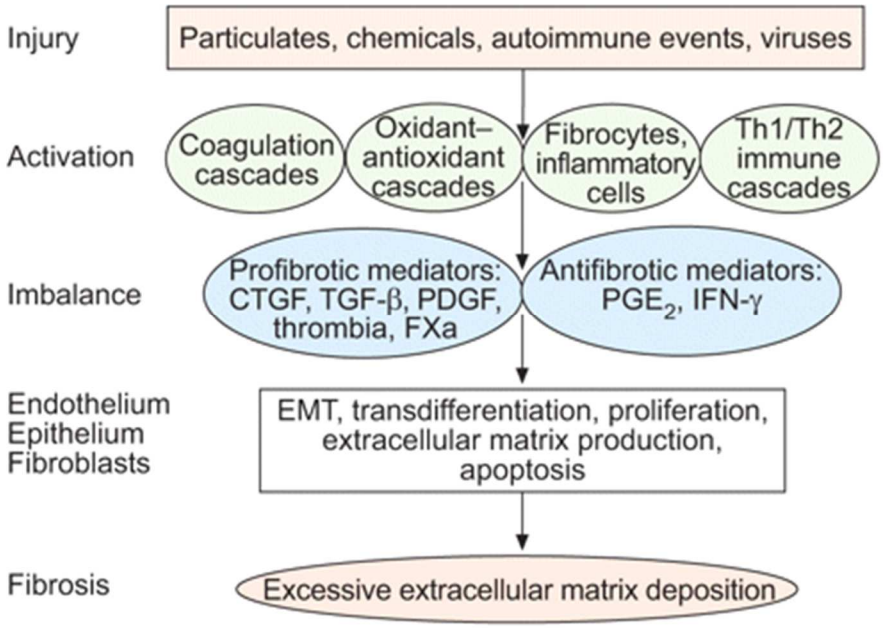


**Figure 5. A new model for the pathogenesis of idiopathic pulmonary fibrosis** (Maher et al., 2007). Th: T-helper cell; CTGF: connective tissue growth factor; TGF-β: transforming growth factor-β; PDGF: platelet-derived growth factor; FXa: factor Xa; PG: prostaglandin; IFN-γ: interferon-γ; EMT: epithelial–mesenchymal transition.

### 1.8.1. Transforming growth factor beta (TGF-β) signaling pathway

More than 60 members of TGF-β family are known: five activins, eight bone morphogenetic proteins (BMPs) and three TGF-βs (Feng and Derynck, 2005). The three mammalian TGF-β isoforms: TGF-β1, 2 and 3 are synthesized as latent precursor molecules (LTGF-β) containing an amino-terminal hydrophobic signal peptide region, the latency associated peptide (LAP) region and the C-terminal potentially bioactive region (Roberts, 1998). The LTGF-β creates the complexes with latent TGF-β-binding proteins (LTBP) and requires activation into a mature form for receptor binding and activation of signaling pathway. The LTBP is removed extracellularly due to a cleavage by plasmin, thrombin, plasma transglutaminase or endoglycosylases, or due to physical interactions of the LAP with thrombospondin-1 (Annes et al., 2003).

The secreted TGF-β binds to two different types of serine/threonine kinase receptor: type I and type II (Figure 6). In vertebrates, there have been identified five type II and seven type I receptors that are referred to as activing- receptor-like kinase (ALKs) (ten Dijke and Hill, 2004). Both receptors are present as homodimers in the plasma membrane. Upon ligand binding, the type II receptors activate the type I receptor kinases through phosphorylation of the juxtamembrane domain (the Gly/Ser-rich domain or GS domain) of type I receptors. Further, the type I receptos activate the signal messengers belonging to Smad family (Marcelo Ehrlich, 2012).

Smads are divided in three subclasses: receptor-regulated Smads (R-Smads), common partner Smads (Co-Smads) and inhibitory Smads (I-Smads). In mammals, Smad2 and Smad3 act as TGF-β/activin-specific R-Smads; Smad1, Smad5 and, presumably, Smad8 are BMP-specific R-Smads. Smad4 is the only Co-Smad; Smad6 and Smad7 act as I-Smads (Miyazono, 2000).

R-Smads are anchored to the cell membrane through membrane-bound proteins such as Smad-anchor for receptor activation (SARA). Phosphorylated Smads-R form heteromeric complexes with Co-Smad- Smad4 and enter to the nucleous where they serve as transcriptional factors with the coactivators CBP and p300. Further, inhibitory Smads antagonize signaling pathway, so they act in opposing manner to R-Smads. They compete with R-Smads for binding to TGF-β RI and inhibit the phosphorylation of R-Smads and/or TGF-β RI degradation by E3-ubiquitin ligases (Shi and Massagué, 2003).

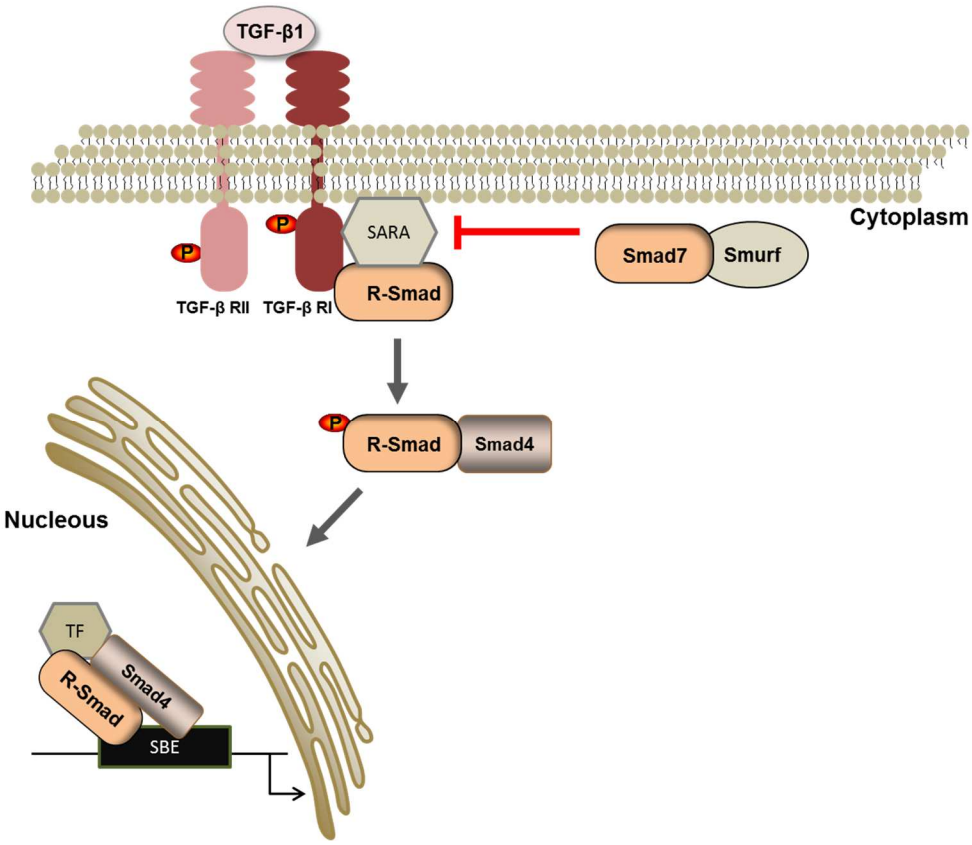


**Figure 6. Transforming growth factor beta (TGF-β) transduction pathway** (Verrecchia and Mauviel, 2007).

### 1.8.2. Connective tissue growth factor (CTGF)

CTGF plays a central role in pulmonary fibrosis. CTGF induces formation of myofibroblasts through transdifferentiation of different types of cells, including epithelial cells (via EMT, epithelial to mesenchymal transition), stellate cells, resident fibroblasts or fibrocytes (bone-marrow-derived, circulating mesenchymal stem cells) that have been recruited to an organ through chemokines. CTGF also activates the myofibroblasts and stimulates their deposition and remodeling of ECM (extracellular matrix) proteins. Moreover, CTGF activates the production of a variety of cytokines such as TGF-β (Yang et al., 2010) and VEGF, which induce higher expression of CTGF (Lipson et al., 2012).

### 1.8.3. Integrins

Various integrins have been found in inflammatory cells during pulmonary fibrosis. Many T cells express αEβ7, which is elevated by TGF-β, and binds to E-cadherin on epithelial cells (Kilshaw, 1999). Additionally, lymphocytes and eosinophils may express

α4 integrins which binds to vascular cell adhesion molecule-1 (VCAM-1). In the bleomycin model, treatment with neutralizing antibody against α4 showed diminished hydroxyproline contenst, histologic fibrosis, cellular inflammation, and α-SMA expression (Todd et al., 2012). Integrins which are expressed on fibroblasts can activate latent TGF-β as well as promote fibrosis. Moreover, the α2β1 integrin is a main type I collagen receptor (Jokinen et al., 2004).

### 1.8.4. Interleukin-13 (IL-13)

Cytokines associated with CD4+ Th1 and Th2 cells have elicited contrasting activity in fibrogenesis. Interleukin-13 (IL-13) is the Th2-associated cytokine and is linked to the development of the fibrosis. Moreover, IL-13 is detected in the BAL fluid of IPF patients; the hyperresponsiveness of IPF fibroblasts to IL-13 and expression of both IL-13 and IL-13Rα1 correlates with the severity of the disease (Murray et al., 2008). Further, fibroblasts isolated from the lungs of patients affected with IPF exhibit an increase in IL-13 receptor expression for both IL-13Rα1 and IL-13Rα2 (Clarke et al., 2013).

### 1.8.5. Platelet-derived growth factor (PDGF)

The importance of PDGF signaling in the fibrotic process is presented by reports showing that a number of fibrogenic mediators such as TGF-β, IL-1, TNF-α, bFGF, and thrombin exhibit PDGF-dependent profibrotic activities. PDGF induces fibroblast chemotaxis, fibroblast proliferation and promotes fibroblast-mediated tissue matrix contraction (Bonner, 2004). The expression of two PDGF isoforms, PDGF-C and PDGF-D, increases during bleomycin-induced lung fibrosis and it has been shown that PDGF receptor tyrosine kinase inhibitors markedly attenuate radiation-induced pulmonary fibrosis (Zhuo et al., 2004).

### 1.8.6. Wnt

The activation of canonical and noncanonical TGF-β signal transduction is involved in myofibroblast differentiation by promoting stress fiber formation (Sousa et al., 2007). Akhmetshina and collegues showed that the crosslink between TGF-β and Wnt pathway is a pivotal factor for fibroblast activation in fibroblast diseases.

During TGF-β-induced myofibroblast differentiation, canonical Wnt signaling is activated by decrease expression of Dickkopf-1, a Wnt inhibitor, in p38-dependent manner and in turn TGF-β requires canonical Wnt activation for fibrosis induction

(Akhmetshina et al., 2012). In IPF, additional to canonical activation, Wnt/ β-catenin pathway might be activated by TGF-β via the phosphorylation of ERK1/2 leading to a secondary activation of other transduction pathways that may regulate cell proliferation and apoptosis (Caraci et al., 2008). Several studies have shown that some pathways are disregulated in pulmonary fibrosis and can explain aberrant behavior of epithelial cells. Wnt/β-catenin is up-regulated in patients with IPF. Moreover, a nuclear accumulation of β-catenin in epithelial cells and fibroblasts suggests that this pathway is switched on in both types of cells (King Jr et al., 2011). When Wnt pathway is blocked by WISP1-neutralizing antibodies, the development of bleomycin-induced fibrosis is inhibited (Königshoff et al., 2009).

### 1.9. Animal models of pulmonary fibrosis

#### 1.9.1. Bleomycin

The bleomycin-induced fibrosis is the most widely used animal model of experimentally induced pulmonary fibrosis. This model is applied in many species: rats, guinea pigs, hamsters, dogs, rabbits, primates, but mice are the most frequently used animals. Bleomycin can be delivered in different manners including: intraperitoneal, subcutaneous, intravenous, inhalational and intratracheal (Degryse and Lawson, 2011), all of which induces DNA strand breaks, oxidative stress and the generation of free radicals (Moeller et al., 2008). This results in epithelial injury and acute inflammation followed by sustained low level of inflammation and development of fibrosis. Various cell types, including fibrocytes, fibroblasts, myofibroblasts, macrophages, lymphocytes, neutrophils, AECs type I and II, pericytes as well as endothelial cells, have been implicated to contribute to bleomycin-induced fibrosis (Degryse and Lawson, 2011). Although the histopathology is not fully consistent with UIP, the intratracheal delivery of a single dose is the most common route to induce pulmonary fibrosis, with alveolar epithelial cells (AECs) on the front line of the injury (Molina-Molina et al., 2007). In the intratracheal model, pulmonary fibrosis can be established in a short period (2-4 weeks) and the acute inflammatory phase appears within the first week; therefore drug intervention during this phase is often protective. To study the effects of antifibrotic agents, the therapy should be delivered after the inflammatory phase (at least 7 days after bleomycin). Further, C57Bl/6 strain mice are known to be more susceptible to bleomycin than Balb/c mice (Moeller et al., 2008).

Degryse and colleagues have compared the effect of repetitive and single dose of bleomycin in intratracheal bleomycin model. Bleomycin was deliverd for 8 weeks,

biweekly with the dose of 0.04 units. This model reveled a prominence of hyperplastic AECs lining the areas of fibrosis with the similarity to usual interstitial pneumonia (UIP) and reduced inflammatory cells in BAL in comparison to single dosing of bleomycin. Fibrosis remains prominent 20 to 30 weeks after the last bleomycin dose (Degryse et al., 2010).

In the case of systemic delivery, pulmonary vascular endothelium is the initial site of injury, which complicates the model with sustained systemic injury, and pulmonary fibrosis develops over a longer time (4 -12 weeks) compared with the intratracheal model. For the systemic administration of bleomycin, 20 mg/kg of bleomycin was administrated twice weekly for 4 to 8 weeks by intravenous route. It resulted in initial endothelial injury followed by epithelial injury, inflammation and fibrosis. The disease is developed by week 4, with the progression through week 12 when the mice were treated for 8 weeks. The bleomycin at dose 0.035 U/g was delivered twice per week by intraperitoneal injections and lung were harvested after 33 days after first dose. Subcutaneous delivery of 0.05 mg bleomycin three times per week for 4 weeks is other repetitive-dosing option. Bleomycin can be also delivered by miniosmotic pumps, presenting other mean of subcutaneous route (B. Moore et al., 2013). In Figure 7, the histological pattern typical for various routes of bleomycin instillation is presented.

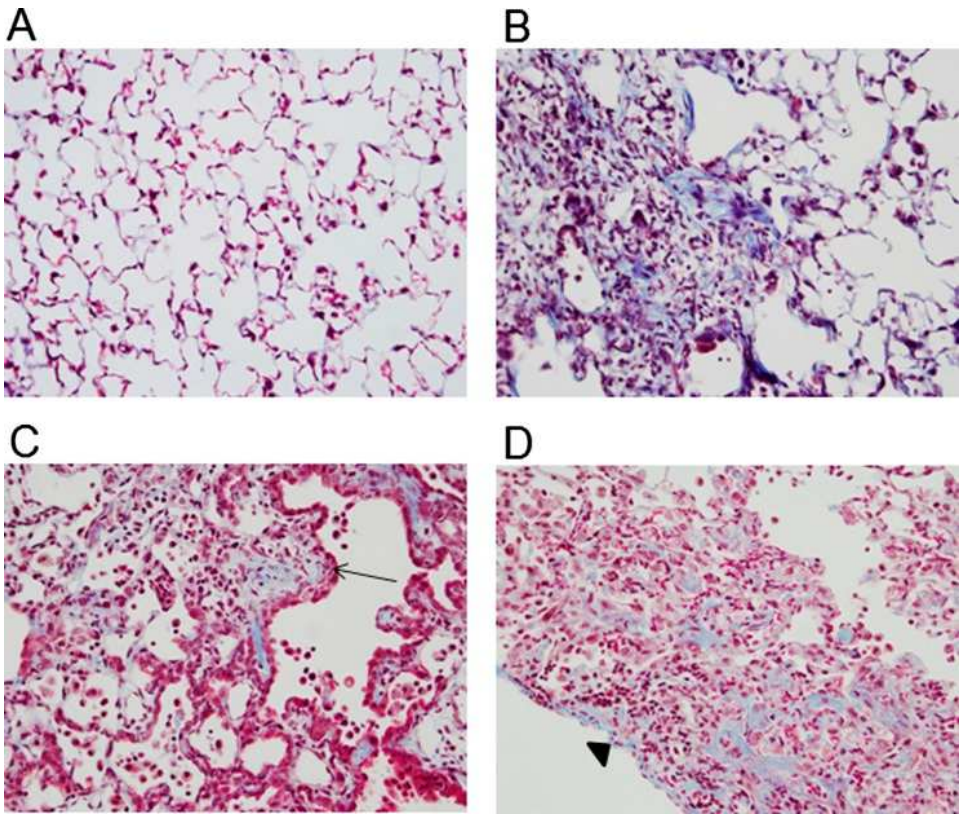


**Figure 7. Different manners of bleomycin administration** (B. Moore et al., 2013)**.** (A) Trichome blue–stained lung sections from normal wild-type C57BL/6 mice. (B) Lung section at 3 weeks after 0.08 of a unit of intratracheal bleomycin demonstrates the development of an area of fibrosis which is typical for this model. (C) Lung section from a mouse at 2 weeks after the eighth biweekly repetitive intratracheal 0.04-unit bleomycin dose. Arrow points to hyperplastic AECs. (D) Lung section from a mouse harvested on day 33 in a twice-weekly intraperitoneal 0.035-U/g bleomycin study. Arrowhead points to pleural edge.

### 1.9.2. Silica

Silica is accumulated in lung and induces persistent, toxic and inflammatory response. In a long term, fibrotic nodules appear around silica deposits which can be easily found by polarization microscopy and histologically (Oberdorster, 1996). There are various routes of silica delivery: aerosolization, intratracheal administration or oropharyngeal aspiration. However, inhalation models mimic human exposure but require longer time to develop pulmonary fibrosis (40-120 days) in comparison to the intratracheal models (14-28 days) (Lakatos et al., 2006). There is strain-dependent response to silica instillation: C57Bl/6 mice are more susceptible than CBA/J mice after intratracheal administration of silica; Balb/c mice are resistant in the aerosolized model, whereas C3H/HeN, MRL/MpJ, and NZB mice show strong response (Davis et al., 1998). It is an important model for investigating the innate

immune regulation of lung fibrotic responses because silicosis involves the strong influence of macrophage NACHT and LRR, PYD domains-containing protein 3 (NALP3) inflammasome activation (Cassel et al., 2008).

### 1.9.3. TGF-β overexpression

The expression of many cytokines such as TGF-β1, TGF-α, IL-13, TNF-α and IL-1β promotes lung fibrosis (Borthwick et al., 2013; Agostini and Gurrieri, 2006). However, TGF-β1 overexpression is studied comprehensively, considering its significant profibrotic potency. TGF-β1 overexpression was first carried out in rats by adenoviral transfection (Sime et al., 1997), where the expression of TGF-β1 was associated with cell infiltration (day 3–7) and the development of alveolar consolidation. Moreover, lung collagen concentration was elevated 2-fold by day 14 (Sime et al., 1997). In the doxycycline-inducible mice model, epithelial cell specific overexpression of TGF-β1 driven by Clara cell 10 promoter led to a transient epithelial apoptosis and resulted in 2-fold increase in collagen concentration over the course of 2 months. Further, the established fibrosis resolved after doxycycline withdrawal (Lee et al., 2004). Both models involve myofibroblast accumulation, alveolar epithelial cell apoptosis, and the induction of epithelial-mesenchymal transition (EMT) (Pulichino et al., 2008).

## 1.10. Treatment options for IPF

Until recently, no pharmacological treatment has been clinically proven for the treatment of IPF. Lung transplantation is the only therapy that prolongs survival in advanced IPF. However, many patients with IPF die before receiving a transplant because they are diagnosed at the late stage. Due to the evolving understanding of the pathogenesis and disappointing clinical outcome of anti-inflammatory and immunosuppressive treatments, there was a shift of paradigm that IPF is an epithelial injury-initiated fibrogenesis rather than an inflammation-driven event (Selman et al., 2001). More recently, two new drugs, pirfenidone and nintedanib, have shown efficacy on disease progression and were licensed for the treatment of IPF. Pirfenidone is the first approved drug for IPF by EMA (The European Medicines Agency) in 2010 (The European Medicines Agency, 2010), followed by FDA (The U.S. Food and Drug Administration) approval in 2014 (The U.S. Food and Drug Administration, 2014a). Pirfenidone was reported to exhibit antifibrotic, anti-inflammatory, and antioxidant effects, although its precise mechanism is not completely clear. Nintedanib, a small molecule tyrosine kinase receptor inhibitor which is originally identified for cancer

treatment, has shown high anti-fibrotic efficacy (Wollin et al., 2015) and was approved by FDA in 2014 (The U.S. Food and Drug Administration, 2014b). Despite of the success with pirfenidone and nintedanib, potential targets of multiple pathways in IPF gain increasing interest of investigators. A summary of such therapeutic targets is outlined in Table 1.

**Table 1. Overview of negative phase III randomized controlled trials in IPF**

| Compound | Mechanism of action | Outcome | Primary endpoint (PE) |
|---|---|---|---|
| **Ambrisentan (ARTEMIS)** | Selective inhibitor, an endothelin A receptor antagonist | Increased risk of hospitalisation due to the increase risk for disease progression (Raghu et al., 2013) | Death or disease progression |
| **Bosentan (BUILD-3)** | Non-selective inhibitor, an endothelin-1 receptor antagonist | No treatment effects in health-related quality of life or dyspnea (King et al., 2011), | Death or disease progression |
| **IFN-ϒ** | Immunoregulatory cytokine | Lack of improve survival for patients with IPF (King Jr et al., 2009) | Death or disease progress |
| **Imatinib** | Tyrosine kinase inhibitor | No improvement of survival or lung function in patients effected by IPF (Daniels et al., 2010) | Time to disease progression or death over 96 weeks |
| **N-acetylcysteine (NAC)** | Precursor of the antioxidant glutathione, stimulator of glutathione synthesis | No significant benefit with respect to the preservation of FV with mild-to-moderate impairment in lung function in IPF patients (Raghu et al., 2014) | Change in FVC |

**Table 1. (continued)**

| | | | |
|---|---|---|---|
| **Sildenafil** | Phosphodiesterase-5 inhibitor | No significant difference between groups (Zisman et al., 2010) | 20% increase in 6MWD at 12 weeks |
| **Warfarin** | Anticoagulant | Increased risk of mortality in an IPF population who lacked other indications for anticoagulation (Noth et al., 2012) | Change in FVC |

### 1.11. Heat shock protein 90 (HSP90)

HSP90 is an evolutionary conserved chaperone that takes part in late-stage maturation, stabilization and activation of more than 200 proteins. It participates in various cellular processes including cell cycle control, hormone signaling, cell survival, trafficking and response to cellular stress (Wandinger et al., 2008).

In eukaryotes, HSP90 is found in the cytoplasm, nucleus, and organelles. In *Homo sapiens,* two cytosolic isoform exist: inducible-HSP90α and constitutive-HSP90β. Those two isoform are encoded by two different genes and share approximately 81% of homology. Moreover, organelle-specific HSP90 forms exist in mitochondria (TRAP1-tumour necrosis factor receptor-associated protein 1), endoplasmic reticulum (GRP94-glucose-regulated protein 94) and chloroplasts (HSP90C) (Miyata et al., 2012). Both GRP94 and TRAP1 have ATPase activity but lack known co-chaperons (Dollins et al., 2007). HSP90α is also secreted from the cells or expressed on cell surface, however there are mostly associated with cancer cells.

#### 1.11.1. Structure of HSP90

Hsp90 forms a dimer at physiological conditions.The chaperone structure consists of three highly conserved domains: N-terminal domain (NTD), middle-domain (MD) and C-terminal domain (CTD). Some members of HSP90 family including cytosolic eukaryotic HSP90 and Grp94 have a charged linker which separates NTD and MD. Additionally, cytosolic eukaryotic HSP90 has a C-terminal extension of MEEVD (Figure 5) (Taipale et al., 2010).

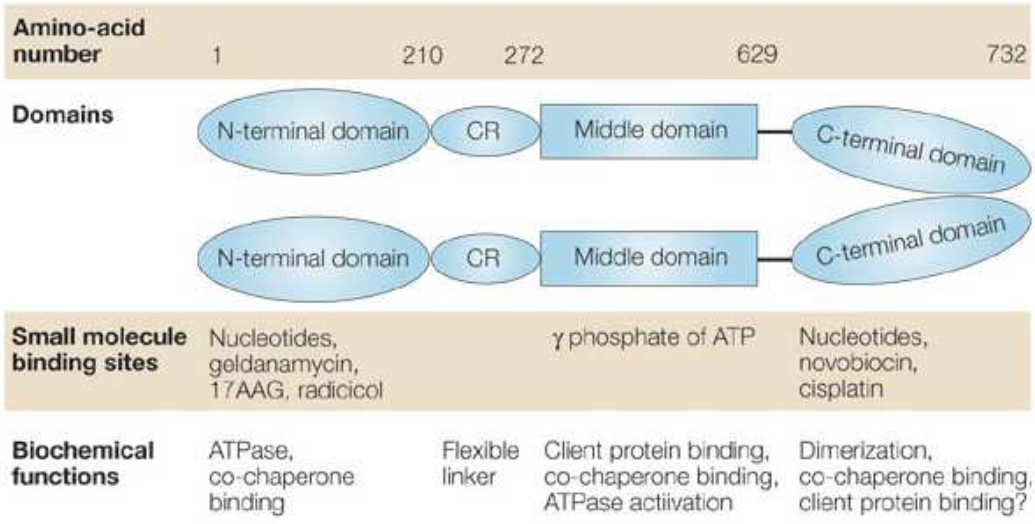


**Figure 8. The scheme of the Hsp90 structure** (Whitesell and Lindquist, 2005)**.** The numbering 1–732 indicates the approximate positions in the amino acid sequence of the human protein that define its functional domains. 'CR' refers to a charged region which serves as a flexible linker between the N-terminal and middle domains. The locations where various small molecules bind HSP90 (heat-shock protein of 90 kDa) and modulate its function are indicated. The biochemical functions of each domain are also shown. 17AAG:17-allylaminogeldanamycin; GA, geldanamycin.

The NTD contains an ATP and drug-binding site (for geldanamycin and ansamycin) and co-chaperone-interacting motifs (for p50 and p23). The MD presents docking sites for client proteins such as Akt, Cdk4, eNOS and co-chaperons such as activator of Hsp90 ATPase (Aha1) and is associated with forming the active ATPase. The CTD is essential for Hsp90 dimerization and possesses a second drug-binding site and interaction regions for other co-chaperons (Wayne and Bolon, 2007; Miyata et al., 2012).

### 1.11.2. Co-chaperons of HSP90

Co-chaperons are the proteins which assist or change the function of other chaperons (Zhao et al., 2005). The cell division cycle 37 homologue (CDC37), prostaglandin E synthase 3 (p23), activator of HSP90 ATPase 1 (AHA1) and STIP1 (p60HOP) regulate the rate of HSP90 cycle by influencing the conformational dynamics of HSP90 (Smith and Workman, 2009). Further, some co-chaperons are adaptors which deliver specific substrates for HSP90. For instance, STIP1 takes part in delivery of steroid hormone receptor clients, while CDC37 is attributed to delivery of protein kinase clients to HSP90. The co-chaperons TAH1 and PIH1 are essential for delivering nascent forms of various ribonucleoproteins that participate in many different processes including

DNA replication, ribosome synthesis and telomerase maintenance (Boulon et al., 2008). Additionally, these co-chaperons are associated with the chromatine-remodelling factors RVB1 and RVB2, elucidating the role of HSP90 in the epigenetic modulation of transcription.

### 1.11.3. Client proteins of HSP90

There are reported more than 200 client proteins for HSP90 (Figure 9). The clients include: transcription factors, chromatin remodeling factors, protein kinases, ribonucleoproteins, steroid hormone receptors, kinetochore complex as well as structural proteins, for instance actin and tubulin (Whitesell and Lindquist, 2005). HSP90 associates with core co-chaperones such as p23 (also known as PTGES3 and as Sba1 in yeast), HSC70 and HSP90-organizing protein (HOP; also known as p60 and STI1) and the HSP40–HSP70 chaperone system; orange) and other co-chaperones (green). Adaptor co-chaperones such as Cdc37 and SGT1 associate with a limited number of proteins or protein domains (blue). However, for most HSP90 clients, it is not known which co-chaperones, if any, are associated in the complex (marked by question mark).

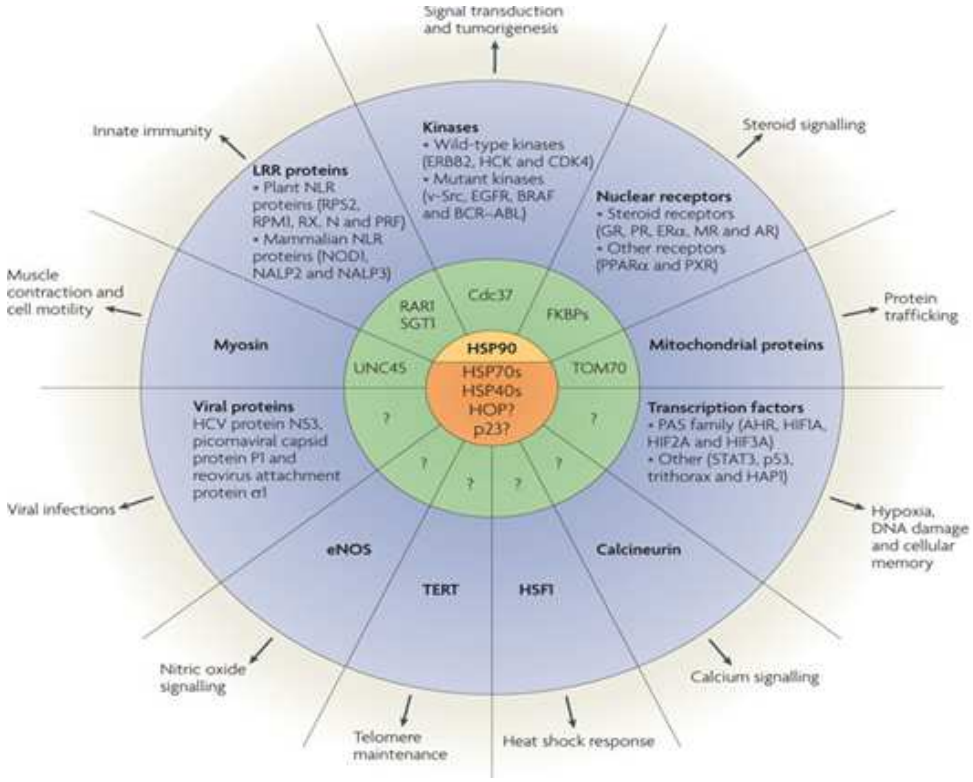


**Figure 9. HSP90 regulates diverse cellular processes through its interaction with client proteins** (Taipale et al., 2010).

### 1.11.4. Heat shock protein 90 (HSP90) in cancer

HSP90 is a master regulator in cancer biology due to the broad spectrum of oncogenic client proteins. Cancer cells proliferate faster and need HSP90 rigorously, while healthy cells rely on HSP90 modestly to maintain physiological functions. This situation is termed 'HSP90 addiction' (Miyata et al., 2012). The higher number of HSP90-dependent proteins may accumulate in cancer cells, therefore HSP90 is more occupied with its clients proteins in cancer cells. Further, the difference in structure and/or post-translational modifications of HSP90-clients can be one of the reasons why the cancer cells are more sensitive to HSP90 inhibition (Kamal et al., 2003). More importantly, highly-unstable mutant oncogenic proteins, which arise during tumor transformation, are stabilized by HSP90 and its co-chaperons. HSP90 and its association with cancer pathobiology are described below.

#### 1.11.4.1. Hypoxia inducible factor (HIF)

HIF is probably one of the most potent proangiogenic proteins regulated by Hsp90. It has been shown that both the HIF-1a and HIF-2a subunits are client proteins for

HSP90 and the chaperone activity is important for HIF stability and function (Milkiewicz et al., 2007; Dörthe M Katschinski, 2004). HIF overexpression correlates with highly vascularized tumors, resistance to chemo- and radiotherapy, and overall poor prognosis (Rankin and Giaccia, 2008).

#### 1.11.4.2.Vascular endothelial growth factor/vascular endothelial growth factor receptors (VEGF/VEGFRs)

Vascular endothelial growth factor (VEGF) are involved in organizing new blood vessels growth during embryonic and postnatal development. Receptors for VEGF (VEGFR1 and VEGFR2) are Hsp90-clients, and their stability and functions rely on the Hsp90 chaperone machinery. The inhibition of HSP90 can leads to tumor regression and suppression of metastasis (Laederich et al., 2011).

#### 1.11.4.3. Epidermal growth factor receptor (EGFR/HER2)

The receptor tyrosine kinase HER-2 (also known as ErbB-2) is a protein whose stability depends on HSP90 function (Zhou et al., 2003). HER-2 is a ligandless receptor and the preferred heterodimerization partner for ligand-bound epidermal growth factor receptor family members HER-1, HER-3, and HER-4 (Citri et al., 2003). Moreover, overexpression of the HER-2 receptor is associated with increased progression and metastasis in human breast cancer (Sidera et al., 2008).

#### 1.11.4.4.Telomerases

The elongation of telomeres by the telomerase is a crucial step for cancer cells to achieve immortalization. Telomerase is overexpressed in the majority of human cancer cells and consists of a reverse transcriptase catalytic subunit hTERT. HSP90 and its co-chaperone p23 were identified as hTERT-binding partners, and they contribute to the formation of functional telomerase complexes in cells. (DeZwaan et al., 2009).

#### 1.11.4.5. p53

p53 tumor suppressor protein is a crucial transcription factor that regulates cell cycle and initiates apoptosis. Inactive mutants are found in more than 50% of human cancers (Brady and Attardi, 2010). Many studies have shown that HSP90 interacts with mutant p53 and inhibition of HSP90 promotes its degradation (Blagosklonny et al., 1996), (Nagata et al., 1999). Interestingly, opposing effects on wild-type and mutant p53 has been observed with HSP90 inhibition (Lin et al., 2008).

### 1.11.5. HSP90 in other diseases

Aside from the focus on HSP90 in cancer biology, HSP90 has gained increasing attention on neurodegenerative disease. It leads to abnormal tau phosphorylation by stabilizing p53 or directly interacting with mutated form of tau protein. Thus it influences the accumulation of toxic tau aggregates in tauopathy like Alzheimer's disease and frontotemporal dementia (FTD) (Dickey et al., 2007).

HSP90 is also a key stress protein involved in both the interaction with and response to microbes and viruses. For example, HSP90 plays a key role in folding of basic viral proteins (Geller et al., 2007), therefore HSP90 inhibition makes possible to block the replication of poliovirus and paramyxovirus (Geller et al., 2013).

### 1.11.6. Therapeutic implications of HSP90 inhibitors

#### 1.11.6.1. Inhibition of N-terminal domain

The first identified inhibitors were the natural benzoquinone ansamycin geldanamycin (GM) and the macrolactone radicicol (RD) extracted in 1970 and 1953, respectively. Both inhibitors bind to the N-terminal ATP binding pocket of HSP90 which results in selective inhibition of ATP binding and hydrolysis of HSP90 (Xu et al., 2002). However, geldanamycin and radicicol have some pharmacological disadvantages like toxicity and limited solubility, they provided the chemical basis for drug development. The semisynthetic GM analogues were developed: 17-allylamino-17-demethoxygeldanamycin (17-AAG, tanespimycin, KOS-953), a carbon-17 substituted derivate which is less toxic and shows similar anti-proliferative effects (Eckl and Richter, 2013) (Figure 10). In phase I studies, 17-AAG presented clinical activity in various malignancies such as HER+, trastuzumab-refractory breast cancer with side effects (diarrhea, fatigue, headache or neuropathy) manageable with supportive medications. However, despite the promising results in the treatment of breast cancer, different animal model studies consistent with the clinical data showed that there is cytostatic arrest and growth inhibition rather than tumor regression (Sawai et al., 2008). Another limitation of 17-AAG is the requirement for reductive metabolism of the benzoquinone by NADPH quinone oxidoreductase 1 (NQO1). This reaction enhances the drug's inhibitory potency but it can also leads to liver toxicity (Gaspar et al., 2009). 17-DMAG (alvespimycin), another geldanamycin analog which is water soluble, displays better pharmacokinetic properties and higher oral (Egorin et al., 1998). In addition, it is less sensitive to and dependent on NQO1, therefore presents low toxicity. The recent phase I studies with intravenous 17-DMAG showed response in patients

with advanced solid cancers such as castrate-refractory prostate cancer and melanoma (Pacey et al., 2011).

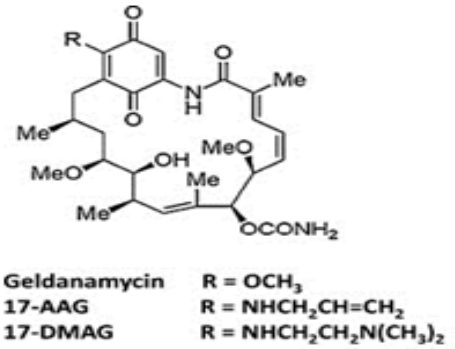


**Figure 10. The structure of geldanamycin, 17-AAG and 17-DMAG** (Li et al., 2009)**.**

### 1.11.6.2. Inhibition of C-terminal domain

Coumarin antibiotics, such as novobiocin, clorobiocin and coumermycin A1 target C domain of HSP90. However, they are all excluded from further evaluation in clinical studies due to the low affinity to HSP90 compared with their affinity to topoisomerases type II (Trepel et al., 2010). Recently, some improving of these compounds has been attained. One of them, such as F-4, presents similar efficacy as 17-AAG in inducing apoptosis in PC-3 and LNCaP prostate cancer cell lines (Matthews et al., 2010). Another novobiocin derivative termed KU135 inhibits proliferation and induced apoptosis of Jurkat T cell (leukaemia lymphocytes) more potently than 17-AAG (Shelton et al., 2009).

### 1.11.6.3. Disruption of co-chaperone/ HSP90 interactions

Besides the drugs which target N and C domain, attempts have been made to develop new inhibitors targeting hydrophobic protein-protein interaction surfaces of HSP90. Recent molecular docking studies and molecular dynamic simulations showed natural product celastrol disrupts the interaction of HSP90 with its co-chaperone CDC37 and destabilizes various HSP90 clients kinases against pancreatic cancer cells (Zhang et al., 2008). However, these strategies remain highly challenging, considering that nowadays little is known about the structural and biochemical interactions between HSP90 and its clients.

# 2. AIMS OF THE STUDY

HSP90 is a highly conserved chaperone protein and is essential for stabilization or degradation of many signaling proteins. HSP90 is centrally involved in the pathobiology of cancer and HSP90 inhibitors have been widely investigated in preclinical and clinical studies against cancer. Recent evidence shows that HSP90 promotes epithelial-mesenchymal transition (EMT) of cancer cells and TGF-β1 signaling via the stabilizing of the TGF-β receptors, however little is known about the role of HSP90 in IPF.

The purpose of the present study is to discover the role of HSP90 in lung fibroblast activation, particularly with regard to TGF-β1-induced profibrotic phenotype, and to determine the effects of HSP90 inhibitor on bleomycin-induced pulmonary fibrosis in mice as well as to offer new selective theraphy targets for IPF.

In this study, a series of study were undertaken as follows:

**1.** Confirm differential HSP90 expression by real-time PCR, western blot and immunohistochemistry:

a. in human lung and interstitial lung fibroblasts (ILFBs) from donor and patients with IPF
b. in mouse lung and ILFBs from healthy mice and bleomycin-administrated mice

**2.** Determine the *in vitro* effects of 17-AAG on:

a. TGF-β-induced fibroblast activation demonstrated by western blot of α-SMA
b. TGF-β-induced fibroblast extracellular matrix (ECM) production carried out by Sircol Soluble Collagen assay and western blot of collagen I and fibronectin
c. FCS-induced fibroblast migration performed by transwell assay and scratch assay

**3.** Characterize TGF-β RII as a target protein and SMAD2 and SMAD3 as downstream molecules of HSP90 by western blot.

**4.** Use the MG-132 inhibitor to prove that 17-AAG block TGF-β/Smad signaling in IFBs by diminishing TGF-βRs levels by proteasome degradadion.

**5.** Perform co-immunoprecipitation to demonstrate the direct interactions between HSP90β and TGF-β RII.

**6.** Investigate the *in vitro* effects of HSP90 inhibition on epithelial-mesenchyman transition (EMT) revealed by western blot and immunofluorescence staining of mesenchymal and epithelial markers.

**7.** Evaluate the *in vivo* effects of 17-DMAG on attenuation of pulmonary fibrosis using the established bleomycin-induced IPF mouse model. The following experiements were investigated:

a. inflammatory cell composition in bronchoalveolar lavage fluid (BALF)
b. respiratory function (lung compliance and tissue damping) by FlexiVent
c. histological assessment including Ashcroft fibrosis scoring and collagen deposition
d. activity of matrix metalloproteases (MMPs) measured by *in vivo* fluorescence molecular tomography (FMT) in combined with micro-computed tomography (µCT)

# 3. MATERIALS AND METHODS

## 3.1. Materials

### 3.1.1. Chemicals, reagents, kits

| Company | Product |
|---|---|
| 17-AAG inhibitor | Selleck, USA |
| 17-DMAG inhibitor | LC Laboratories, USA |
| 2-propanol | Sigma- Aldrich, Germany |
| Acetic acid | Sigma- Aldrich, Germany |
| Acrylamid | Roth, Germany |
| Ammonium persulfate (APS) | Sigma- Aldrich, USA |
| Ampicillin sodium salt | Sigma, USA |
| Bis(sulfosuccinimidyl)suberate (BS3) | Thermo Scientific, USA |
| Bleomycin | Sigma-Aldrich, USA |
| Bovine serum albumin powder | Serva, Germany |
| Bovine serum albumin (2 mg/ml) | Bio-Rad, USA |
| Bromophenol blue | Merck, Germany |
| Cell proliferation ELISA, BrdU | Roche, USA |
| Citric acid monohydrate | Sigma, Germany |
| Collagenase type IV | Sigma-Aldrich, USA |
| Crystal violet solution 2.3% w/v | Sigma-Aldrich, USA |
| DAPI | Dakocytomation, USA |
| *DC*™Protein Assay | Bio-Rad, USA |
| DEPC water | Roth, Germany |
| Disodium phosphate ($Na_2HPO_4$ x $H_2O$) | Roth, Germany |
| Dithiothreitol (DTT) | Sigma-Aldrich, USA |
| Dynabeads Protein G | Life Technologies, USA |
| Enhanced chemiluminescence (ECL) kit | Amersham, USA |
| Eosin-Y alcoholic | Thermo Scientific, UK |
| Ethanol 70% | SAV LP, Germany |
| Ethanol 96% | Otto Fischhar, Germany |
| Ethanol 99.9% | Berkel AHK, Germany |
| Ethylenediaminetetraacetic acid (EDTA) | Sigma-Aldrich, USA |
| Formaldehyde 3.5-3.7% | Fischer, Germany |
| Giemsa | Merck, Germany |
| Glycerol | Sigma-Aldrich, USA |

| | |
|---|---|
| Hematoxilin Haemalaun nach Mayer | Waldeck, Germany |
| iScript cDNA synthesis kit | Bio-Rad, USA |
| Isoflurane | Baxter, UK |
| iTaqSYBR Green Supermix | Bio-Rad, USA |
| May-Gruenwald | Merck, Germany |
| Methanol | Sigma-Aldrich, USA |
| MMPSense™ 680 | Perkin Elmer, USA |
| MG-132 inhibitor | Calbiochem, USA |
| Monopotassium phosphate ($KH_2PO_4$) | Roth, Germany |
| Non-fat milk | Roth, German |
| Paraformaldehyde | Sigma-Aldrich, USA |
| Paraplast® Plus paraffin embedding medium | Sigma-Aldrich, USA |
| Pertex® mounting medium | Medite, Germany |
| Picric acid solution 1.2% | AppliChem, Germany |
| Positively charged glass slides | Langenbrinck, Germany |
| Potassium chloride (KCl) | Sigma-Aldrich, USA |
| Precision Plus Protein Standards | Bio-Rad, USA |
| RIPA buffer | Santa Cruz, USA |
| S.O.C solution | Invitrogen, USA |
| Saline (NaCl 0.9%) | B. Braun, Germany |
| SDS Solution, 10% w/v | Promega, USA |
| SIRCOL collagen assay | Biocolor Ltd., UK |
| Sirius red F3B | Niepoetter, Labortechnik |
| Sodium chloride (NaCl) | Sigma-Aldrich, USA |
| Sodium citrate tribasic dehydrate | Sigma, Germany |
| Tetramethylethylenediamine (TEMED) | Sigma-Aldrich, USA |
| TGF-β1 | R&D System, USA |
| Tissue-Tek® O.C.T™ Compound | Sakura, Japan |
| Tris-HCl 0.5 M, pH 6.8 | Amresco SOLON, USA |
| Tris-HCl 1.5 M, pH 8.8 | Amresco SOLON, USA |
| Tris-HCl | Roth, Germany |
| Triton-X100 | Sigma-Aldrich, USA |
| TRIzol® Reagent | Life Technologies, USA |
| Trypsin 2.5% | Invitrogen, USA |

| | |
|---|---|
| Tween®20 | Sigma-Aldrich, USA |
| UltraPure water | Cayman Europe, Estonia |
| Xylol (isomere) >98% pure, for histology | Roth, Germany |
| ZytoChem-Plus AP Kit, Broad Spectrum | Zytomed Systems |
| β-Mercaptoethanol | Sigma-Aldrich, USA |

### 3.1.2. Cell culture medium

MCDBI-131 medium, HBSS (Hank´s buffered saline solution) PBS, L-glutamine, penicillin/streptomycin and Trypsin/EDTA are all purchased from PAN (Germany). Fetal calf serum (FCS) is from Biowest (Germany) and insulin from Sigma-Aldrich (USA). Basic fibroblast growth factor (bFGF) and human epidermal growth factor (EGF) are purchased from Peprotech (USA). The rest including DMEM/F12 medium, Opti-MEM medium, MEM vitamin solution and MEM non-essential amino acids solution are all from Gibco, Life Technologies (USA).

### 3.1.3. Antibodies

**Table 2. Primary antibodies**

| Antibody (catalog number) | Host | Dilution | Company |
|---|---|---|---|
| **Alpha smooth muscle actin (α-SMA), (ab5694)** | rabbit polyclonal antibody | 1:1000<br>1:100 | Abcam, UK |
| **Beta- actin (β-actin), (ab6276)** | mouse monoclonal antibody | 1:4000 | Abcam, UK |
| **Collagen type I, (T40777R)** | rabbit monoclonal antibody | 1:1000 | Meridian, USA |
| **E-cadherin, (07-697)** | rabbit polyclonal antibody | 1:1000 | Millipore, USA |
| **E-cadherin, (610181)** | mouse monoclonal antibody | 1:100 | BD Biosciences, USA |
| **Fibronectin, (F0916)** | mouse monoclonal antibody | 1:1000<br>1:200 | Sigma-Aldrich, USA |
| **HSP90α, (ADI-SPS-771)** | rabbit polyclonal antibody | 1:1000<br>1.100 | Enzo Life Sciences, USA |
| **Hsp90β, (ab53497)** | rabbit polyclonal antibody | 1:100 | Abcam, UK |
| **HSP90β, (ADI-SPA-844)** | rabbit polyclonal antibody | 1:1000 | Enzo Life Sciences, USA |
| **IgG control, (NB810-56910)** | rabbit polyclonal antibody | 1:75 | Acris, USA |
| **IgG control, (sc-2027)** | rabbit polyclonal antibody | 2 µg/ 0.75 mg lysate | Santa Cruz, USA |
| **SMAD2 (pSer465, pSer467), NB200-629** | rabbit polyclonal antibody | 1:1000 | Novus Biologicals, UK |
| **SMAD2, (5339)** | rabbit monoclonal antibody | 1:1000 | Cell Signaling, USA |
| **SMAD3 (pSer423, pSer425), (PS1023)** | rabbit monoclonal antibody | 1:1000 | Calbiochem, USA |
| **SMAD3, (9523S)** | rabbit monoclonal antibody | 1:1000 | Cell Signaling, USA |
| **TGF-β receptor I, (3712)** | rabbit polyclonal antibody | 1:1000 | Cell Signaling, USA |

**Table 2. (continued)**

| | | | |
|---|---|---|---|
| **TGF-β receptor II, (3713)** | rabbit polyclonal antibody | 1:1000 | Cell Signaling, USA |
| **TGF-β receptor II, (sc-400)** | rabbit polyclonal antibody | 1:1000<br>2 µg/ 0.75 mg lysate | Santa Cruz, USA |
| **TTF1, (ab76013)** | rabbit monoclonal antibody | 1:100 | Abcam, UK |

**HRP-conjugated secondary antibody**

Rabbit anti-mouse IgG (1:40000), Sigma-Aldrich, USA

Goat anti-rabbit IgG (1:50000) Pierce, USA

**Fluor-conjugated secondary antibody**

Goat anti-mouse DyLight549 IgG (1:5000), Zytomed, Germany

### 3.1.4. Primers

**Table 3. Primers for quantitative RT-PCR**

| Gene | | Primer Sequence |
|---|---|---|
| **HumaHSP90A class A1 (HSP90AA1)** | Forward | 5’ TGCCTTTTGCCTTAAGGTCTC 3’ |
| | Reverse | 5’GAT TGG TGA CAT CTC CATGCT 3’ |
| **Human HSP90A class B1 (HSP90AB1)** | Forward | 5’CTT GAC TGC CAA GTG GTCTTC 3’ |
| | Reverse | 5’GAT CGA AGA TGT GGGTTCAGA 3’ |
| **Human HSP90B1** | Forward | 5’CCC GTC CTA GAG TGT TTCCTC 3’ |
| | Reverse | 5’ CCA GTT TGG TGT CGGTTTCTA 3’ |
| **Mouse HSP90A class A1 (HSP90AA1)** | Forward | 5’ GAC TCC CAG GCA TAC TGC TC 3’ |
| | Reverse | 5’ AAT AAC CTT GGC ACC ATT GC 3’ |
| **Mouse HSP90A class B1 (HSP90AB1)** | Forward | 5’AGG GTT GAT CTC CAG GTGTTT 3’ |
| | Reverse | 5’TGG GAA CCA TTG CTA AGTCTG 3’ |
| **Human HSP90B1** | Forward | 5’TCC ACG ACC TAG TGT GTT TCC 3’ |
| | Reverse | 5’ CCA GTT TGG TGT CGG TTT TTA3’ |

### 3.1.5. Equipments

| Equipment | Company |
|---|---|
| Balance 1.0-3000g RP 3000 | August Sauter, Switzerland |
| Balance PCB 200-2 Precision | Kern, Germany |
| Balance XS205 | Mettler Toledo, Switzerland |
| BioDoc Analyzer | Biometra, USA |
| Cell culture incubator | Hera Cell Heraeus, |
| Centrifuge Roranta 460R | Hettich, Germany |
| Cooling plate for paraffin-embedding EG1150C | Leica, Germany |
| Cytospin™ 4 Cytocentrifuge | Thermo Scientific, USA |
| Electrophoresis chamber | Bio-Rad, USA |
| FlexiVent | SCIREQ, Canada |
| Fluorescence Molecular Tomography 2000 | Perkin Elmer |
| Freezer (+4°C, -20 °C, -80 °C) | Bosch, Germany |
| Incubator hood TH 15 | Edmund Buehler |
| Infinite® 200 microplate reader | Tecan, Switzerland |
| Inolab PH meter | WTW, Germany |
| Light microscope DM IL | Leica, Germany |
| Light and fluorescence microscope DM6000 B | Leica, Germany |
| Live imaging microscope DMI6000 B | Leica, Germany |
| Material test chamber with mechanical convection F53 | Binder, Germany |
| Microtome RM2165 | Leica, Germany |
| Mounting bath HI1210 | Leica, Germany |
| Mounting heating plate HI1220 | Leica, Germany |
| Multifuge centrifuge | Heraeus, Germany |
| Mx3000P qPCR System | Stratagene, USA |
| NanoZoomer | Hamamatsu, Germany |
| Paraffin-embedding system EG1140H | Leica, Germany |
| Pipetboy and pipettes | Eppendorf, USA |
| Power supply | Bio-Rad, USA |
| Precellys®24 homogenizer | Bertin Technologies, France |
| Rotator Staurt®SB3 | Bibby Scientific, U.K. |

| | |
|---|---|
| Shaker | Bruker, Belgium |
| SkyScan 1178 high-throughput micro-CT | Biometra, USA |
| Tissue processor TP1050 | Leica, Germany |
| Tissue processor ASP 300S | Leica, Germany |
| Thermocycler T3000 | Biometra, USA |
| Vortex machine | VWR, Germany |
| Water bath for cell culture | HLC, Germany |
| Water bath for tubes | Medingen, Germany |
| Western blot unit | Bio-Rad, USA |

### 3.1.5. Other materials

| **Material** | **Company** |
|---|---|
| 6-well, 24-well, 96-well microplate | Corning, USA |
| AGFA cronex 5 medical X-ray film | AGFA, Belgium |
| Chromatography column | Bio-Rad, USA |
| Cover glass 60 x 24 (0.13-0.18 mm) | Langenbrinck, Germany |
| Falcon tubes | BD Biosciences, USA |
| Film cassettes | Kodak, USA |
| Filter tips (10, 100, 1000µl) | Nerbe plus, Germany |
| Gel blotting paper | Whatman, USA |
| Glass pipettes, cell culture dishes, plates | Sarstedt, Germany |
| Glass slides Super Frost® Plus | R. Langenbrinck, Germany |
| Needles 26-20G (0.45-0.9mm) Microlance™ 3 BD | Drogheda, Ireland |
| Nitrocellulose membrane | Bio-Rad, USA |
| Osmotic minipump (2 mL) | Durect Corparation, USA |
| Precellys bead mill sample tube | Bertin Technologies, France |
| Radiographic films hypersensitive | Amersham, USA |
| Radiographic films | Santa Cruz, USA |
| Scalpels | Feather, Japan |
| Scissors, forceps, clamps | Fine Scientific Instruments |
| Shandon™ Single Cytofunnel™ with Cytoclips™ and White Filter Shandon | Thermo Scientific, USA |
| Shandon™ Single Cytoslides™ | Thermo Scientific, USA |
| Syringes 1, 2, 5, 10, 25 ml | B. Braun, Germany |

| | |
|---|---|
| Tips (10, 100, 1000µl) | Eppendorf, USA |
| Tissue culture chamber slide | BD Falcon, USA |
| Transwell permeable support | Corning, USA |

### 3.1.6. Softwares

| **Software** | **Company** |
|---|---|
| FlexiWare 7.0 | SCIREQ, Canada |
| i-Control | Tecan, Austria |
| Leica Application Suite Advanced Fluorescence (LAS AF) Microscope Software | Leica, Germany |
| Leica QWin imaging software | Leica, Germany |
| Magellan v.6.3 | Tecan, Austria |
| MS® Excel and Word 2013 | Microsoft, USA |
| MxPro™ QPCR software | Agilent Technologies, USA |
| Prism® v6.05 | GraphPad Software, USA |

## 3.2. Methods

### 3.2.1. Patients

Human lung tissue was obtained from three donors and three patients suffering from IPF who underwent lung transplantation at the Department of Thoracic Surgery, University of Vienna Hospital in Austria. The study protocol for human tissue donation was approved by the Ethics Committee of the Justus-Liebig-University School of Medicine (No. 31/93, 29/01, and No. 111/08: European IPF Registry), and written informed consent was obtained from each individual patient or the patient's next of kin. The material was prepared accordingly to the further assessment.

#### 3.2.1.1. Human interstitial lung fibroblasts (hILFBs)

Human interstitial lung fibroblasts were isolated, as described previously (Jablonska et al., 2010). Lung specimens of the pulmonary parenchyma were chopped into <1-mm3 pieces. The minced pieces were washed twice with PBS and then plated in 100-mm dishes. After fibroblasts have grown out from the tissues, the slices were removed by aspiration, and the cells were allowed to reach confluence. Confluent fibroblasts were then passaged by trypsin treatment and used for the experiments between passages 3 and 4. After the second passage, fibroblasts were frozen in 10% DMSO, 10% FCS and DMEM. The experiments were started from frozen aliquots of human ILFBs.

#### 3.2.1.2. RNA and protein

Human lung tissue was obtained from three donors and four IPF patients that underwent lung transplantation in Medical University of Vienna (Vienna, Austria) and had a confirmed UIP histological pattern. Pieces of lung tissue were snap-frozen immediately upon lung excision and used for mRNA and protein extraction.

#### 3.2.1.3. Histology examination

At the surgical theatre, peripheral lung tissue samples (of explanted IPF-) were immeresed in 4% (PFA, pH 7.0) immediately after transplantation. The remaining lung tissue was flushed, cooled down to +4°C, and sent (together with the formalin-fixed lung tissue samples) immediately to Giessen. There the lung lobes were prepared according to a predefined algorithm; and additional lung tissues samples from subpleural and hilar regions were placed in 4% PFA. Next, the lung was processed according to lung tissue preparation protocol described in further section.

### 3.2.2. Animals

Adult male 12-week-old C57BL/6 mice in body weight between 20-25 g were obtained from Charles River Laboratories. Both the University Animal Care Committee and the Federal Authorities for Animal Research of the Regierungspraesidium Giessen (Hessen, Germany) approved the study protocol (GI20/10, number 59/2012). Animals were housed under room temperature and 12/12-hour light/dark cycle with free access to food and water.

### 3.2.3. Bleomycin administration

At day 0 mice were anesthetized with 5% isoflurane following orotracheal instillation of bleomycin at the dose of 3.5 units/kg mouse body weight or sterile saline (0.9% NaCl). The animal was fixed in a vertical position under a binocular. During instillation nose of a mouse was kept pinched to ensure that during inspiration bleomycin or saline solutions were inhaled and distributed throughout the lung. Bleomycin was dissolved in sterile saline to achieve the required dose.

### 3.2.4. Experimental groups

Animals were divided in the following four groups. Group I served as normal control mice, which received instillation of sterile saline at day 0 and was given vehicle alone (saline); Group II served as bleomycin-induced pulmonary fibrosis mice, which received instillation of bleomycin at day 0 and were given vehicle; Group III and Group IV served as the treatment groups where mice received bleomycin at day 0 and were treated every second day from day 8 to day 21 with 10 mg/kg or 25 mg/kg 17-DMAG (LC Laboratories), respectively. 17-DMAG was prepared freshly in saline at 2 or 5 mg/ml and administrated *per os* via gavage needle, all in the same manner. Survival of each group was expressed as percentage of mice alive at the specific time points of the experiment.

### 3.2.5. Measurement of lung function

At day 21 after bleomycin instillation, respiratory function measurement was performed using a computer-controlled piston ventilator FlexiVent. This system introduces the forces oscillation technique (FOT) which is a powerful tool allowing the experimental performance of lung function in mice. It ensures measurements of respiratory system mechanics through the analysis of volume and pressure signals acquired in reaction to predefined, small amplitude, oscillatory airflow waveforms. Lung function

measurements were performed in dead mice. After system and cannula calibration, mice ware placed on flexiVent system followed by the insertion of tracheal cannula. Further, the deep inflammation was executed to recruit closed lung areas and standardize lung volume history and the pressure of 30 $cmH_2O$ over a 3 second period without excessive volume displacement. Three single-compartment perturbations and three constant-phase perturbation were obtained. The averages of these three measurements were determined for each animal and averaged for each experimental group. Lung function parameters were automatically calculated by the software, by fitting pressure and volume data to the single compartment model measuring dynamic compliance (C) with the Snapshot-150 perturbation and measuring the constant-phase and tissue damping (G) with the QuickPrime-3 perturbation, respectively. Dynamic compliance captures the ease with which the lung can be extended. Tissue damping is closely related to tissue resistance and reflects the energy dissipation in the lung. Only measurements with coefficient of determination (COD) ≥0.9 were used for further analysis (McGovern et al., 2013).

### 3.2.6. Bronchoalveolar lavage fluid (BALF) cell count

After respiratory function measurement, lungs were lavaged three times with 0.3 ml of ice cold saline and all aliquots were pooled for each lung. Further, BAL fluid was centrifuged and cell pellet was resuspended in 1 ml of saline. Cells in constant volume of 0.2 ml of PBS were deposited in a cytospin funnel and transferred to a glass slide with Shandon Cytospin-3® centrifuge at 500 rpm for 5 minutes followed by drying. Slides were stained with May Gruenwald-Giemsa using the following protocol:

**Table 4. Gruenwald-Giemsa staining protocol**

| Step duration | Duration (min) |
|---|---|
| May Gruenwald | 10 min |
| Washing with distilled water | 1 min |
| Giemsa | 5 min |
| Washing with distilled water | 1 min |

Numbers of macrophages, neutrophils and lymphocytes were determined by counting of 100 cells under the Leica light microscope DM6000 B. Different cell count was expressed in %.

### 3.2.7. Lung tissue harvest and preparation

After respiratory measurement, whole lungs were flushed through the pulmonary artery with saline due to remove red cells. Three right lobes were snap frozen in liquid nitrogen and stored in -80º C for molecular biology assessment, while left lobe was placed in OCT mounting medium, snap frozen in liquid nitrogen and stored in -80º C for cryosections. Further, one left lobe was perfused under 22 $cmH_2O$ pressure through the pulmonary artery with 3.5-3.7 % of formalin and immersed in formalin for 24 hours. Formalin-fixed lung tissue samples were transferred to embedding cassettes and stored in phosphate-buffered saline (PBS). The dehydration was performed overnight in Leica ASP 300S tissue processor. Next day, the lung tissues were embedded in 65°C warmed paraffin with the usage of a heated Leica paraffin embedding module. Then the paraffin-embedded lung tissues were cooled down for hardening on a Leica cooling plate followed by sectioning into 3 µm-thickness on Leica fully-automated rotation-microtome, and mounted on positively charged glass slides. Finally, lung tissue sections were allowed to dry on Leica heating plate at 40°C and incubated at 37° C (for 12 hours) in a drying oven.

### 3.2.8. Fibrosis score and collagen quantification in lung tissue sections

To examine fibrosis morphological changes, lung tissue sections were stained with hematoxylin and eosin according to the protocol below. Next, fibrosis scores were quantified according to a numerical scale as described by Ashcroft and colleagues (Ashcroft et al., 1988) with slight modifications: 0- healthy lungs were referred to score “0”; whereas score “6” represented the most severe degree of fibrosis. Main scores are 0, 2, 4, 6. 0- normal lung, 2- minimal fibrosis (septae thickening without distortion of lung architecture), 4- substantial fibrosis (fibroblastic foci, distortion of lung architecture), 6- maximal fibrosis (scar formation). There also intermediate scores: 1, 3, 5 which are used in case weakly expressed scores 2, 4, 6.

**Table 5. Hematoxylin and eosin staining**

| Step duration | Duration, min |
|---|---|
| 3 x Xylol | 10 |
| Ethanol 99.6% | 5 |
| Ethanol 99.6% | 5 |
| Ethanol 96% | 5 |
| Ethanol 70% | 5 |
| Distilled water | 2 |
| Haemalaun nach Mayer, acidic | 20 |
| Tap water | 5 |
| Ethanol 96% | 1 |
| Eosin-Y alcoholic | 4 |
| Distilled water | rinse |
| Ethanol 96% | 2 |
| Ethanol 96% | 2 |
| Ethanol 99.6% | 5 |
| Isopropanol 99.8% | 5 |
| 3 x Xylol | 5 |

Collagen deposition on slides, expressed in %, was assessed by Sirius Red staining according to the protocol below. The sections were examined under a Leica DM 600B microscopy using Leica QWin imaging software. 0.1% picro Sirius red (0.1g Sirius Red in 100 ml picric acid).

**Table 6. Sirius Red staining**

| Step duration | Duration, min |
|---|---|
| Incubation at 58°C | 60 |
| 3 x Xylol | 10 |
| Ethanol 99.6% | 5 |
| Ethanol 99.6% | 5 |
| Ethanol 96% | 5 |
| Ethanol 70% | 5 |
| Deionized water | shortly |
| 0.1% picro Sirius red | 60 |
| Acidifier water (1% glacial acetic acid) | 2 |
| Acidifier water (1% glacial acetic acid) | 2 |
| Acidifier water (1% glacial acetic acid) | 2 |
| Dip in deionized water and shake | shortly |
| Ethanol 70% | 5 |
| Ethanol 96% | 5 |
| Ethanol 99.6% | 5 |
| 2 x Xylol | 2 |

### 3.2.9. Fluorescence molecular tomography and micro computed tomography (FMT- µCT)

FMT system (FMT2000) is a small-animal fluorescence *in vivo* imaging system for murine preclinical research use. It is designed to provide calibrated quantitative tomographic images and data of fluorescence signal within biological tissue (in lungs) throughout the depth of the subject. This two channel instrument operates on two near-infrared channels excited at 670 nm and 746 nm, and emitting at 700 nm and 750 nm respectively.

The SkyScan 1178 is an ultra-fast micro-CT system for high throughput *in vivo* scanning of small laboratory animals. During scanning the source-camera assembly turns around the object 360$^{o}$C whole body scan, which remains statically in the carbon-composite bed. The instrument is supplied with integrated physiological monitoring for

*in vivo* small animal scanning, including color real-time imaging of the animal during investigation, gating from breathing, body temperature measurement, heart beats and stabilization.

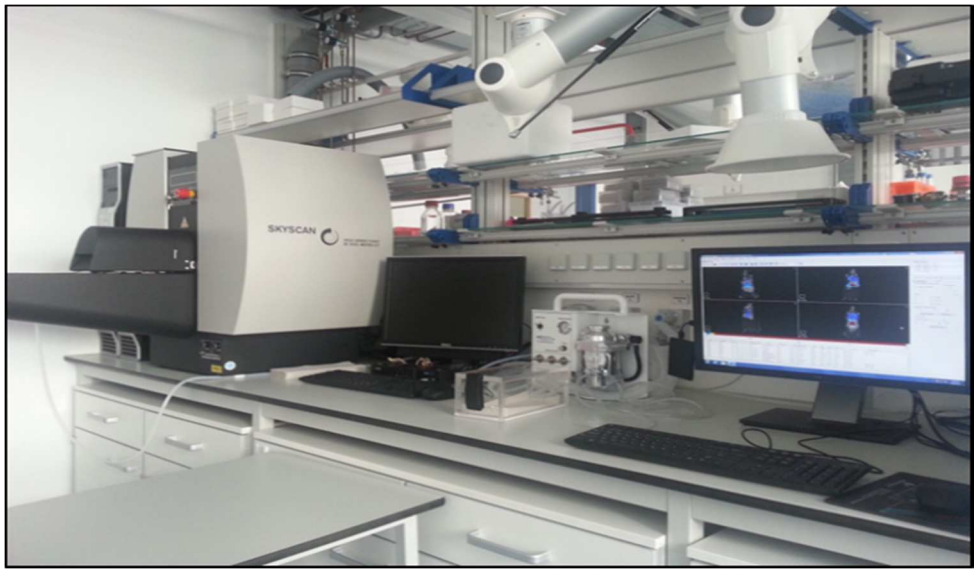


**Figure 11. PerkinElmer FMT and 3D tomographic imaging**

Mice were shaved and depilated to remove all hair to avoid absorb autofluorescence. Further, animals were anesthetized with isoflurane and fixed into a portable animal imaging cassette that lightly compressed the anesthetized mouse between optically translucent windows thereby preventing the motion during FMT and CT imaging. The animal holder with the anesthetized mouse was put to μCT (micro computed tomography), followed by transfer of the holder to FMT system.

The MMP activatable fluorescent probe, MMPSense680, was administrated via tail vein 24 hours before the FMT measurement. MMPSense680 probes (~ 450kDa) is optically quenched in its native form and becomes highly fluorescent with an excitation at 670 nm and emission at 700 nm and activated by Matrix Metalloproteinases MMP-2, -3, -9 and -13 (http://www.perkinelmer.com/catalog/category/id/in vivo imaging). In vivo MMP activity in mice lung was monitored by quantitative FMT at day 21 after bleomycin administration in sham and bleomycin-challenged mice (Bleo) in the absence or presence of 17-DMAG (10 mg/kg or 25 mg/kg, every two days from day 8 to day 21). Micro CT was performed for organ and accurate signal localization.

After setting regions of interest on the basis of the anatomic μCT data, MMPSense680 concentration in the lungs were determined by Analyze11.0, a software package developed by the Biomedical Imaging Resource (BIR) at Mayo Clinic for scanning, reconstruction and calculation of three-dimensional fluorochrome concentration and

distribution of MMPSense680. The FMT2000 TrueQuant software was used for the calculation of the MMP concentration (pmol).

### 3.2.10. Mouse interstitial lung fibroblasts (mILFBs) isolation

The tip of right ventricle was cut and the needle was stuck into the left ventricle close to the pulmonary artery. The lungs were perfused with saline until they became white. Then lungs were washed with HBSS until blood is removed and minced into 1 to 2-$mm^3$ pieces. Lung pieces were incubated in 5 ml digestion buffer (0.3 mg/ml type IV collagenase and 0.5 mg/ml trypsin, in HBSS-Ca/Mg) in a shaker at 37°C for 1 hour, at each of six 10-minutes intervals, the lung pieces were pipetted through a 10 ml pipette for 10 times to dissociate the cells. The digestion buffer was passed through a 40 µm Nylon cell strainer into a 50 ml tube to get rid of the undigested lung tissue. Next, cells were centrifuged for 5 minutes under 800 rpm. At the end the cell pellet was suspended with 9 ml pre-balanced culture medium (DMEM/F12, 10% fetal calf serum, penicillin (10,000 U/100 ml), streptomycin (10,000 µg/100 ml), glutamine (29.2 mg/100 ml) and seeded in the dish. After attachment for 2 hours and cells were refreshed with new medium after washing twice with PBS.

### 3.2.11. Human interstitial lung fibroblasts (hILFBs)

Human interstitial lung fibroblasts were obtained from three donors and three patients with idiopathic pulmonary fibrosis (IPF). Cells were cultured in MCDB-131 medium, supplemented with 5% fetal calf serum, penicillin (10,000 U/100 ml), streptomycin (10,000 µg/100 ml), glutamine (29.2 mg/100 ml), 5 µg/ml insulin, 2 ng/ml basic fibroblast growth factor (bFGF), 0.5ng/ml human epidermal growth factor (EGF) in humidified atmosphere of 95% air with 5% $CO_2$ at 37°C.

Human ILFBs were stimulated with recombinant TGF-β1 (10 ng/ml) for 24 hours (western blots and co-immunoprecipitation), 72 hours (Sircol collagen assay), and 16 hours (transwell assay), in the absence or presence of 17-AAG (50 nM), following 24 hours of serum-starvation.

Human ILFBs were pretreated with 17-AAG (50 nM) in the absence or presence of MG-132 (30 µM) for 5 hours and then stimulated with TGF-β1 (10 ng/ml) (treatment with MG-132, proteasome degradation inhibitor).

### 3.2.12. Epithelial- mesenchymal transition of A549 cells

A549 (human lung adenocarcinoma cell line) cells were seeded in DMEM/F12 medium, supplemented with 10% FCS, penicillin (10,000 U/100 ml), streptomycin (10,000 µg/100 ml), glutamine (2 mM), 1% MEM vitamins solution, 1% MEM nonessential amino acids in humidified atmosphere of 95% air with 5% $CO_2$ at 37°C. After attachment, A549 cells were kept in medium with 1% FCS for 24 hours and cultured in medium with 5 ng/ml TGF-β1 and 1% FCS for 72 hours in the absence or presence of 50 nM 17-AAG. Further, the cell morphology was examined by light microscopy, and the expression of epithelial and mesenchymal markers was carried out by fluorescence microscope and western blots.

### 3.2.13. Polymerase chain reaction (PCR)

#### 3.2.13.1. RNA isolation

Total RNA from tissues or cells was extracted using Trizol according to the manufacturer's protocol. 50 mg lung tissue was mixed with 1 ml Trizol and homogenized by Precellys24 homogenizer, or $1\times10^6$ of ILFBs were collected in 1 ml Trizol. These lysates were kept for 5 minutes at RT to dissociate the RNA from histone proteins. After adding of 0.2 ml chloroform, the sample was vigorously mixed and centrifuged at 12000 rpm for 15 minutes at 4°C. Next, the clear upper layer was carefully transferred to a new tube and gently mixed with 0.5 ml of 2-propanol. After 10 minutes the mixture was centrifuged at 12000 rpm at 4°C for 15 minutes and the RNA pellet was washed with 1 ml of 75% ethanol and dried with opened lid. Finally, RNA was dissolved in DEPC-water and stored at -80°C. The quality and concentration of RNA was measured by NanoDrop spectrophotometer.

#### 3.2.13.2. Reverse transcription- polymerase chain reaction (RT-PCR)

cDNA was synthesized by RT-PCR using Bio-Rad iScript cDNA synthesis kit according to the manufacturer’s instructions. 1 µg RNA in 20 µl mastermix was prepared according to the protocol. The reverse transcription reactions were subjected to cDNA synthesis by firstly annealing at 25°C for 5 minutres and incubating at 42°C for 30 minutes, followed by thermal inactivation of reverse transcriptase at 85°C for 5 minutes. The cDNA was stored at -20°C.

**Table 7. Reverse transcription- PCR**

| RT- PCR reaction component | Volume per reaction |
|---|---|
| RNA (0.1 µg/µl) | 10 µl |
| 5x iScript reaction mix | 4 µl |
| iScript reverse transcriptase | 1 ul |

### 3.2.13.3. Quantitive realtime- polymerase chain reaction (qRT-PCR)

The intron-spanning primer pairs were designed using the Primer3 program and are shown in Table 3. Primers were cross checked to insure the specificity by blasting to the whole genome. The product size is within the range of 80 bp-150 bp.

**Table 8. qRT- PCR reaction components**

| qRT- PCR reaction component | Volume per reaction | Final concentration |
|---|---|---|
| cDNA | 2 µl | 0.2 |
| Forward primer 10 µM | 0.5 µl | 0.2 µM |
| Reverse primer 10 µM | 0.5 µl | 0.2 µM |
| iTaq SYBR Green supermix with Rox | 12.5 µl | |
| Nuclease-free water to a final volume | 20 µl | |

qRT- PCR was performed on a Mx3000P® QPCR system machine using SYBR® iTaq SYBR Green Supermix with Rox kit according to manufacturer's instructions. The cDNA was omitted for the negative control. The annealing temperature for every gene was 59°C. By using the MxPro™ QPCR software, a dissociation curve was generated for each gene to ensure a single product amplification and the threshold cycle (Ct values) was determined for each gene. The mRNA changes between sham and bleomycin mice or between donor and IPF patients were calculated as ΔCt (Ct reference - Ct target). The Ct value was normalized to the reference gene hypoxanthin-phosphoribosyl-transferase (HPRT) obtained for the same cDNA sample. Each reaction was run in duplicate and repeated three times independently.

**Table 9. qRT- PCR program**

| qRT- PCR program | Temperature | Time | Cycle |
|---|---|---|---|
| Activation | 95°C | 10 min | 1 |
| Denaturation | 95°C | 30 sec | 40 |
| Annealing | 58°C | 30 sec | |
| Extension | 72°C | 30 sec | |
| Denaturating | 95°C | 1 min | |
| Dissociation curve | 55-95°C | indefinite | 1 |
| Soak | 4°C | indefinite | 1 |

### 3.2.14. Western blotting

#### 3.2.14.1. Protein isolation

Total protein was extracted in RIPA buffer (containing: 1x TBS, 1% Nonidet P-40, 0.1% SDS, 0.5% sodium deoxycholate, 0.004% sodium azide) according to manufacturer's instructions. Proteinase inhibitor cocktail, sodium orthovanadate and PMSF were added to RIPA freshly before use. 100 mg lung tissue homogenized in 600 µl RIPA or $2\times10^6$ hILFBs in 300 µl RIPA was centrifuged at 12000 rpm for 30 minutes at 4°C and the supernatants were kept at -80°C.

**Table 10. RIPA buffer recipe**

| Component of RIPA | Final concentration |
|---|---|
| RIPA buffer | 1x |
| Protease inhibitor cocktail | 1x |
| Sodium orthovanadate | 1% |
| PMSF | 1% |

### 3.2.14.2. Protein concentration measurement

Protein concentration was determined with Bio-Rad DC protein assay according to manufacturer's instructions. The assay is based on Lowry assay with slight modifications. There are two steps leading to color development: the reaction between protein and copper in an alkaline medium (Reagent A) and the subsequent reduction of Folin (Reagent B) reagent by the copper-treated protein (Bio-Rad Manual instructions). A series of bovine serum albumin (BSA) concentration: 0.25- 0.5- 1- 2 mg/ml were used as standard. The protein samples were pre-diluted into the range of the standard and the protein concentration of each sample was estimated in duplicate. After developing of color samples were measured at 750 nm using Tecan microplate reader. Final protein concentration was calculated with accompanying Magellan™ software.

### 3.2.14.3. SDS-polyacrylamide (SDS-PAGE) gel electrophoresis

Protein samples with equal concentration were mixed with 5× SDS gel loading buffer at a ratio of 4:1 (v/v) and denatured at 100°C for 5 minutes. Protein samples (10 µg for β-actin; 30 µg for other antibodies) or dual protein marker were loaded in the lanes of 8% SDS-PAGE gel and run at 100-130V for 2 hours to separate. Buffers are listed below.

**Table 11. 5×SDS gel-loading buffer recipe**

| 5×SDS gel-loading buffer component | Final concentration |
|---|---|
| Tris-HCl (2 M, pH 6.8) | 375 mM |
| SDS | 10% (w/v) |
| Glycerol | 50% (v/v) |
| β-Mercaptoethanol | 12.5% (v/v) |
| Bromophenol blue | 0.02% (w/v) |

Polyacrylamide gels were prepared according to following procedure. The space between the glass plates was filled with 8%-resolving gel mixture. Next, 2- propanol was poured on top of this mixture until the gels polymerized. After 30 minutes, water from resolving gel was removed and 6% stacking gel solution was added. A comb was inserted and polymerization took 30 minutes. The protocols for SDS-PAGE gels are listed below.

**Table 12. Running buffer components**

| Running buffer component | Final concentration |
|---|---|
| Tris-HCl | 25 mM |
| Glycine | 192 mM |
| SDS | 10% (w/v) 0.1% (w/v) |

**Table 13. Resolving gel (8%) components**

| Resolving gel (8%) component | Volume | Final concentration |
|---|---|---|
| Tris-Cl (1.5 M, pH 8.9) | 2.25 ml | 375 mM |
| Acrylamid 30% (w/v) | 2.4 ml | 10% (w/v) |
| SDS 10% (w/v) | 90 µl | 0.1% (w/v) |
| APS 10% (w/v) | 45 µl | 0.05% (w/v) |
| TEMED | 9 µl | 0.1% (w/v) |
| $H_2O$ | 4.2 ml | |

**Table 14. Stacking gel (6%) components**

| Stacking gel (6%) component | Volume | Final concentration |
|---|---|---|
| Tris-Cl (0.5 M, pH 6.8) | 0.625 ml | 375 mM |
| Acrylamid 30% (w/v) | 0.5 ml | 10% (w/v) |
| SDS 10% (w/v) | 25 µl | 0.1% (w/v) |
| APS 10% (w/v) | 12.5 µl | 0.05% (w/v) |
| TEMED | 2.5 µl | 0.1% |
| $H_2O$ | 1.34 ml | |

### 3.2.15. Immunoblotting

The proteins separated on the SDS-PAGE were transferred to nitrocellulose membrane and at 100V for 1 hour using a blotting apparatus. The membranes were blocked with 5% non-fat milk for 1h at RT and probed with primary antibodies (diluted in TBST with 5% BSA) at 4°C overnight. After three times washes with TBS containing 0.1% Tween-20, horse radish peroxidase (HRP)-conjugated secondary antibodies (diluted in TBST

with 5% BSA) were applied for 1 hour at RT. Following washing, the blots were developed using an enhanced chemiluminescence (ECL) kit. The blots were captured by X-ray films and the intensity of bands was quantified by densitometry. Antibodies were listed as follows: TGF-β receptor I (1:1000, Cell Signaling), TGF-β receptor II (1:1000, Cell Signaling), SMAD2 (1:1000, Cell Signaling), SMAD3 (1:1000, Cell Signaling), fibronectin (1:1000, Sigma-Aldrich), collagen type I (1:1000, Meridian), β-actin (1:4000, Abcam), α-SMA (1:1000, Abcam), SMAD2 (pSer465/467) (1:1000, Novus), SMAD3 (pSer423/425) (1:1000, Calbiochem), E-cadherin (1:1000, Millipore), HSP90α and HSP90β (1:1000, Enzo).

**Table 15. Blotting buffer recipe**

| Blotting buffer | Final concentration |
|---|---|
| Tris-HCl | 50 mM |
| Glycine | 40 mM |
| Methanol | 20% (v/v) |

**Table 16. TBST buffer (pH 7.6) recipe**

| TBST buffer ( pH 7.6) component | Final concentration |
|---|---|
| Tris-HCl | 20 mM |
| NaCl | 150 mM |
| Tween | 0.1% (v/v) |

### 3.2.16. HSP90 inhibitors

17-AAG and 17-DMAG are selective inhibitors for HSP90. *In vitro* experiments were carried out using 17-Allylamino-17-demethoxygeldanamycin (17-AAG) inhibitor. 17-(Dimethylaminoethylamino)-17-demethoxygeldanamycin (17-DMAG) is a water-soluble derivative of geldanamycin which has excellent bioavailability and tissue distribution in animals and was applied in *in vivo* experiments.

### 3.2.17. Immunohistochemistry

Formalin-fixed, paraffin-embedded lung tissues were cut into sections with the thickness of 3 μm. After deparaffinization in xylene and rehydration in a series of grade-decreasing ethanol solutions, the sections were washed in distilled water. The

antigen retrieval was carried out by boiling the slides in citrate buffer (0.1 M citric acid monohydrate + 0.1 M Sodium citrate tribasic dihydrate). Next, the streptavidin-biotin-alkaline phosphatase (AP) method with use of the ZytoChem-Plus AP Kit (Fast Red, red dye) or the streptavidin-biotin-HRP-method by using the ZytoChem-Plus HRP-DAB Kit (brown dye, both kits from Zytomed Systems, Berlin, Germany), according to a previously published protocol (Korfei et al., 2013). As control experiments, sections were treated with isotype IgG control (1:75, Acris Antibodies) to determine the specificity of the staining. To block the endogenous peroxidases, cells were treated with 3% hydrogen peroxide in methanol solution for 20 minutes. Further, slides were blocked with blocking solution (provided by the kit) for 5 minutes. Primary antibodies (diluted in PBS containing 2% BSA) such as: Hsp90α, Hsp90β and αSMA rabbit were applied for 3 hours.

For staining of human lung tissue sections, the concentrations of primary antibodies were: α-SMA (1:150, Abcam), HSP90α (1:75, Enzo Life Sciences), and HSP90β (1:100, Abcam). For staining of murine lung tissue sections, the concentrations of primary antibodies were: α-SMA (1:100, Abcam), TTF1 (1:100, Abcam), HSP90α (1:70, Enzo Life Sciences), and HSP90β (1:100, Abcam). Double-IHC-stainings were performed on mice lung tissue sections for alpha-SMA (red dye, cytoplasmic staining of smooth muscle cells and myofibroblasts) and TTF1 (brown dye, nuclear staining of alveolar epithelial type-II cells (AECII)).

After washing, the slides were treated with the corresponding biotinylated (polyvalent) antibody (diluted in solution provided by the kit) for 20 minutes and then with streptavidin-AP-conjugate for next 20 minutes. After washing, color development was carried out with Fast Red in Naphthlon solution, followed by counterstaining with hematoxylin. The sections were examined under a Leica DM 6000 B using Leica QWin imaging software. Sections from three mice and three donor/ IPF patients were stained with the representative staining shown. 1 x PBS (pH 7.4) was prepared for washes; 1 x PBS composition: 137 mM NaCl, 2.7 mM KCl, 10 mM $Na_2HPO_4$, 2 mM $KH_2PO_4$.

### 3.2.18. Immunocytochemistry

1.5 x $10^4$ human ILFBs were seeded in 8-well chamber slides. After serum-starvation for 24 hours, cells were stimulated with 10 ng/ml of human recombinant TGF-β 1 in the presence or absence of 50 nM 17-AAG for 72h. Further, cells were fixed with 4% paraformaldehyde (PFA) for 20 min at RT and permeabilized with 0.3% Triton-X100 in PBS containing 1% glycine at RT for 15 min. After three times washing steps cells were

blocked in blocking buffer (PBS containing 3% BSA and 0.05% Tween) for 1hr at RT. Cells were then incubated overnight at 4°C with primary antibodies: E-cadherin (1:100, BD Biosciences) and fibronectin (1:200, Sigma-Aldrich). Primary antibodies were diluted in blocking buffer. Next, cells were washed three times and DyLight 549-conjugated secondary antibodies (1:5000, Zytomed, diluted in Fluorescence Antibody Diluent from the kit) were applied for 1 hour at RT followed by DAPI nuclear staining. For each antibody, the images were captured under the same exposure time and conditions by the Leica fluorescence microscope.

### 3.2.19. Collagen assay

Human ILFBs were plated in 6 cm dish. After serum-starvation for 24h, the cells were stimulated with 10 ng/ml of human recombinant TGF-β 1 in the presence or absence of 50nM 17-AAG for 72h. Soluble collagen content in cells was assessed by Sircol collagen assay (Biocolor) according to manufacturer's instructions. Briefly, cells were incubated with 0.5 M acetic acid and soluble collagen collected from the cells was stained with Sirius red dye. The extracts were centrifuged at 12000 rpm for 10 min to precipitate collagen-Sirus red complexes. Next, pellet was washed with ice-cold acid-salt wash reagent. The absorbance was measured at 555nm with the spectrophotometer. Amount of collagen was presented as µg, using a standard curve prepared from the kit at the same time.

### 3.2.20. In vitro scratch assay

Human ILFBs were seeded on 24-well plates. After serum-starvation for 24 hours, scratches were created using a p10 pipette tips. Next, cells were washed twice with PBS and cultured in medium containing 5% FCS in the presence or absence of 50 nM 17-AAG. The images were captured by Leica realtime microscope system at the start of the experiment and every one hour until 24 hours later. Cell migration distance between the scratched line and the growing edge of the cells was measured at five points by Leica Application Suite Advanced Fluorescence (LAS AF) Microscope software. The migration rate was expressed in %.

### 3.2.21. Transwell assay

After serum-starvation for 24 hours, human ILFBs from donor and IPF patients were trypsinized and $1.2 \times 10^4$ cells were plated in 100 µl of MCDB-131, in the 6.5-mm transwell inserts with 8.0-µm pore size polycarbonate membrane. The lower chambers

were filled with 600 µl of serum-free medium alone or serum-free medium containing 5% FCS or 5% FCS with 50nM 17-AAG inhibitor. All conditions were supplemented with 0.1% BSA. Further, fibroblasts were incubated at 37°C for 16 hours to allow cells to migrate through the membrane. Cells on the upper side of the inserts were removed with a cotton swab, whereas cells on the lower side of the inserts were fixed in 3.7% PFA for 10 minutes followed by merging the insert in water. The migrated cells were then stained with 0.1% crystal violet in 20% methanol and were counted from nine randomly taken fields per membrane with the 20-fold magnification using Leica DM6000 B microscope. The migration rate was expressed in %.

### 3.2.22. Co- immunoprecipitation

ILFBs from patients with IPF were cultured in 10 cm dish. After serum-starvation for 24 hours, cells were stimulated with 10 ng/ml of human recombinant TGF-β 1 in the absence or presence of 50 nM 17-AAG for 24 hours. Total proteins of donor ILFBs were isolated using cell lysis buffer (components are described in the table below). Dynabeads Protein G (Life Technologies) was incubated with TGF-β receptor II antibody (2 µg/ 0.75 mg of total proteins, Santa Cruz) or with IgG control antibody (2 µg/ 0.75 mg of total proteins, Santa Cruz) for 1 hour at RT. The antibodies were diluted in PBST (PBS + 0.02% Tween 20).

**Table 17. Cell lysis buffer recipe**

| Components of cell lysis buffer | Final concentration |
|---|---|
| Tris-HCl | 50nM |
| EDTA, pH 8 | 15mM |
| NaCl | 170nM |
| Triton x100 | 0.1% |
| Glycerol | 20% |

Further, 0.75 mg of total proteins was applied and incubated with Dynabeads-TGF-β RII complexes overnight at 4°C. The precipitated complexes were washed three times using PBST (PBS containing 0.02% Tween 20) for each step and eluted by adding 50 mM glycine, pH 2.8. Next, the complexes were mixed with 5 × SDS gel loading buffer at a ratio of 4:1 (v/v) and denatured at 100°C for 5 minutes. The experimental samples were separated by 8% SDS-PAGE and transferred to nitrocellulose

membranes. The membranes were blocked using 5% non-fat milk for 1 hour at RT and probed with TGF-β RII (1:1000, Santa Cruz) and HSP90β (1:1000, Enzo) antibody (diluted in TBST containing 5% BSA). Horse radish peroxidase (HRP)-conjugated secondary antibodies (diluted in TBST containing 5% BSA) were applied for 1 hour at RT. After three times washing, the blots were developed using an enhanced chemiluminescence (ECL) kit and were captured by films. The input lane represents 5% of the protein used in co-immunoprecipitation.

### 3.2.23. Statistics

GraphPad Prism® v6.05 was used for all statistical analysis. Data are expressed, when appropriate, as mean ± SEM. Significance was assessed using unpaired t test (when two groups analyzed) or one-way ANOVA- Newman-Keuls test (for more than two groups). $P < 0.05$ was considered significant.

# 4. RESULTS

## 4.1. Heat shock protein 90 (HSP90) expression at RNA level is not changed in human interstitial lung fibroblasts (hILFBs) and lungs derived from patients with interstitial lung fibrosis (IPF).

To check the expression of HSP90 at RNA level in human, the real-time PCR was performed. Human interstitial lung fibroblasts (hILFBs) express similar level of HSP90AA1 and HSP90AB1 isoforms, except for HSP90B1 which is significantly up-regulated in patients with IPF when compared with donors (Figure 12A). Similarly, relative mRNA level of all HSP90 isoforms in human lung homogenates is not altered (Figure 12B). There is no significant changes at transcriptional level in both human interstitial fibroblast (IFBs) and lung homogenates from donor and patients with IPF.

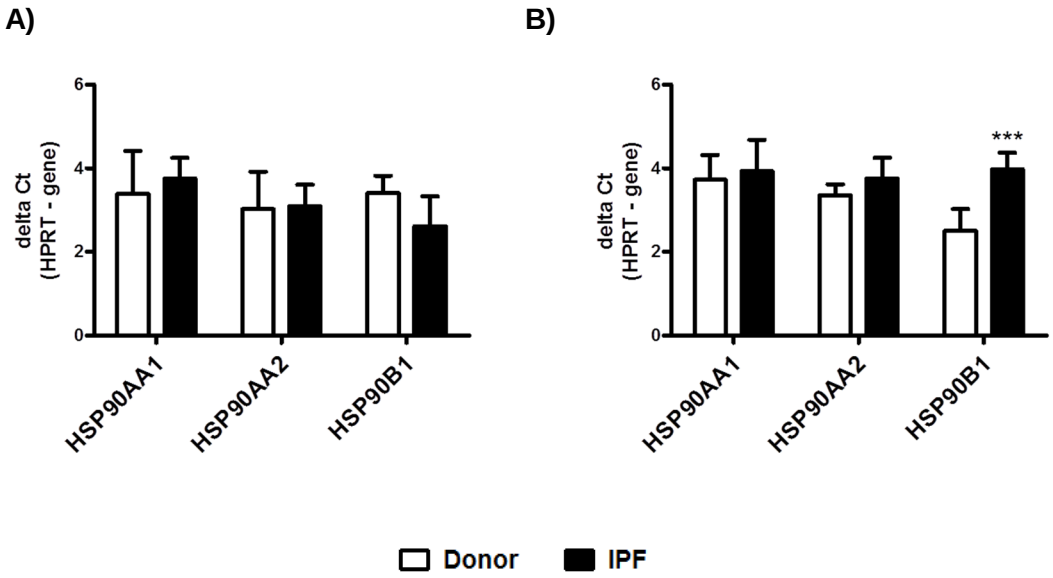


**Figure 12. HSP90 at RNA level is not changed in hILFBs and lungs from IPF patients.** Relative mRNA levels of HSP90AA1, HSP90AB1 and HSP90B1 isoforms in **(A)** human interstitial lung fibroblast (ILFBs) and **(B)** human lungs from donor and patients with IPF were shown as delta Ct value after normalization to HPRT. All values are expressed as mean ± SEM of n = 3 or n = 5 per group. ***P < 0.001 versus Donor.

**4.2. HSP90 at protein level is increased in ILFBs and lung homogenates from patients with IPF.**

Next the expression of HSP90 was examined at protein level in human ILFBs and lungs from donors and patients with IPF. In the initial protein expression profiling there was a significant up-regulation of the HSP90 isoforms (HSP90α and HSP90β) in both ILFBs (Figure 13A-13C) and lung homogenate from patients with IPF (Figure 13D-13F) compared with donors.

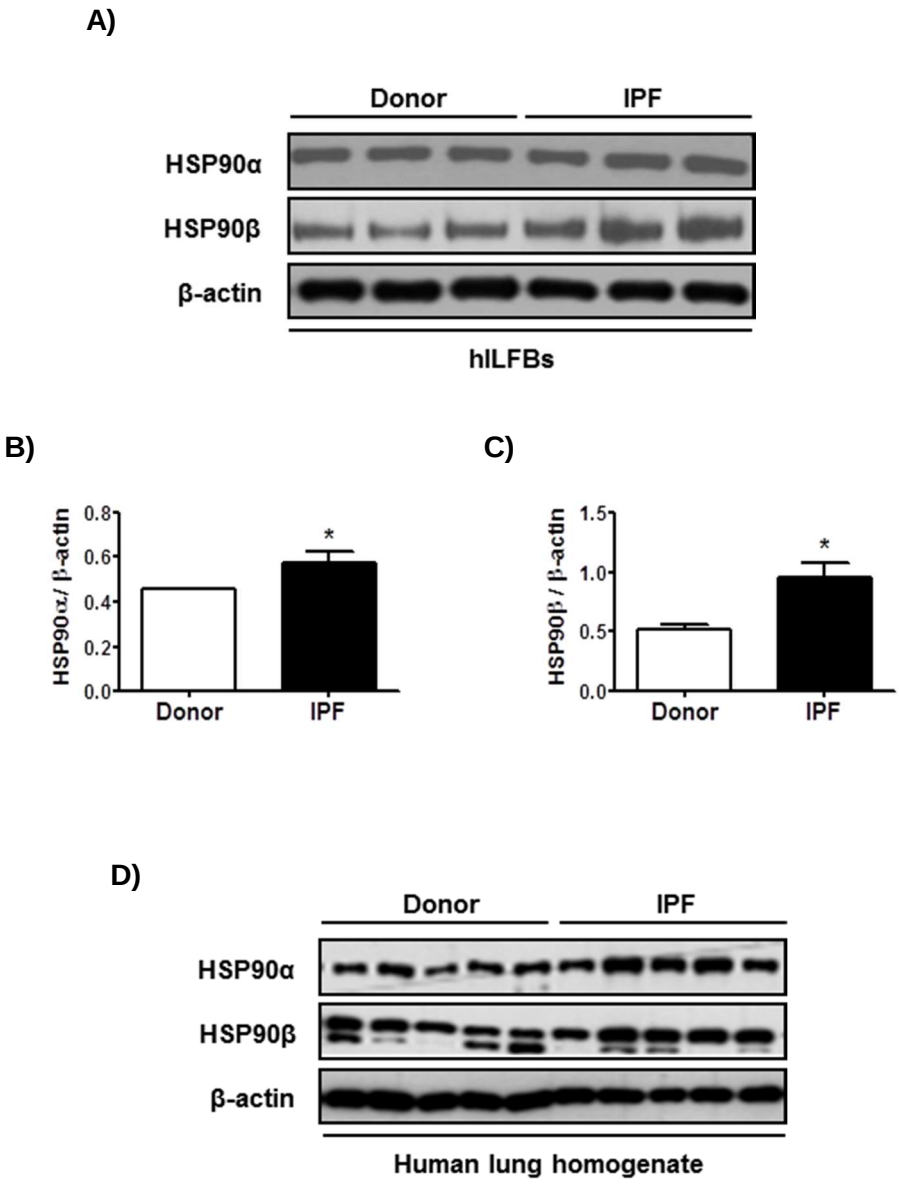

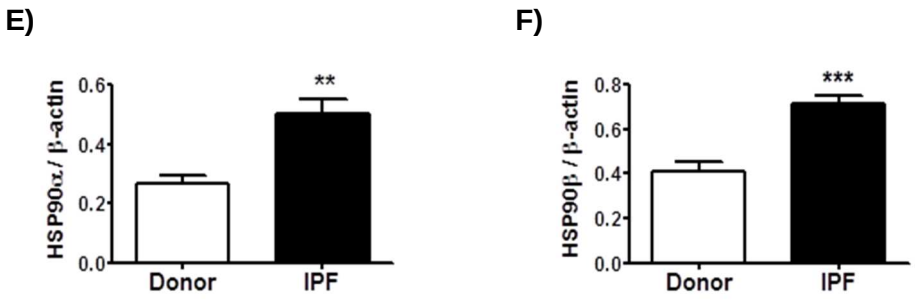


**Figure 13. HSP90 is increased in hILFBs and lungs from patients with IPF.** Representative western blots with densitometry quantification of HSP90α and HSP90β in (A-C) human interstitial lung fibroblast (ILFBs) and (D-F) human lungs from donor and patients with IPF. β-actin serves as the loading control. All values are expressed as mean ± SEM of n = 3 or n = 5 per group. *P < 0.05, **P < 0.01, ***P < 0.001 versus Donor.

### 4.3. HSP90 is up-regulated in myofibroblasts from lung of IPF patients.

The up-regulated HSP90 expression at protein level was confirmed by immunochemistry. The staining revealed the presence of HSP90α and HSP90β in the pulmonary interstitium of donor and IPF lungs, but with an increased signal in myofibroblasts and fibroblast foci in the IPF lungs (indicated by asterisks and α-SMA positive staining of a serial sections; Figure 14).

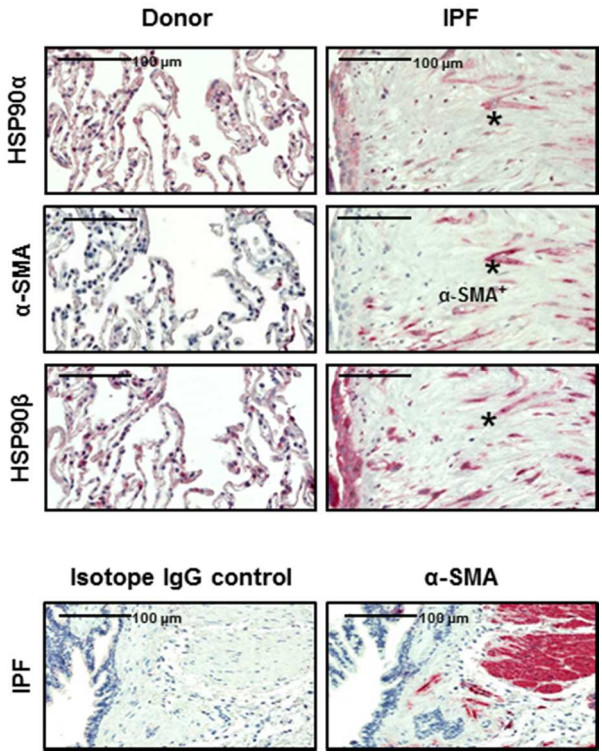


**Figure 14. HSP90 is up-regulated in human lung tissue sections from IF patients.** Representative immunohistochemical staining of heat shock protein (HSP) 90α, HSP90β and α-smooth muscle actin (α-SMA) in serial lung sections obtained from five organ donors and five patients with IPF. Myofibroblasts are shown by α-SMA (asterisks) staining. Red coloring indicates positive staining. Scale bar = 100 μm.

### 4.4. 17-AAG reduces ILFBs transdifferentiation and collagen production.

Having observed the upregulation of HSP90 in hILFBs from IPF patients, 17-AAG (a highly selective HSP90 inhibitor) was employed *in vitro*, to investigate the function of HSP90 on TGF-β1-induced fibrotic response in ILFBs, considering a central role of TGF-β1 in IPF. Western blots revealed that collagen I, fibronectin and α-SMA were all increased in hILFBs by the stimulation of TGF-β1, indicating fibroblast transdifferentiation and excessive extracellular matrix (ECM) production. This response was stronger in IPF ILFBs than in donor ILFBs (Figure 15A-15F). The effects of TGF-β1 were blocked by co-administration of 17-AAG. Moreover, extracellular collagen deposition examined by Sircol collagen assay was 2-fold or 4-fold increased by TGF-β1 in donor ILFBs or IPF ILFBs, respectively, and this increase was prevented by 17-AAG (Figure 15.G). Taken together, these results suggest that 17-AAG might suppress fibroblast transdifferentiation and collagen production.

Additionally, HSP90 expression in hILFBs was not changed after *in vitro* treatment with 17-AAG, which is consistent with the fact that HSP90 inhibitors only block the

chaperone ability of HSP90 rather than inhibit the expression (Figure 15A, 15F, 15G). Furthermore, proteomic analysis in previous studies showed induction of the HSP70 family members after Hsp90 inhibition (Mayor-López et al., 2014), (Munje et al., 2014), therefore the level of HSP70 in *in vitro* experiment was investigated. The donor and IPF hILFBs treated with 17-AAG expressed higher level of HSP70 in comparison to untreated or TGF-β1-stimulated fibroblasts (Figure 15A, 15E).

**A)**

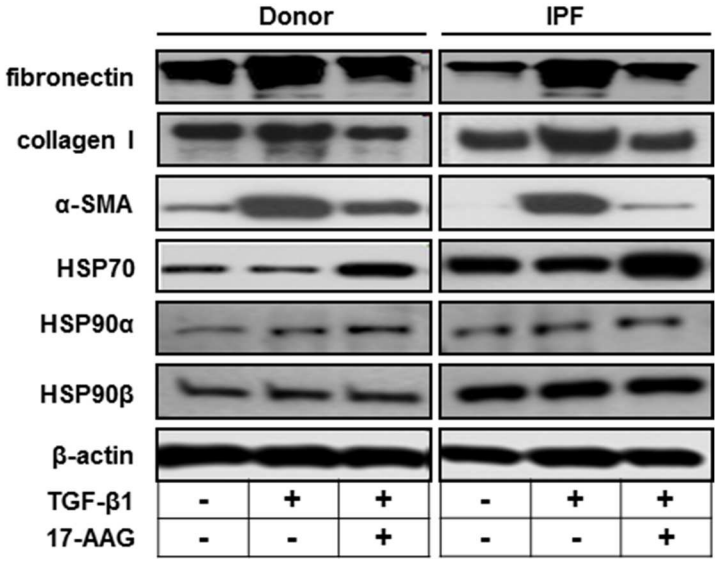


**B)**

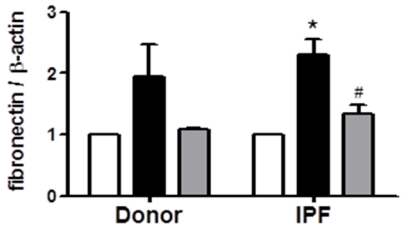


**C)**

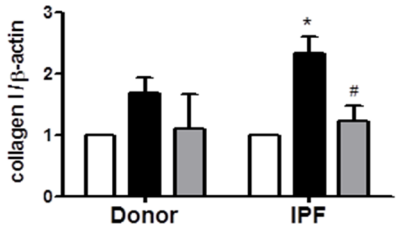

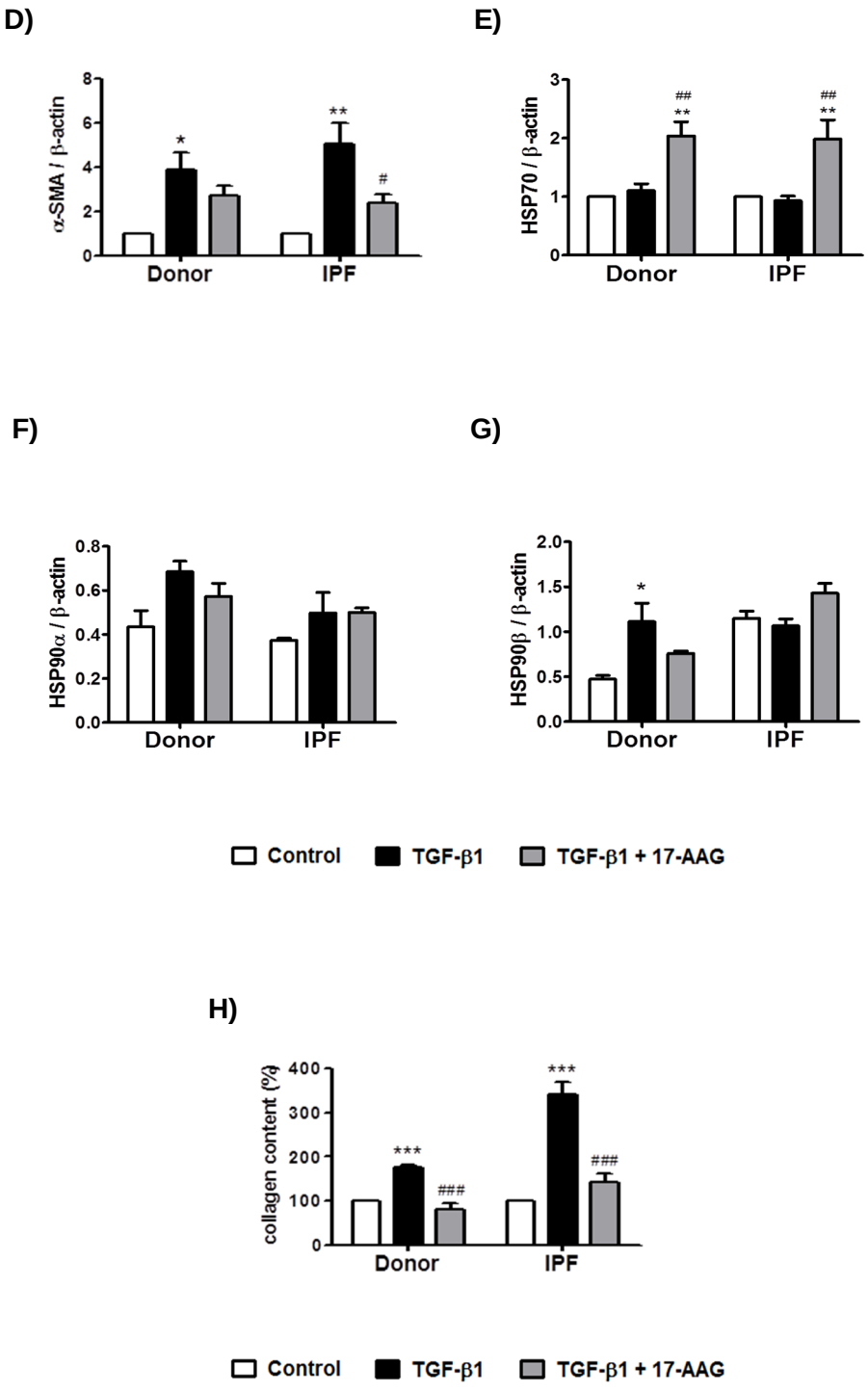


**Figure 15. 17-AAG inhibits hILFBs transdifferentitation and collagen production induced by TGF-β1.** Expression of collagen I, fibronectin, α-SMA, HSP70, HSP90α and HSP90β expression detected by western blot **(A)** and quantified by densitometry using β-actin as the loading control **(B-G)**. The level of protein expression is presented as the fold change from the level in the unstimulated cells which is presented as control. *P < 0.05, **P < 0.01 versus NTC; #P < 0.05, ##P < 0.01 versus TGF-β1. **(H)** Extracellular collagen production measured by Sircol soluble collagen assay. Collagen content is expressed as a percentage of collagen content in control group. ***P < 0.001 versus NTC, ###P < 0.001

versus TGF-β1. ILFBs were stimulated with recombinant TGF-β1 (10 ng/ml) for 24 hours (western blot) and 72 hours (Sircol collagen assay) in the absence or presence of 17-AAG (50 nM), following 24 hours of serum-starvation. Panels represent results from cells of three different donors and three different patients with IPF, and all values are given as the mean ± SEM of n = 3 per group.

### 4.5. 17-AAG inhibits ILFBs migration induces by FCS.

Uncontrolled fibroblast migration is a pathological feature during the progressive pulmonary fibrosis, so the effect of 17-AAG on ILFBs migration by transwell assay was determined. The migration was increased after FCS stimulation in both donor and IPF ILFBs, while the treatment with 17-AAG inhibits significantly the migration by approximately 70% in both donor and IPF ILFBs (Figure 16A-16B).

Additionally, cell migration monitored by real-time microscope in the scratch assay demonstrated a 60% and 70% decrease of FCS-induced gap closure after 17-AAG treatment in donor and IPF ILFBs, respectively (Figure 16C, 16D), which was consistent with the transwell results. These data strongly suggests that 17-AAG suppresses FCS-induced migration of ILFBs.

**A)**

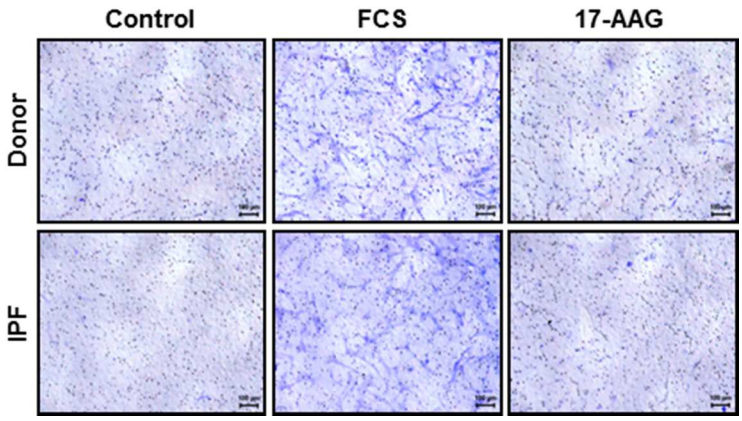


**B)**

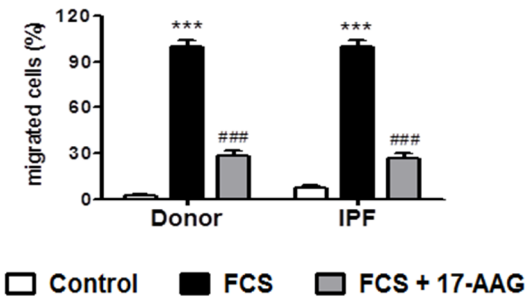

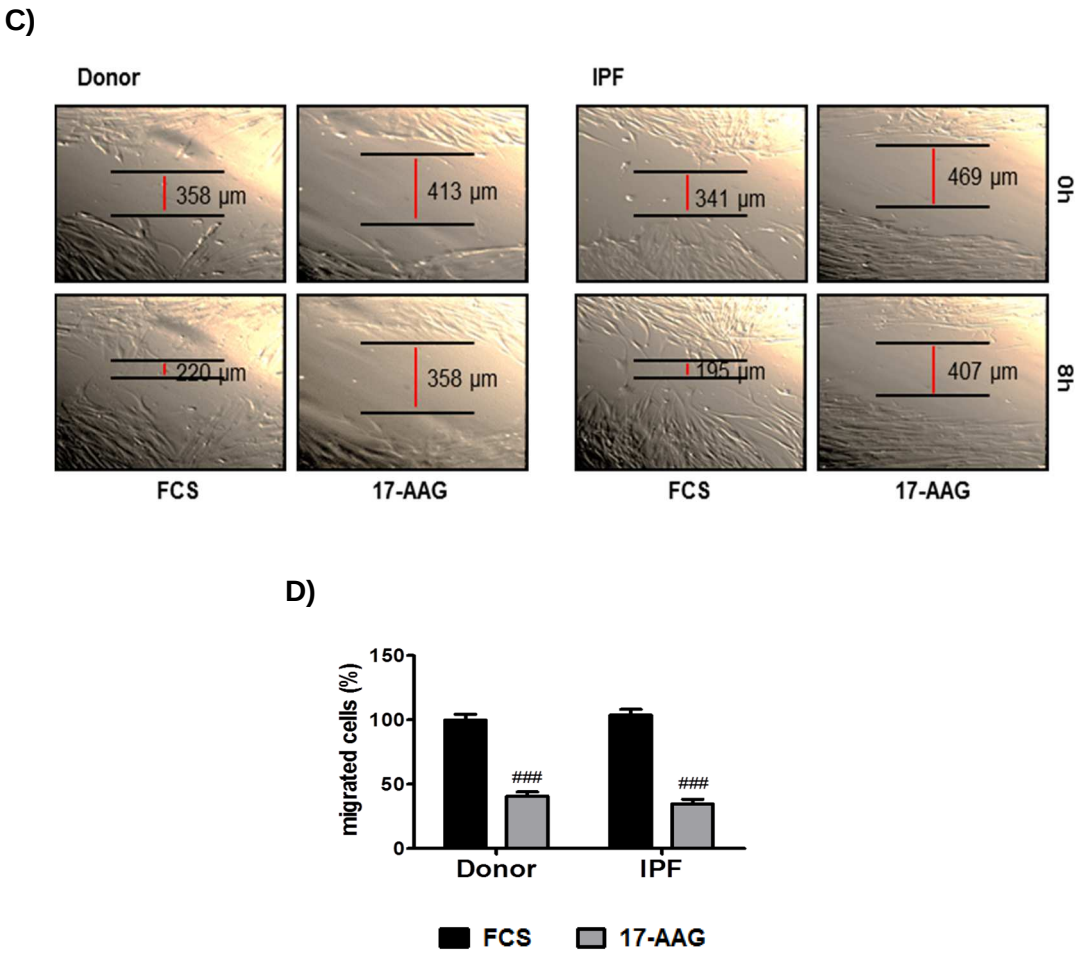


**Figure 16. 17-AAG inhibits hILFBs migration induced by FCS. (A-B)** ILFB transwell migration induced by fetal calf serum (FCS). The migration rate is expressed as a percentage of the migration rate in FCS-stimulated cells. Representative images of cells on transwell membranes were taken using light microscopy. Scale bar = 100 µm. **(C-D)** Images of the scratch at the same position were captures every hour and the degree of gap closure of both donor and patients with IPF. The migration rate is expressed as a percentage of the migration rate in FCS-stimulated cells. Representative images at the time of scratch 0 hours and 8 hours were shown. ILFBs were stimulated with FCS for 8 hours (scratch assay) or 16 hours (transwell assay) in the absence or presence of 17-AAG (50 nM) following 24 hours of serum-starvation. All panels represent results from cells of three different donors and three different patients with idiopathic pulmonary fibrosis (IPF), and all values are given as the mean ± SEM of n= 3 per group. ***P < 0.001 versus Control; ###P < 0.001 versus FCS.

### 4.6. 17- AAG blocks TGFβ/Smad signaling in IFBs by diminishing TGF-βRs levels by proteasome degradation.

TGF-β receptor I and/or TGF-β receptor II were suggested to be potential target proteins chaperoned by HSP90 in cancer cell studies (Zhang et al., 2012; Tomcik et al., 2014), therefore the next question was asked if the same regulation applies to IFBs.

Stimulation of IPF ILFBs with TGF-β1 led to increased levels of TGF-βRI and TGF-βRII, both of which were reduced to control levels by co-administration of 17-AAG along with Smad2/3 activation indicated by Smad2 phosphorylation (Figure 17A-17D). However, donor ILFBs showed only mild decrease of TGF-βRI when treated with 17-AAG. Nevertheless, TGF-β1-induced Smad2/3 activation indicated by Smad2 phosphorylation was blocked by 17-AAG in both donor and IPF ILFBs (Figure 17A-17D). More interestingly, 17-AAG-induced loss of TGF-βRs and Smad3 phosphorylation were restored by MG-132, a proteasome inhibitor (Figure 17E). These data suggest that 17-AAG blocks the TGF-β/Smad signaling by disrupting the stability of TGF-βRs and promoting proteasome degradation.

**A)**

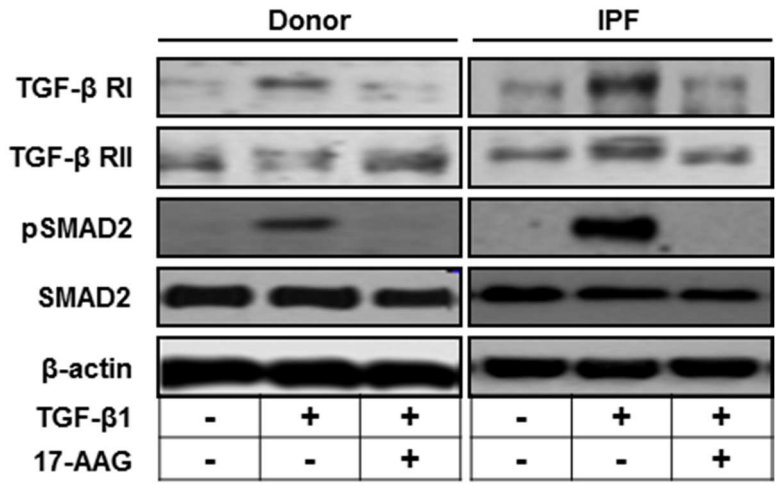


**B)**

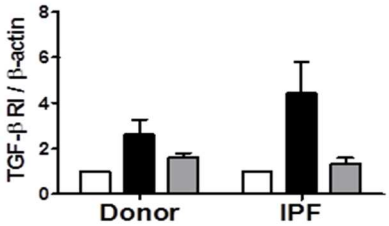


**C)**

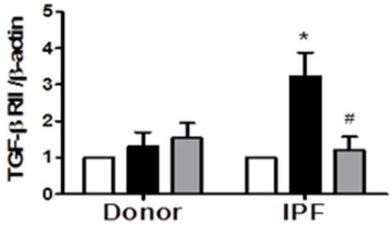

**D)**

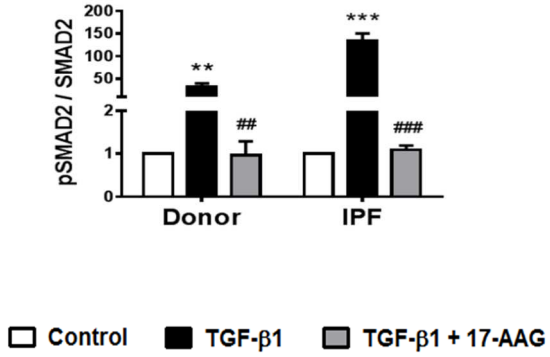


**E)**

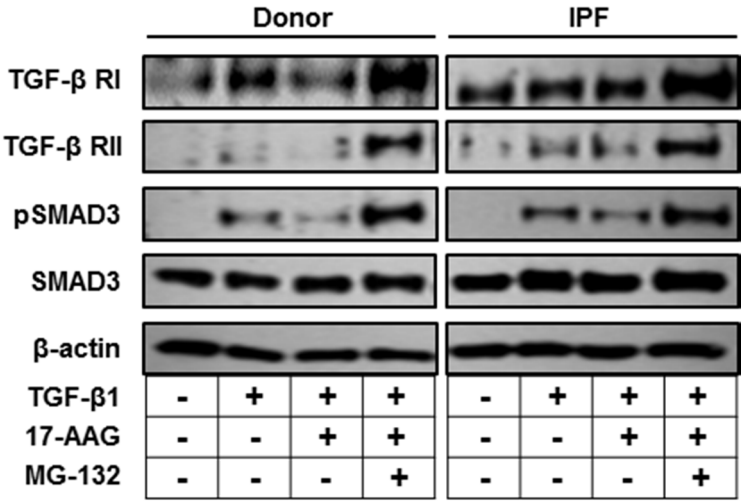


**Figure 17. 17-AAG blocks TGFβ/Smad signaling in hILFBs by diminishing TGF-βRs levels by proteasome degradation. (A-D)** Western blot analysis of TGF-β receptor I (TGF-βRI), TGF-β receptor II (TGF-βRII), phospho-Smad2 (phospho-Ser465, phospho-Ser467) and Smad2. β-actin serves as the loading control. The level of protein expression is shown as the fold change from the level in the control group. All panels represent results from cells of three different donors and three different patients with idiopathic pulmonary fibrosis (IPF), and all values are given as the mean ± SEM of n = 3 per group. *P < 0.05, **P < 0.01, ***P < 0.001 versus Control; #P < 0.05, ##P < 0.01, ###P < 0.001 versus TGF-β1. **(E)** Representative WB analysis of TGF-β receptor I (TGF-βRI), TGF-β receptor II (TGF-βRII), phospho-Smad3 (phospho-Ser423, phospho-Ser425) and Smad3. β-actin serves as the loading control. The experiment was repeated independently three times in one donor and one patient with IPF. After 24 hours of serum-starvation, ILFBs were stimulated with recombinant TGF-β1 (10 ng/ml) for 24 hours (western blots), in the absence or presence of 17-AAG. For MG-132 experiment, ILFBs were treated with 17-AAG (50 nM) in the absence or presence of MG-132 (30 μM) for 5 hours, followed by 1 hour stimulation with TGF-β1.

### 4.7. HSP90β interacts with TGF-βRII in hILFBs.

To further delineate whether HSP90 directly interacts with TGF-βRs and acts as a molecular chaperone, endogenous co-immunoprecipitation was performed in donor and IPF ILFBs followed by western blotting, which revealed that HSP90β was specifically co-immunoprecipitated by TGF-βRII in both cells (Figure 18A). More importantly, the binding TGF-βRII and HSP90β was profoundly disrupted by 17-AAG. Taken together, the results suggest that HSP90 regulates TGF-β/Smad signaling by stabilizing TGF-βRs via direct interaction with TGF-βRII.

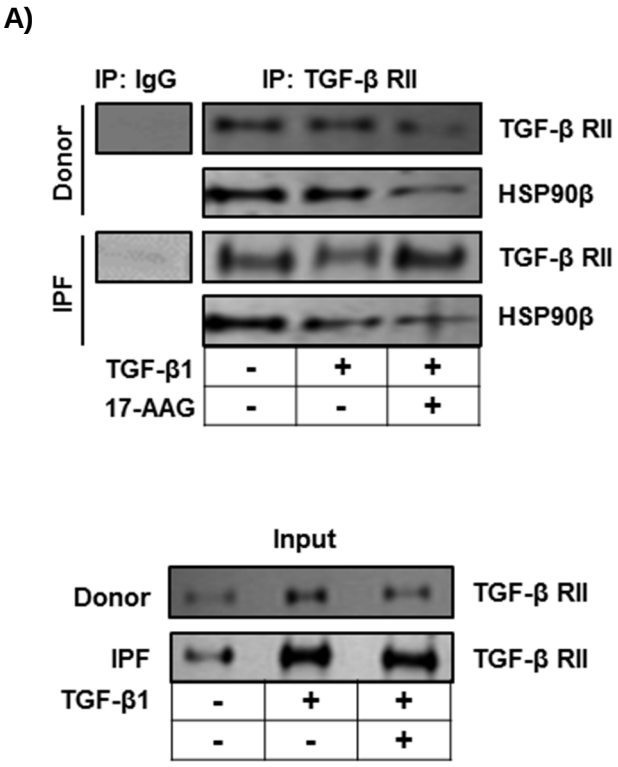


**Figure 18. HSP90β interacts with TGF-βRII in hILFBs. (A)** Western blots of heat shock protein HSP90β and TGF-βRII after protein lysate from donor and IPF ILFBs was immunoprecipitated with anti-TGF-βRII antibody or IgG antibody. After 24 hours of serum-starvation, ILFBs were stimulated with recombinant TGF-β1 (10 ng/ml) for 24 hours in the absence or presence of 17-AAG.

### 4.8. 17-AAG prevents epithelial-mesenchymal transition (EMT) of A549 cells.

Except for the residential interstitial fibroblasts in the lung, epithelial-mesenchymal transition (EMT) has been implied as a source of myofibroblasts (Fernandez and Eickelberg, 2012b). The study was also directed toward the effect of 17-AAG on TGF-β1-induced EMT of A549 cells, which is a model of human alveolar type-II epithelial

cells. A549 cells without exposure to TGF-β1 exhibited a cubic cell shape in cluster formation (epithelial phenotype); administration of TGF-β1 caused the cells to develop an individualized, elongated spindle-shape, whereas cells exposed to TGF-β1 and concomitant 17-AAG retained the epithelial phenotype (Figure 19A). Additionally, immunofluorescence staining (Figure 19A) and western blotting (Figure 19B-19F) demonstrated that TGF-β1 exposure led to elevation of the mesenchymal marker-fibronectin (Figure 19C) and reduction of the epithelial marker- E-cadherin (Figure 19D) in A549 cells, indicating an on-going EMT event. The shift of markers induced by TGF-β1 was prevented by co-administration of 17-AAG, concomitant with decreased TGF-βRII expression and Smad2 phosphorylation (Figure 19E-19F).

**A)**

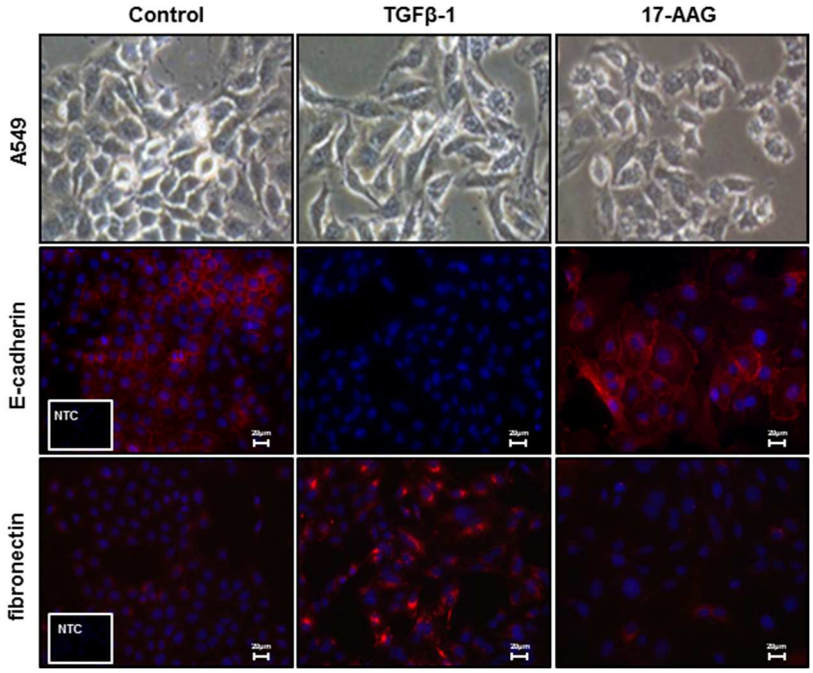

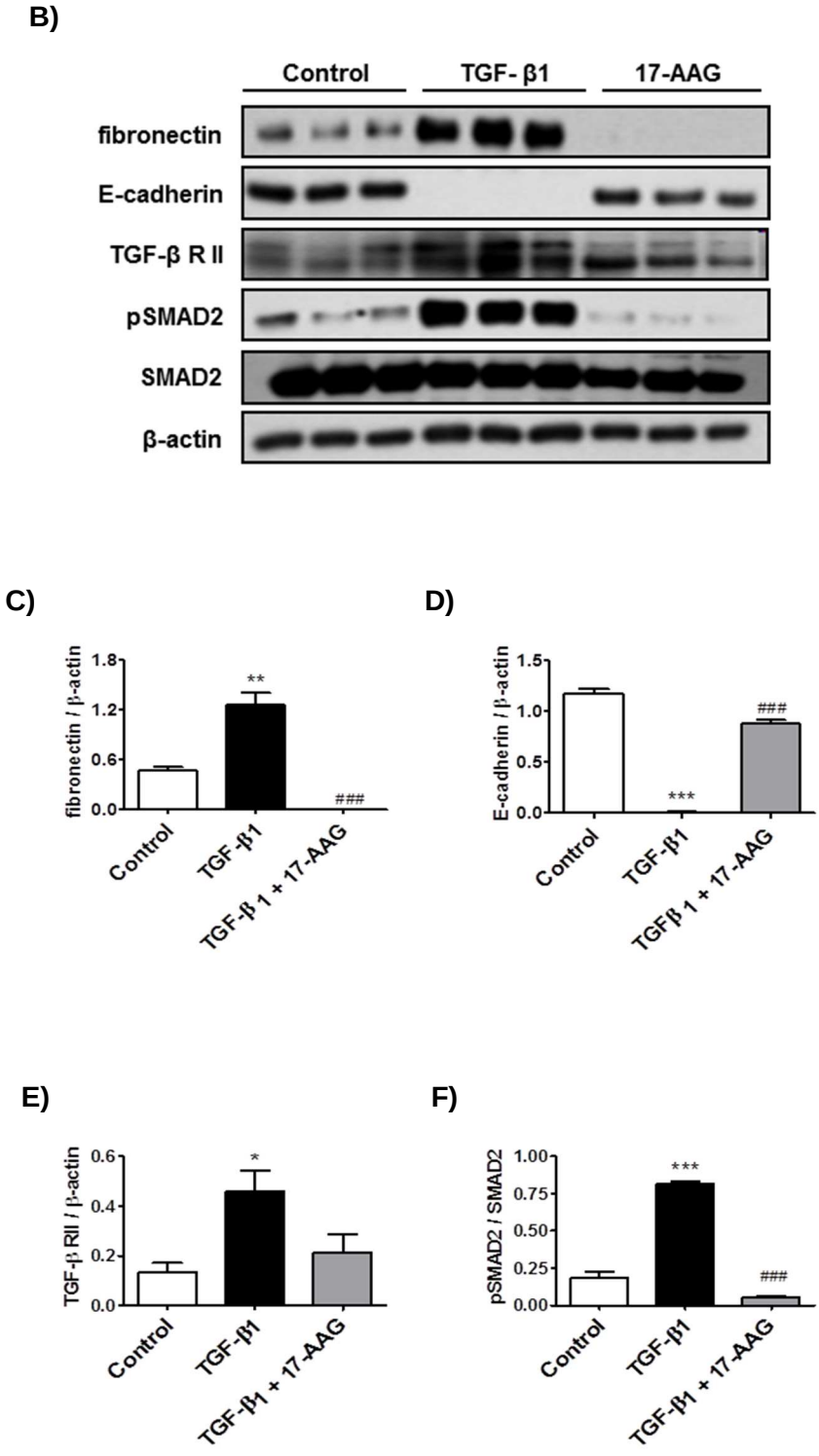


**Figure 19. 17-AAG prevents TGF-β1-induced EMT of A549 cells. (A)** Representative images of A549 cell morphology examined by phase contrast microscopy under 20 x magnification (upper panel) and representative immunofluorescence staining of E-cadherin (red) and fibronectin (red) with DAPI (blue) counter-staining for nuclei (lower 2 panels). Scale bar = 20 μm. **(B-F)** Representative western blots of E-cadherin, fibronectin, TGF-β receptor II (TGF-βRII), phospho-Smad2 (phospho-Ser465, phospho-Ser467),

and Smad2, with β-actin as the loading control. A549 cells were stimulated with TGF-β1 (5 ng/ml) for 72 hours in the absence or presence of 17-AAG (50 nM) after 24 hours of serum-starvation. All values are given as the mean ± SEM of n = 3 per group. The experiment was repeated independently three times. *P < 0.05, **P < 0.01, ***P < 0.001 versus Control; ###P < 0.001 versus TGF-β1.

### 4.9. Administration schedule using 17-DMAG on the bleomycin-induced pulmonary fibrosis model.

Based on the fact that HSP90 plays an important role in ILFB transdifferentiation and EMT by manipulating the TGF-β pathway, and HSP90 inhibition with 17-AAG blocks the fibrotic response to TGF-β in vitro, the in vivo studies with 17-DMAG were carried out, a water-soluble HSP90 inhibitor, in mice with bleomycin-induced pulmonary fibrosis. Animals were divided in the following four groups:

I. Control mice- received instillation of sterile saline at day 0 and was given vehicle alone (saline);
II. Bleomycin-administrated mice- received bleomycin at day 0 and were given vehicle;
III. Mice treated with 10 mg/kg 17-DMAG- received bleomycin at day 0 and were treated every second day from day 8 for 2 weeks with 10 mg/kg.
IV. Mice treated with 25 mg/kg 17-DMAG- received bleomycin at day 0 and were treated every second day from day 8 for 2 weeks with 25 mg/kg.

17-DMAG was prepared freshly in saline at 2 or 5 mg/ml and administrated *per os* via gavage needle, all in the same manner.

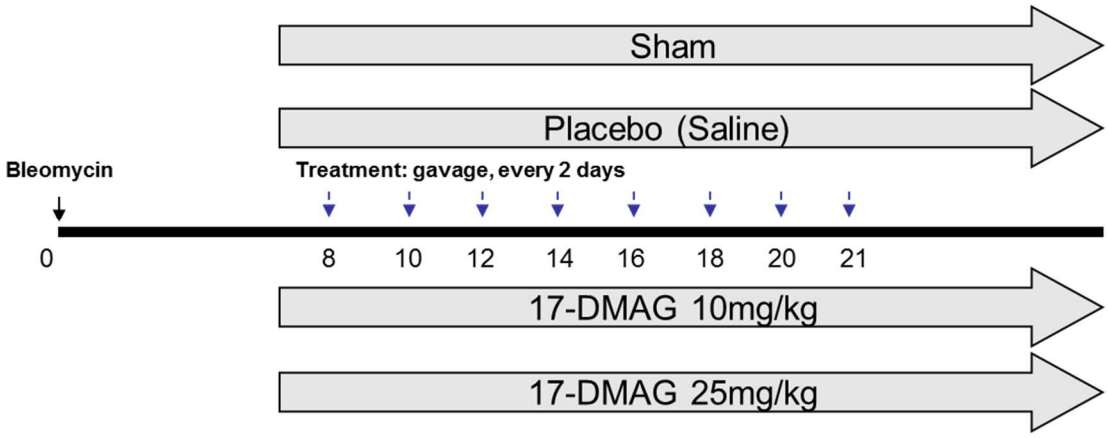


**Figure 20. Schedule using 17-DMAG in the bleomycin-induced pulmonary fibrosis model.**

### 4.10. HSP90 at RNA level is not up-regulated in ILFBs and lungs from bleomycin-challenged mice.

To investigate the transcriptional level of HSP90 in mouse, the real-time PCR was carried out. There was no differences in the expression of HSP90AA1, HSP90AB1 and HSP90B1 isoforms between sham control and bleomycin-challenged mice, in both mouse interstitial fibroblasts (Figure 21A) and lung homogenate (Figure 21B).

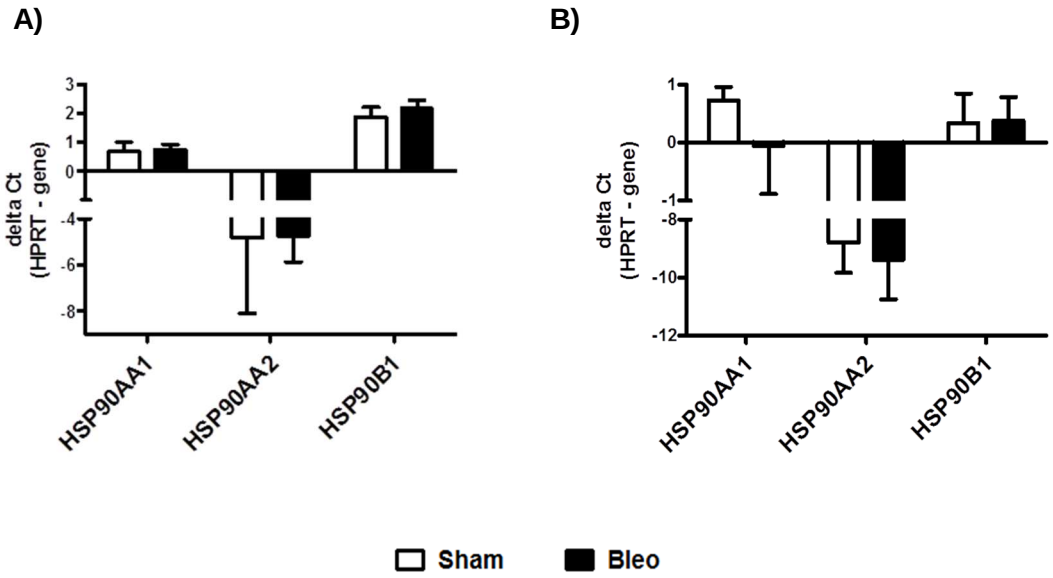


**Figure 21. HSP90 at RNA level is not up-regulated in mILFBs and lung homogenates from bleomycin-challenged mice. (A)** Relative mRNA levels of HSP90AA1, HSP90AB1 and HSP90B1 in mouse ILFBs and **(B)** mouse lungs from sham control and bleomycin-challenged mice (Bleo) presented as delta Ct value after normalization to HPRT. All values are expressed as mean ± SEM of n= 3 per group.

### 4.11. HSP90 is increased at protein level in ILFBs and lung homogenates from bleomycin- challenged mice.

Next, the expression of HSP90 in the 21-day bleomycin-challenged mice was examined. Western blots demonstrated a 2-fold increase of HSP90α and HSP90β in ILFBs from bleomycin-challenged mice (Figure 22A-22C) and no significant differences in the expression of HSP90 in lung homogenates from bleomycin-challenged mice (Figure 22D-22F) when compared with sham control.

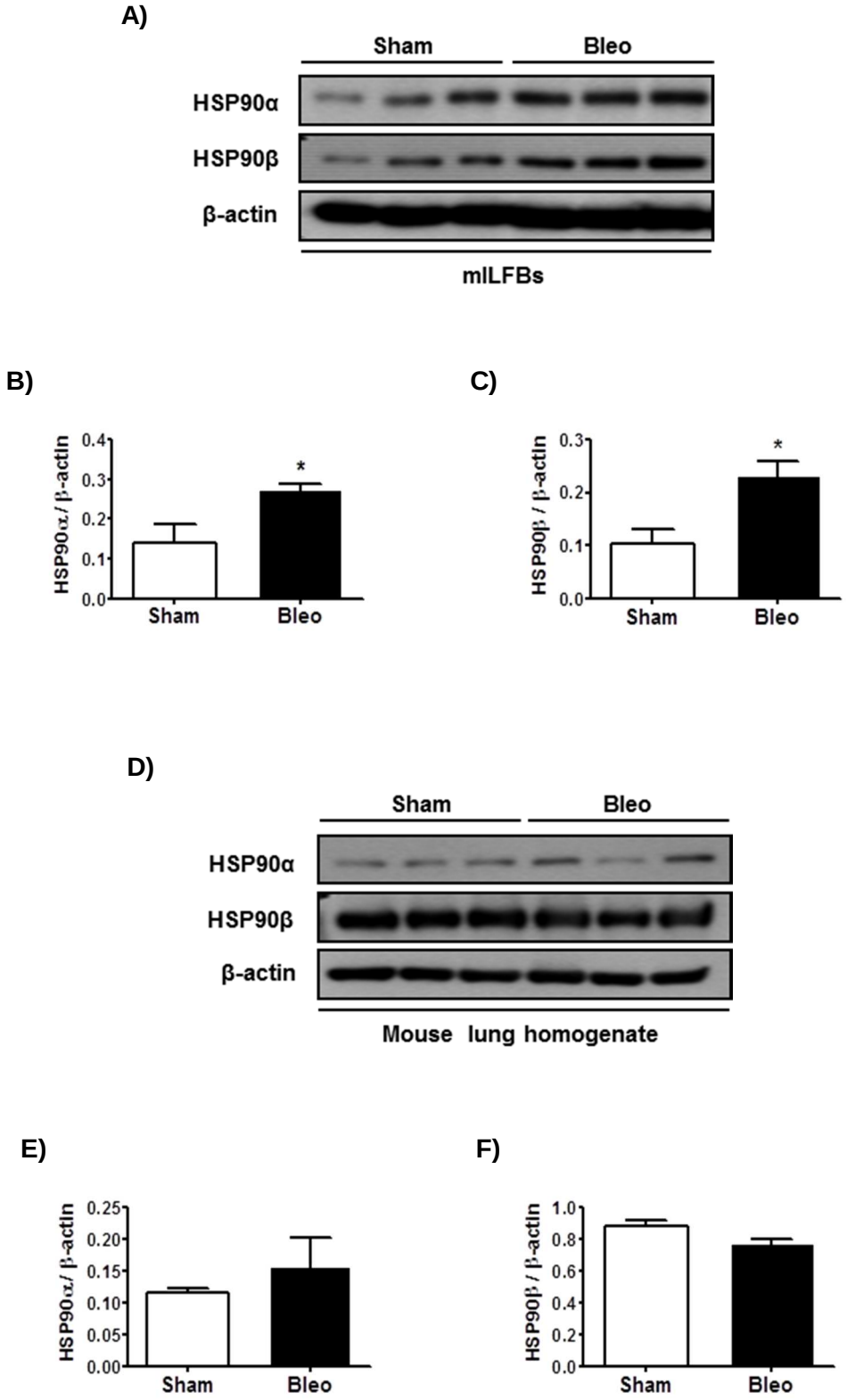


**Figure 22. HSP90 is increased in mILFBs and lung homogenates from bleomycin- challenged mice.** Representative western blots of HSP90α and HSP90β in **(A-C)** mouse ILFBs and **(D-F)** mouse lungs from

sham and bleomycin-challenged mice (Bleo), with densitometry quantification. β-actin serves as the loading control. All values are expressed as mean ± SEM of n= 3 in the group. *P < 0.05 *vs* Sham.

### 4.12. HSP90 is up-regulated in myofibroblasts from lung of bleomycin-challenged mice.

The expression of HSP90 in the lungs of bleomycin-challenged mice and sham controls was examined. Immunohistochemistry exhibited increased interstitial immunoreactivity of HSP90α and HSP90β in myofibroblasts (indicated by asterisks and α-SMA staining of a serial section) in the lungs of bleomycin-challenged mice compared with sham controls (Figure 23). In addition, a pronounced overexpression of HSP90β (but not HSP90α) was observed in AECII in bleomycin-challenged lungs (indicated by arrows and TTF1 staining) compared with sham controls (Figure 23).

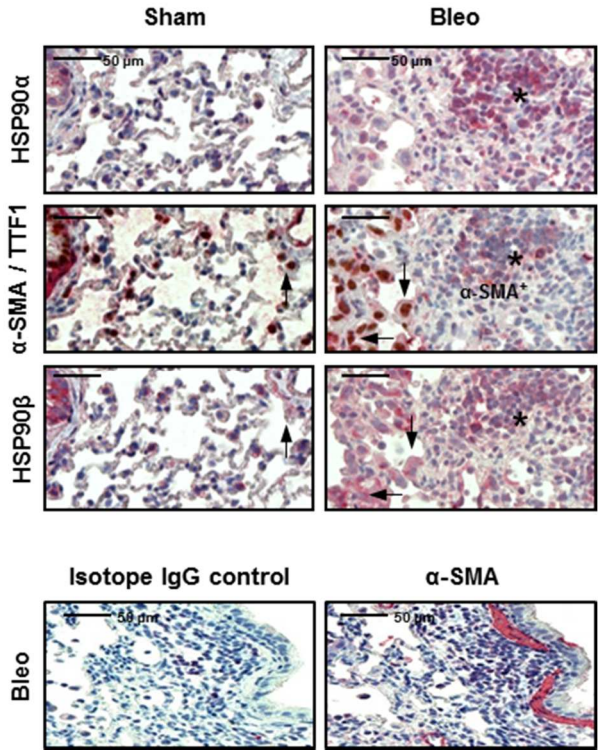


**Figure 23. HSP90 is up-regulated in lung tissue sections from bleomycin-challenged mice.** Representative immunohistochemical staining of HSP90α, HSP90β, TTF1 and α-SMA in serial lung sections obtained from three sham controls and three bleomycin-challenged mice (Bleo). Myofibroblasts and AECII are shown by α-SMA (asterisks) and TTF1 (arrows) staining, respectively. Red coloring indicates positive staining for Hsp90α, Hsp90β and α-SMA; brown coloring for TTF1. Scale bar = 50 µm.

### 4.13. TGF-β RI, TGF-β RII and TGF-β1 at RNA level is not changed in mouse homogenate after treatment with 17-DMAG.

It was shown in this study that the antifibrotic effects of HSP90 inhibitor were a consequence of significant depletion of TGF-β receptors on the post-translational level. To prove that there are not changes on the transcriptional level, RT-PCR was performed. The results indicated that there was no differences in expression of TGF-β1, TGF-β receptor I and receptor II at RNA level between sham control, bleomycin-challenged mice and mice treated with both doses of 17-AAG (10 mg/kg and 25 mg/kg; Figure 24A-24C).

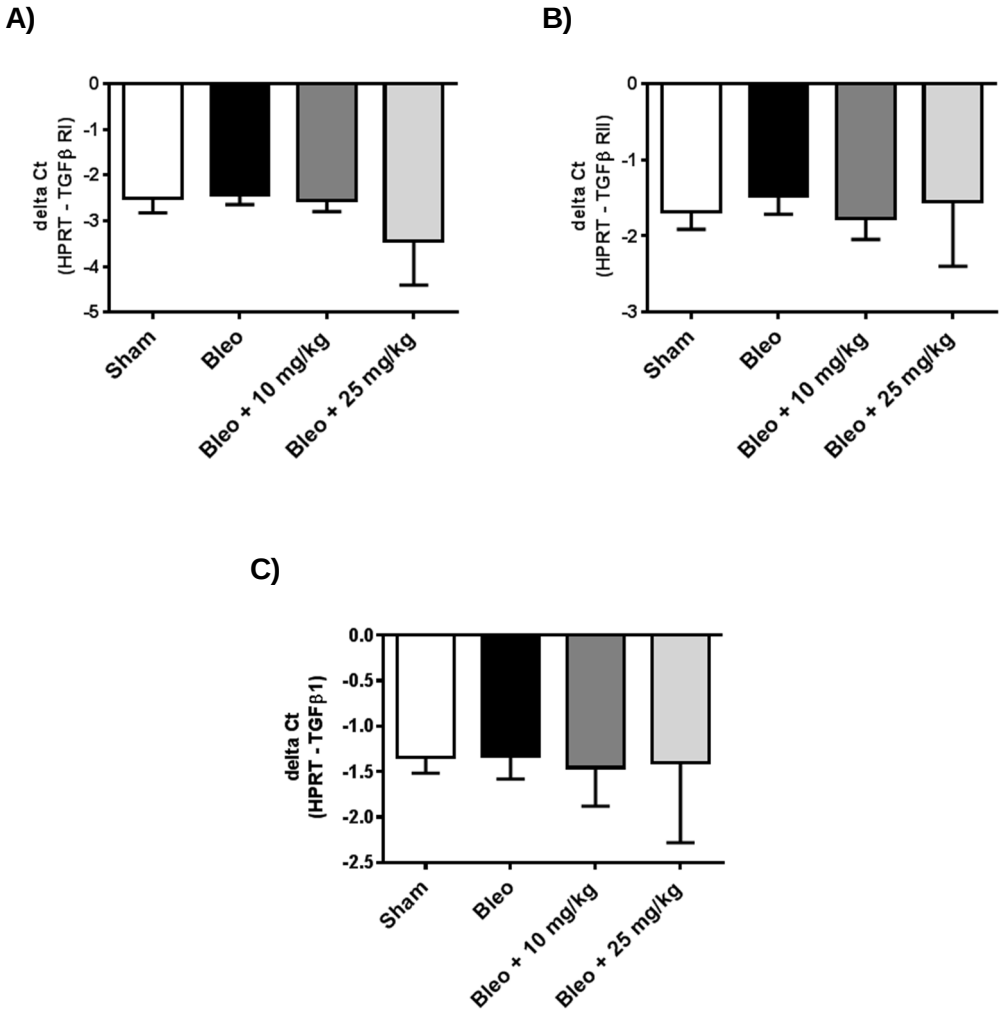


**Figure 24. TGF-β RI, TGF-β RII and TGF-β1 at RNA level is not changed in mouse lung homogenate after the 17-DMAG treatment. (A-C)** Relative mRNA levels of TGF-β RI, TGF-β RII and TGF-β1 in mouse lung homogenates from sham control, bleomycin-challenged mice (Bleo) and mice treated with 17-DMAG

(10 mg/kg and 25 mg/kg) presented as delta Ct value after normalization to HPRT. All values are expressed as mean ± SEM of Sham= 6, Bleo= 9, 10 mg/kg= 9, 25 mg/kg= 8.

### 4.14. HSP90 expression at the protein level is not changed in the mouse homogenate after treatment with 17-DMAG.

WB was performed to check if the protein level of HSP90 was unaltered after the *in vivo* treatment with 17-DMAG. The expression supposes to be equal because the Hsp90 inhibitor only disrupts protein interactions between HSP90 and its clients, it does not affect protein level of Hsp90 itself. Indeed, these data indicated that the HSP90 level is unaltered in bleomycin-challenged mice treated with the both doses of 17-DMAG (10 mg/kg and 25 mg/kg) when compared with sham controls or bleomycin-challenged mice (Figure 25A-25C).

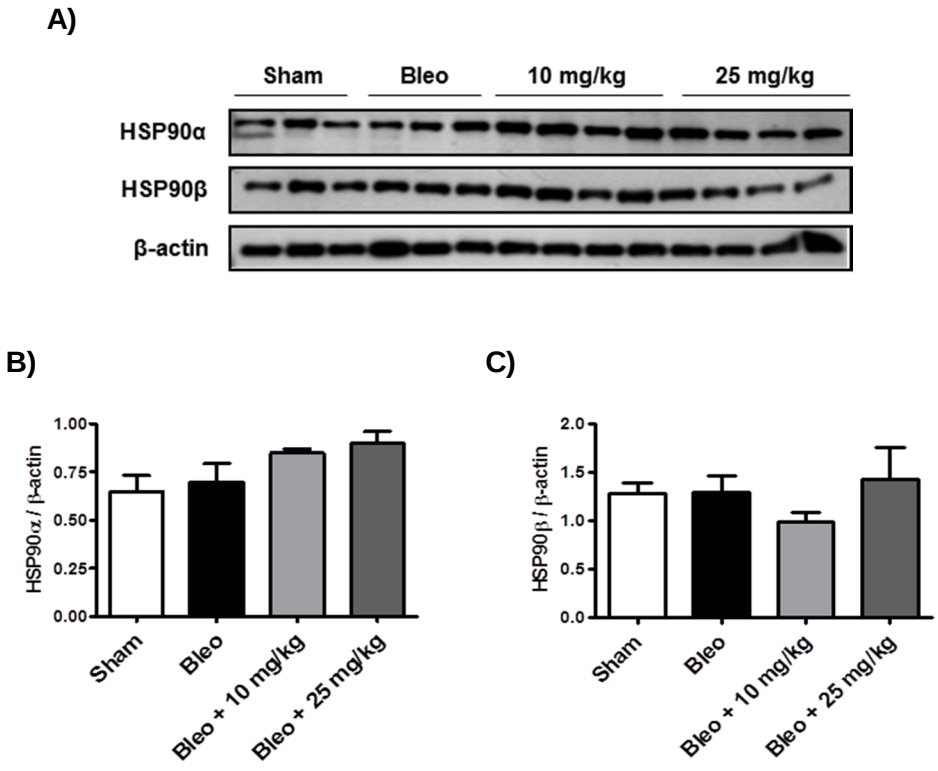


**Figure 25. HSP90 expression at the protein level is not changed in the mouse lung homogenate after treatment with 17-DMAG. (A)** Representative western blots of HSP90α and HSP90β with densitometry quantification **(B-C))** in mouse lung homogenates from sham control, bleomycin-challenged mice (Bleo) and mice treated with 17-DMAG (10 mg/kg and 25 mg/kg) with densitometry quantification. β-actin serves as the loading control. All values are expressed as mean ± SEM of n= 3 or n= 4 per group.

### 4.15. HSP70 protein expression is up-regulated in the homogenate from bleomycin-administrated mice after treatment with 17-DMAG.

Proteomic analysis in previous studies showed induction of the HSP70 family members after Hsp90 inhibition (Mayor-López et al., 2014); (Munje et al., 2014). The level of HSP70 was investigated in this study. The bleomycin-challenged mice treated with both doses of 17-DMAG (10 mg/kg and 25 mg/kg) expressed higher level of HSP70 when compared with sham or bleomycin-administrated mice (Figure 26A and 26B).

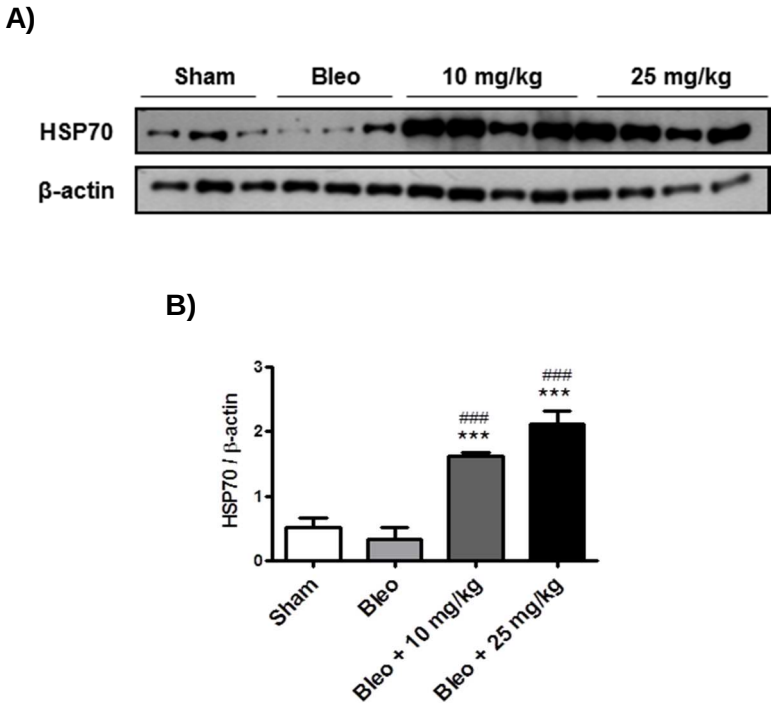


**Figure 26. HSP70 protein expression is upregulated in the homogenate from bleomycin-administrated mice after treatment with 17-DMAG. (A-B)** Representative western blots of HSP70 with densitometry quantification in mouse lung homogenates from sham control, bleomycin-challenged mice (Bleo) and mice treated with 17-DMAG (10 mg/kg and 25 mg/kg) with densitometry quantification. β-actin serves as the loading control. All values are expressed as the mean ± SEM of n= 3 or n= 4 mice per group. ***P < 0.001 versus Sham; ###P < 0.001 versus Bleo.

### 4.16. 17-DMAG suppresses inflammation in bleomycin-challenged mice.

Bleomycin-induced pulmonary fibrosis model is initiated by a severe acute injury and inflammatory response, followed by chronic inflammation and fibrosis (Scotton and Chambers, 2010), therefore the inflammatory cell composition of BALF collected on day 21 was analyzed. The cell counting revealed increased proportions of lymphocytes and neutrophils, at the expense of the proportion of macrophages, in bleomycin-

challenged mice compared with sham controls. 17-DMAG partially restored the inflammatory cell composition in BALF (Figure 27A-27C), suggesting a favorable effect of HSP90 inhibition on sustained pulmonary inflammation in bleomycin-challenged mice.

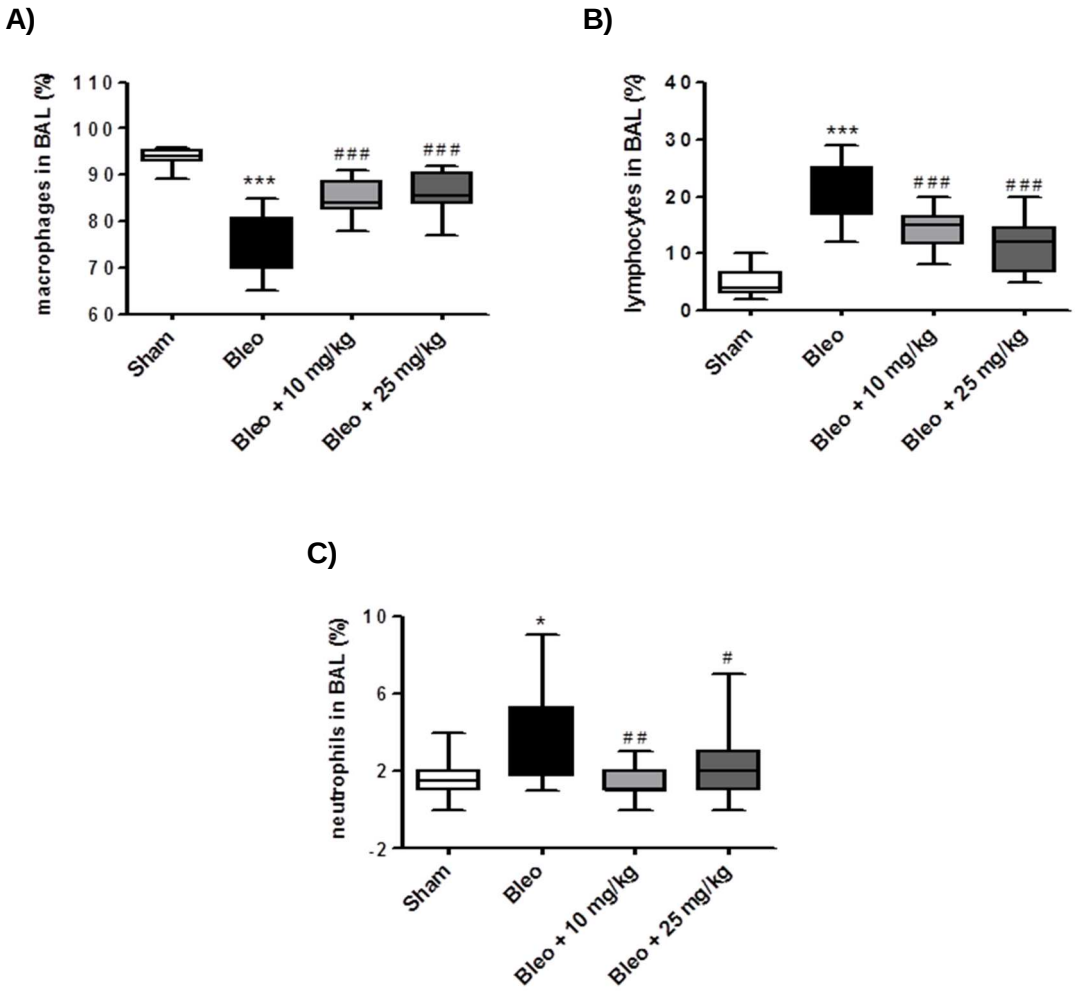


**Figure 27. 17-DMAG suppresses inflammation in bleomycin-challenged mice. (A-C)** Infiltrated inflammatory cells in bronchoalveolar lavage fluid (BALF) were counted. At day 21 after instillation of bleomycin (Bleo) or saline (Sham), in the absence or presence of 17-DMAG treatment (10 mg/kg or 25 mg/kg every 2 days from day 8 to day 21). All values are given as the mean ± SEM of n= 10 mice in each group. *P < 0.05, ***P < 0.001 versus Sham; #P < 0.05, ##P < 0.01, ###P < 0.001 versus Bleo.

### 4.17. 17-DMAG improves physiological parameters in mice with bleomycin-induced pulmonary fibrosis.

Bleomycin causes significant loss of body weight (up to 20%) one week after instillation. The body weight gain of 17-DMAG-treated mice was effectively improved compared with bleomycin-challenged mice (Figure 28A). Moreover, lung function monitored by FlexiVent exhibited a significant decrease of lung compliance in bleomycin-chalenged mice compared to sham (0.025 mL/cm$H_2O$ ± 0.006 *vs* 0.035 mL/cm$H_2O$ ± 0.005), and 17-DMAG dose-dependently ameliorated lung compliance (0.0283 mL/cm$H_2O$ ± 0.0067 in 10 mg/kg group and 0.0325 mL/cm$H_2O$ ± 0.0046 in 25 mg/kg group mice; Figure 28B).

Further, tissue damping was elevated in bleomycin-treated mice in comparison to sham control (5.77 cmH2O/mL ± 0.43 vs 4.39 cmH2O/mL ± 0.2). The treatment with both doses of 17-DMAG improves the tissue damping (5.17 cmH2O/mL ± 0.18 in 10mg/kg group and 4.63 cmH2O/mL ± 0.19 in 25 mg/kg group; Figure 28C). These results showed that 17-DMAG restores the impaired lung function.

**A)**

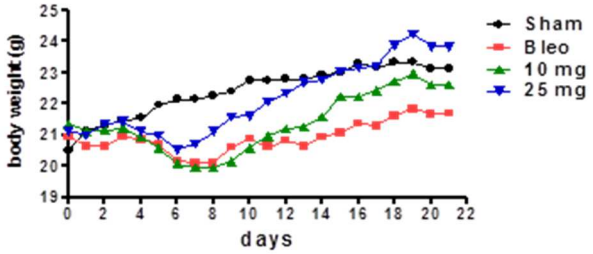

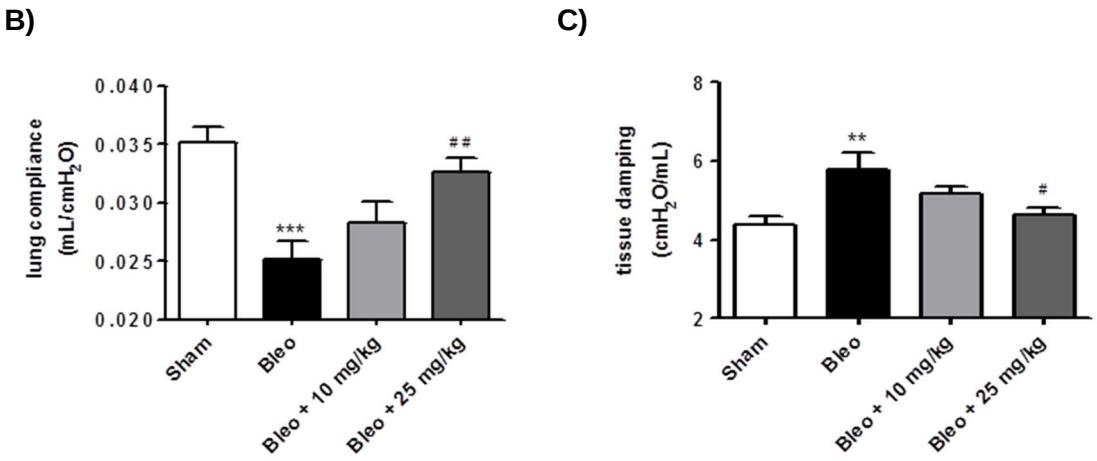


**Figure 28. 17-DMAG treatment improves lung function in bleomycin-challenged mice. (A)** Body weight curve monitored throughout the whole experiment, **(B)** Lung compliance and **(C)** lung tissue damping, measured at day 21 after instillation of bleomycin (Bleo) or saline (Sham), in the absence or presence of 17-DMAG treatment (10 mg/kg or 25 mg/kg every 2 days from day 8 to day 21). All values are given as the mean ± SEM of n= 10 mice in each group. **P < 0.01, ***P < 0.001 versus Sham; #P < 0.05, ##P < 0.01 versus Bleo.

### 4.18. 17-DMAG decreases fibrosis scores and collagen deposition in bleomycin-challenged mice.

To understand the role of HSP90 in lung parenchyma remodeling, a comprehensive histological evaluation was carried out. Hematoxylin and eosin (H&E) staining revealed a significant distortion of bleomycin-challenged lungs, while 17-DMAG partially restored the lung architecture (Figure 29A). The fibrosis score demonstrated a moderate degree of fibrosis in bleomycin-challenged mice compared with sham controls (3.83 ± 0.56 versus 0.50 ± 0.14; Figures 29A and 29B). 17-DMAG dose-dependently decreased fibrosis scores (3.06 ± 0.38 in the 10 mg/kg group and 2.85± 0.25 in the 25 mg/kg group). Based on the pronounced effect of 17-AAG on collagen production *in vitro*, collagen deposition *in vivo* was further examined using sirius red staining. Bleomycin-challenged mice exhibited excessive collagen deposition compared with sham controls (4.64% ± 0.56 versus 0.94% ± 0.19), whereas 17-DMAG treatment narrowed the collagen areas (2.33% ± 0.58 in the 10 mg/kg group and 2.19% ± 0.54 in the 25 mg/kg group; Figures 29A and 29C).

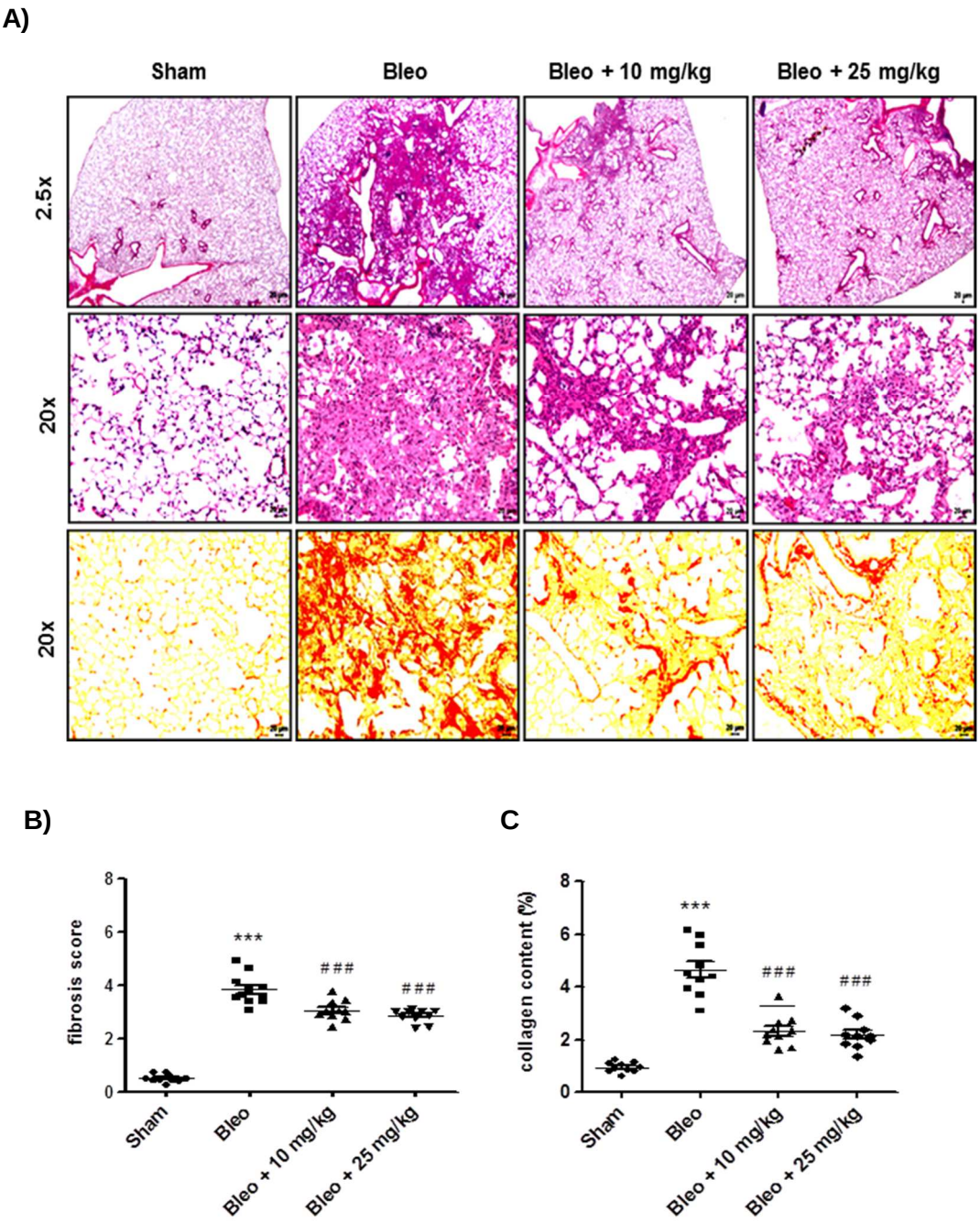


**Figure 29. 17-DMAG treatment decreases fibrosis scores and collagen deposition in bleomycin-challenged mice. (A)** Histological images of lung paraffin sections with hematoxylin and eosin (H&E) staining for pulmonary fibrosis (upper 2 panels) and sirius red staining for collagen deposition (lower panel). Scale bar = 20 μm. **(B)** Fibrosis score (based on H&E staining) expressed on a numerical scale ranging from 0 (healthy) to 6. **(C)** Collagen content (based on sirius red staining) expressed as a percentage of the total area of lung section. All values are given as the mean ± SEM of n = 10 mice per group. **P < 0.01, ***P < 0.001 versus Sham; #P < 0.05, ##P < 0.01, ###P < 0.001 versus Bleo.

### 4.19. 17-DMAG suppresses metalloproteinase (MMP) activity in bleomycin-challenged mice.

MMP-associated proteinase activity is reported to reflect inflammation and IPF patients show elevated MMPs levels in BALF (Dancer et al., 2011), (McKeown et al., 2009). To monitor the MMP activity *in vivo*, a MMP-responsive probe, named MMP680Sense, was introduced into mice and measured the signal with FMT. MMP activity was increased in lungs from bleomycin-challenged mice compared with sham control (4.67 pmol ± 1.22 vs 0.54 pmol ± 0.24). Mice treated with 17-DMAG after the bleomycin challenge showed lower MMP activity (2.11 pmol ± 1.44 in the 10 mg/kg group and 0.99 pmol ± 0.66 in the 25 mg/kg group; Figure 28A-28C).

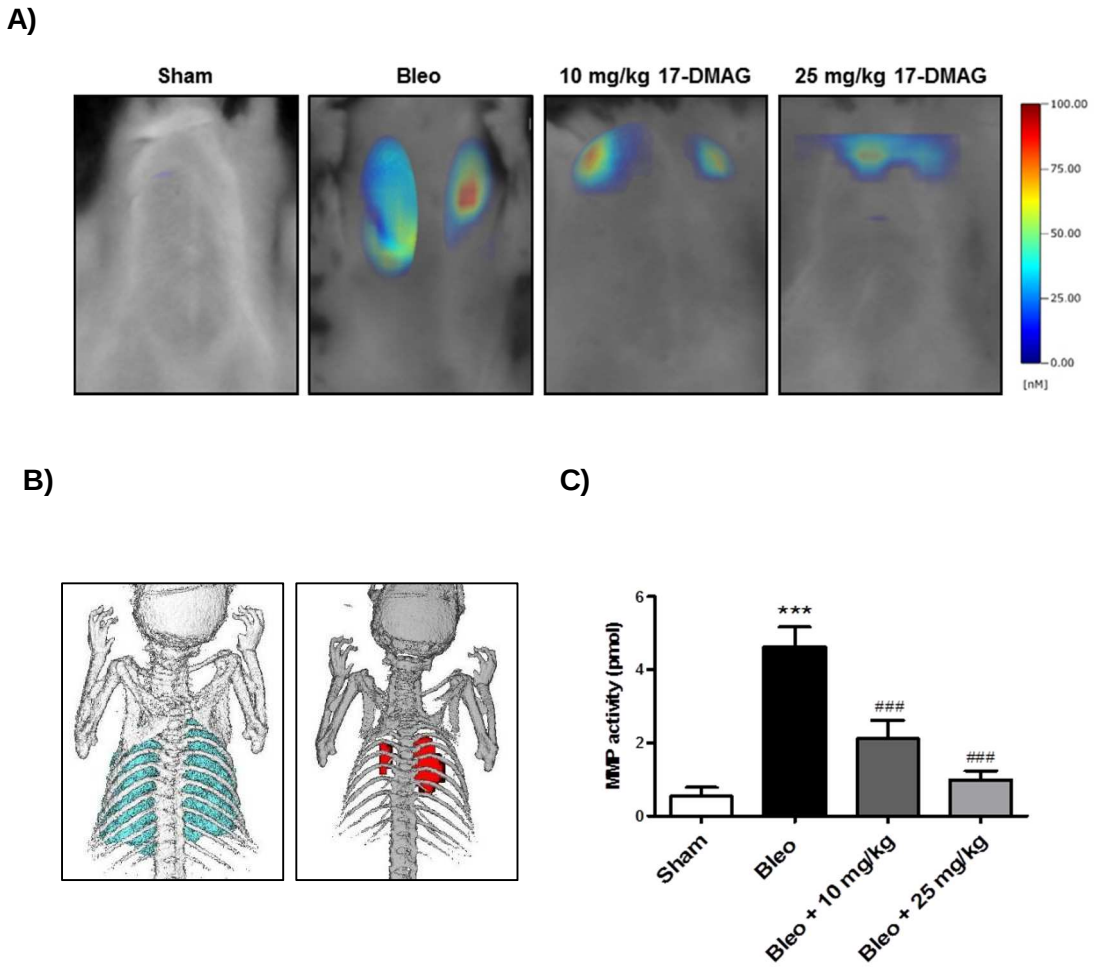


**Figure 30. 17-DMAG suppresses metalloproteinase (MMP) activity in bleomycin-challenged mice.** **(A)** Representative images of MMP activity in mouse lungs. **(B)** Virtual 3D rendering of skeleton, lungs and MMP activity in bleomycin-challenged lung acquired by FMT in combination with microcomputed tomography (µCT). **(C)** Quantitative FMT measurement of MMP activity in mouse lungs. MMP activity in mouse lungs was measured *in vivo* by quantitative fluorescence molecular tomography (FMT) at day 21

after instillation of bleomycin (Bleo) or saline (Sham), in the absence or presence of 17-DMAG treatment (10 mg/kg or 25 mg/kg every 2 days from day 8 to day 21). MMP activatable fluorescent probe, MMPSense680, was injected via the tail vein 24 hours before the FMT measurement. All values are given as the mean ± SEM of n = 5 mice. ***$P$ < 0.001 versus Sham; ###$P$ < 0.001 versus Bleo

# 5. DISCUSSION

This study provides direct experimental proof that HSP90 plays a pathological role in pulmonary fibrosis. HSP90 inhibition presents antifibrotic effects *in vitro* by preventing the myofibroblasts transdifferentiation from both fibroblasts and alveolar epithelial cells. Furthermore, the treatment of bleomycin-induced pulmonary fibrosis mice with HSP90 inhibitor shows significant antifibrotic effects *in vivo*.

## 5.1. HSP90 expression

HSP90 has a broad spectrum of pathophysiological functions depending on cell types and stresses. HSP90 has been intensively studied in tumors. Many tumor-promoting factors are HSP90-dependent and cancer cell proliferation relies on HSP90 function. Cancer cells proliferate faster and need rigorously HSP90 function, while healthy cells rely on HSP90 modestly. This phenomenon is termed 'HSP90 addiction'. The role of HSP90 has been investigated in other diseases such as neurodegenerative and infectious diseases. In neurodegenerative diseases, HSP90 stabilizes p53 and lead to abnormal tau phosphorylation and directly interacts with mutated form of tau protein. Thus it influences the accumulation of toxic tau aggregates in tauopathy like Alzheimer's disease (AD) and frontotemporal dementia (FTD) (Dickey et al., 2007). In viral infections HSP90 plays a key role in folding of basic viral proteins (Geller et al., 2007) and HSP90 inhibitors can block the replication of poliovirus and paramyxovirus (Geller et al., 2013). However, little is known on the role of HSP90 in pulmonary fibrosis.

To better understand the pathophysiology of IPF, many studies have tried to identify molecules by comparing the transcriptome or proteome of healthy lungs and lungs derived from IPF patients (Korfei et al., 2013). In the 2-D gel proteomic study, Korfei and colleagues have reported that HSP90 along with other stress-related proteins such as HSP27 was elevated in IPF lungs (Korfei et al., 2013); however the function of HSP90 in IPF has not been elucidated. In this study, theup-regulation of HSP90 was observed in IPF lungs, more interestingly up-regulated protein expression of both HSP90α and HSP90β was found in ILFBs from IPF patients as well as from human lung homogenate. Moreover, ILFBs derived from bleomycin-administrated mouse exhibit significantly increased level of both isoforms of HSP90.

Additionally, in this study the protein level of HSP90 was not changed neither after *in vitro* treatment with 17-AAG in donor and IPF ILFBs nor after *in vivo* treatment of

bleomycin-administrated mice with 17-AAG. This situation takes places because the Hsp90 inhibitor only disrupts protein interactions between Hsp90 and its clients, it does not change the protein level of Hsp90 itself. Similarly, the increased expression of HSP90α and HSP90β was detected by immunochemistry in patients with systemic sclerosis (SSc) and in experimental fibrosis in a transforming growth factor β (TGF-β)-dependent manner (Tomcik et al., 2014).

### 5.2. TGFβ signaling in pulmonary fibrosis

It is well known that TGF-β is actively involved in initiation and progression of pulmonary fibrosis (Fernandez and Eickelberg, 2012b), (Khalil et al., 1996), therefore inhibition of aberrant TGFβ signaling cascade has long been pursued as a potential strategy for the treatment of pulmonary fibrosis, among other fibrotic diseases. Despite of intensive *in vivo* investigations or even clinical trials, attempts to directly block TGF-β signaling by either TGF-β neutralizing antibodies (Khalil et al., 1996) or TGFβR kinase inhibitors (Bonniaud et al., 2005) have thus far been ineffective or are still in the experimental stage. To overcome this challenge, it is of great interest to identify other mediators of TGF-β signaling which can be targeted pharmacologically. HSP90 was proposed as such a mediator and HSP90 inhibitor as a novel therapeutic approach for pulmonary fibrosis.

### 5.3. 17-AAG reduces extracellular matrix (ECM) production

During the progress of pulmonary fibrosis, a range of cellular abnormalities are present in the lung, one of which is myofibroblasts transdifferentiation. As the effector cells, myofibroblasts are mostly responsible for EMC production, remodelling and fibrotic foci formation (Fernandez and Eickelberg, 2012a). Having observed the upregulation of HSP90 in pulmonary fibrotic lungs or ILFBs, we employed 17-AAG, a highly selective HSP90 inhibitor, *in vitro* to investigate the function of HSP90 on TGF-β1-induced fibrotic response in hILFBs, considering TGF-β1 plays a central role in IPF. Western blots revealed that collagen I, fibronectin and α-SMA were all increased in hILFBs under the stimulation of TGF-β1 indicating fibroblast activation and excessive ECM production, with a higher level on IPF hIFBs compared to the donor cells. And the effects of TGF-β1 were sufficiently blocked by 17-AAG. Moreover, extracellular collagen deposition examined by sircol red assay was increased by TGF-β1 in both donor hILFBs and IPF hILFBs and was reversed to the basal level by 17-AAG.

Similarly, in a study on systematic sclerosis, 17-DMAG was shown to block TGF-β1-induced mRNA expression of collagen and fibronectin in skin fibroblasts (Tomcik et al., 2014). Further, Noh and colleagues described in renal NRK49F fibroblasts increased level of TGFβ1-induced ECM production, while the treatment with 17-AAG inhibited the expression of collagen I, fibronectin and α-SMA (Noh et al., 2012). In hepatic fibrosis, Myung and colleagues showed that α-SMA protein expression was suppressed by the treatment with 17-AAG what indicated that the inhibitor prevented HSC (hepatic stellate cells) cell activation. Additionally, TGF-β1-induced collagen synthesis on RNA level was suppressed by 17-AAG in HSC cells which are main source of ECM proteins in hepatic fibrosis (Myung et al., 2009).

### 5.4. 17-AAG inhibits fibroblast migration

Besides myofibroblasts transdifferentiation and ECM production, one other pathological features of fibroblasts contributing to pulmonary fibrosis are uncontrolled migration which is also a feature of cancer cells (Vancheri et al., 2010; Vancheri, 2013). HSP90 inhibitor suppress tumor growth and metastasis via abrogating proliferation and mobility (Fortugno et al., 2003)(Annamalai et al., 2009). Annamalai and colleagues demonstrated that HSP90 may regulate the activity of EphA2 and presented the potential interaction between EphA2 receptor signaling and chaperone function. Geldanamycin reduced the migration of U251 (human malignant glioblastoma) cell line suggesting that EphA2 signaling plays a major role in HSP90-dependent cell migration (Annamalai et al., 2009). Nagaraju and colleagues investigated the role of HSP90 in colorectal cancer. The treatment with HSP90 inhibitor (ganetespib) inhibited migration in HCT-116 (human colon carcinoma) cell line. Moreover, the effect of ganetespib on cellular pathways involved in motility were evaluated. Phosphorylated S6K and FAK was down-regulated at both RNA and protein level (Nagaraju et al., 2014).

### 5.5. 17-AAG reverses epithelial-mesenchymal transition (EMT)

The origin of myofibroblasts remains unclear (Willis et al., 2005). There are three theories that seek to explain the origin of myofibroblasts: activated resident lung fibroblasts, epithelial cells via the process of EMT and bone marrow–derived fibrocytes. Myofibroblasts have been long believed to arise through transdifferentiation of residential parenchymal fibroblasts, initiated by multiple growth factors or cytokines such as PDGF, FGF and TGF-β (Fernandez and Eickelberg, 2012a). Compelling evidence has also suggested that alveolar epithelial cells may transdifferentiate to

myofibroblasts by activation of TGF-β signaling (Willis et al., 2005) or Wnt signaling (Königshoff et al., 2009), by process referred as EMT. However, the relative quantitative contribution of each cell types in the onset and progression of IPF is unknown. Reporter mice with marked cells of lung epithelial lineage with β-galactosidase were created to study EMT, and bone marrow chimeras expressing green fluorescent protein under the control of the fibroblast-associated S100A4 promoter were generated to examine bone marrow–derived fibroblasts. In bleomycin-induced fibrosis in mice, EMT comprised about 33% of fibroblasts and bone-marrow progenitors (fibrocytes) accounted for 20% of fibroblasts. It can be speculated, that 50% of fibroblasts originate from resident mesenchymal cells or other undisclosed source, at least in this model (Tanjore et al., 2009).

The association of EMT with the cancer progression has been investigated in various types of cancer such as breast cancer, prostate cancer, pancreatic cancer and hepatoma (Lamouille et al., 2014). Several studies have also revealed the association between loss of E-cadherin expression and poor prognosis in lung cancer (Xiao and He, 2011). Balanis and colleagues showed that the EMT is capable to increase the invasion and metastasis of breast cancer cells via activation of Stat3. Moreover, cancer cells undergo fibronectin production that supports Stat3 activation and metastatic outgrowth (Balanis et al., 2013). Further, Nagaraju and colleagues proved the inhibition of EMT in the animal model, in HCT-116 and HT-29 xenograft. Tumors resected from the gantespib-treated mice had significantly down-regulated expression of vimentin and increased E-cadherin when compared with untreated mice (Nagaraju et al., 2014). Based on the close association of HSP90 with the EMT in cancer metastasis, this study was directed toward the effect of 17-AAG on TGF-β1-induced EMT by applying A549 cells (human pulmonary epithelial cells). And our results confirm this theory, showing that 17-AAG reversed the switch between the epithelial and mesenchymal markers induced by TGF-β1, at the expense of TGF-βR2 and Smad2 activation. A549 cells under untreated conditions present a cubic epithelial shape in cluster formation compared with an individualized, elongated and spindle shape after TGF-β1 stimulation, whereas 17-AAG restored A549 cells to the epithelial phenotype. Additionally, TGF-β1 led to elevated mesenchymal marker (fibronectin) and diminished epithelial marker (E-cadherin) in A549 cells indicating an on-going EMT event, demonstrated by immunofluorescence staining and western blots. The shift of markers

induced TGF-β1 by was reversed by 17-AAG, accompanied by decreased TGF-β receptor II expression and SMAD2 phosphorylation.

The role of HSP27, another family of HSP proteins, was also studied in fibrogenesis and EMT. HSP27 was reported to bind to and stabilize Snail and consequently contribute to EMT. HSP27 knockdown caused Snail proteosomal degradation, thus blocking TGF-β-induced EMT. Wettstein and colleagues also demonstrated that HSP27 is up-regulated in patients suffered from IPF and in different *in vivo* models. The inhibition of HSP27 with OGX-427 (in phase II clinical trials as anticancer compound) efficiently inhibited EMT and fibrosis development (Wettstein et al., 2013).

### 5.6. HSP70 expression

Heat shock protein 70 (HSP70) is involved in the protection against various stressors and has anti-inflammatory activity. A wide variety of stresses, for example ischemia and inflammation, induce the up-regulation of HSPs including HSP70. HSP70 in particular has been showed to be involved not only in cytoprotective function via anti-apoptosis processes against stress *in vitro* , but also influence strong cytoprotection in the stomach, heart and liver *in vivo* (Otaka et al., 2007; Suemasu et al., 2009). It has been investigated the protective role of HSP70. Tanaka and colleagues found that transgenic mouse overexpressing HSP70 exhibit the blockade of the bleomycin-induced pulmonary inflammatory response and tissue damage. Moreover, HSP70 expression inhibited the bleomycin-dependent increase in myofibroblasts (Tanaka et al., 2010).

Based on those evidences, the expression of HSP70 was investigated by western blots using 17-AAG (*in vitro*) or 17-DMAG (*in vivo*). The alteration of HSP70 chaperone expression was evaluated in the absence or presence of 17-AAG/ 17-DMAG. The HSP70 expression increased after treatment with HSP90 inhibitor in both hILFBs and bleomycin-administrated mice when compared with untreated control or sham control, respectively. It is known that HSP70 exhibits antiapoptotic effects vie different mechanisms such as binding to apoptotic protease activating factor 1 (Apaf-1) in order to prevent the activation of caspase-9 and suppress downstream of apoptotic pathway of caspase-3 activation. Further, it was recently demonstrated that HSP70 blocks the activation of Bcl-2-associated X protein (BAX), which is crucial for apoptosis-associated mitochondrial dysfunction (Suemasu et al., 2009). This mechanism might be

considered as a crucial in the HSP70-dependent suppression of bleomycin-induced lung epithelial cell apoptosis. It is well documented that BAX and caspases activation play the important role in bleomycin-induced apoptosis in epithelial cells (Lee et al., 2005). Additionally, it might be possible that HSP70 exhibits inhibitory effects on EMT via the inhibition of NF-κB. There are many reports indicating that NF-κB stimulates EMT independently on TGF-β1 (Lee et al., 2005).

### 5.7. HSP90 regulates TGFβRs

Although HSP90 is essential for the viability of healthy cells, cancer cells might demand a higher level of HSP90-dependent clients and therefore require an increased level of HSP90 activity (Zhao and et al., 2005), as opposed to normal tissues, which may provide a favorable therapeutic window. It may also hold true for the fibrotic diseases. We found that the antifibrotic effects of HSP90 inhibition were a consequence of significant depletion of TGF-βRs on the post-translational level, but not on the transcriptional level, followed by decreased Smad2/3 activation. Indeed, present results demonstrate that the response to TGF-β1 in terms of fibroblast activation and ECM production was greater in ILFBs derived from patients with IPF than in ILFBs from donors. However, HSP90 inhibition shows similar potency for cells from both sources, suggesting that HSP90 is accountable for the higher sensitivity of the canonical TGF-β-Smad2/3 pathway in ILFBs derived from patients with IPF compared with donor-derived cells. Interestingly, recent study has proved that TGF-β signaling is activated in SSc (systemic sclerosis) fibroblasts, and also has showed that the overexpression of constitutively active TGF-β1 up-regulates HSP90β expression in murine skin (Tomcik et al., 2014).

Furthermore, endogenous co-immunoprecipitation proves that TGF-βRII directly interacts with HSP90β, indicating that TGF-βRII is a client of HSP90 and can be stabilized by HSP90. And the result with MG-132, a proteasome inhibitor, indicates that the compromised interaction of HSP90 and TGF-βRs lead to proteasome degradation of TGF-βRs. In support of this finding, recent studies using epithelial cell lines have demonstrated a direct interaction of TGF-βRs with HSP90 (Zhang et al., 2012), (Wrighton et al., 2008). Additionally, the investigators showed that the HSP90 inhibitor 17-AAG disrupts this interaction and recruits Smurf2 to TGF-βRs which promotes TGF-βR ubiquitination and subsequent degradation (Zhang et al., 2012). HSP90 chaperone machinery maintains protein homeostasis of various set of client proteins either by

assisting protein folding and maturation or by stabilizing protein complexes (Taipale et al., 2010).

### 5.8. *In vivo* studies with 17-DMAG

The various reports investigated the effectiveness of HSP90 inhibitor in many diseases such as systemic sclerosis, LPS-induced lung and liver inflammation as well as renal fibrosis. Tomcik and colleagues also showed that HSP90 inhibitor (17-DMAG) prevents skin fibrosis induced by overexpression of a constitutively active TGF-β RI. Moreover, the 17-DMAG decreases potent antifibrotic effects as well in Tsk-1 mice (they have a dominant mutation in the fibrillin-1 gene which occurs in elevated activation of latent TGF-β). These results were showed by reduced dermal thickening, hydroxyline content and number of myofibroblasts on tissue sections as well as decreased nuclear accumulation of phosphorylated pSMAD2/3 (Tomcik et al., 2014).

Ambade and colleagues also elucidated the role of 17-DMAG in prevention of LPS-induced liver injury. They found that pro-inflammatory cytokines, TNF-α and IL-6 were significantly blocked at both mRNA and protein level in liver treated with 17-DMAG and LPS. Moreover, the inhibition of HSP90 in the liver induces HSF1 (heat shock factor 1) and blocked LPS-induced NFκB activation and pro-inflammatory cytokine production attenuating liver injury (Ambade et al., 2012). Noh and colleagues determined the therapeutic efficacy of HSP90 inhibitor in unilateral ureteral obstruction (UUO) kidney model of renal fibrosis in mice. They found that the treatment with 17-AAG significantly attenuates α-SMA, fibronectin and collagen I in UUO kidneys and restores E-cadherin. Finally, the phosphorylation of SMAD2 induced by UUO was decreased by the treatment with17-AAG, indicating that these events were dependent on TGF-β1. Lilia and colleagues assessed the ability of HSP90 inhibitor (ganetespib) a non-geldanamycin HSP90 blocker, to suppress LPS-induced proteases, inflammatory mediators and cellular infiltrates. Ganetespib also suppressed B cells and NK cell recruitment, MMP9 level and chemokine and cytokine induction. Further, this inhibitor is introduced as a potential inhibitor in therapies for inflammatory diseases, in particular those of the lung (Lilja et al., 2015).

Based on earlier evidence from others and present *in vitro* results from my doctoral thesis, it is reasonable to speculate that HSP90 may be more than a cancer target, but also a target for pulmonary fibrosis. In consistent with expression patterns of human

ILFBs, the increased HSP90 expression was observed in ILFBs from bleomycin-challenged mice.

17-DMAG, an analogue of 17-AAG, is water soluble and displays high oral bioavailability and low toxicity, which make it desirable for therapeutic purposes (Egorin et al., 1998). In the bleomycin-challenged mice model, therapeutic dosing (10 mg/kg or 25 mg/kg, every 2 days) of the small molecular HSP90 inhibitor 17-DMAG was demonstrated for the first time.

Further, HSP90 inhibitor *in vivo* can attenuate experimental pulmonary fibrosis and improves lung function. Bleomycin-challenged mice exhibited significant loss of body weight compared to sham control, whereas 17-DMAG improved bodyweight, with a greater gain of body weight in the higher dose (25 mg/kg)-treated mice. The fibrosis scoring and collagen content was decreased in the group treated with 17-DMAG in comparison with bleomycin-challenged mice. It was also shown that in unilateral ureteral obstruction (UUO) model of kidney fibrosis, the HSP90 inhibitor reduces collagen deposition on tissue sections as well as prevents the elevation of TGF-β receptor II expression at protein level (Noh et al., 2012).

### 5.8.1. The role of inflammation in IPF

The inflammatory response is the initial response following injury challenges and fibrosis is generally a final outcome of the inflammatory process in the lung. The response is characterized by migration and activation of both resident and circulating inflammatory cells, including macrophages, neutrophils, lymphocytes, the production of cytokines and growth factors (Gong et al., 2005). Inflammatory and epithelial cells release cytokines/growth factors, such as TNF-α, TGF-β, interleukin 1 (IL)-1, 6 and 8, insulin-like growth factor (IGF)-1 and platelet-derived growth factor (PDGF) as well as stimulate migration, secretory activities and collagen production by fibroblasts. Meanwhile, injury causes increased permeability of the pulmonary epithelium and endothelium, resulting in extravasation of plasma proteins and ultimately extracellular matrix remodeling and fibrin deposition in the alveolar lumen and interstitium (Ou et al., 2009).

The changes in cellular profiles in BAL fluid has been well investigated in bleomycin-induced fibrosis (Oku et al., 2008). Kim and collegues demonstrated dose response effects of bleomycin on inflammation and pulmonary fibrosis. They found the modest increase of the number of neutrophils and leukocytes on day 7, whereas at day 24 the

neutrophil number dropped (Kim et al., 2010). In this study, inflammatory cell composition in bronchoalveolar lavage fluid (BALF) was evaluated. BALF collected on D21 revealed a significant reduced percentage of macrophages in bleomycin-challenged group compared to sham control and elevated percentage of lymphocytes and neutrophils. After treatment with two doses of 17-DMAG, the percentage of macrophages was partially restored and the percentage of lymphocytes and neutrophils was markedly decreased compared to the bleomycin-challenged mice. Taken together, *in vivo* data suggest that 17-DMAG reduces bleomycin-induced fibrosis.

### 5.8.2. The role of matrix metalloproteinases in IPF

MMP is a key element of tissue repairing, cell invasion and epithelium basement membrane destruction (Dancer et al., 2011)(Clarke et al., 2013). Fluorogenic MMP substrates noninvasively present that tumors have elevated MMP activity compared to non-tumor-bearing animals. Littlepage and colleagues suggest distinct contribution by MMPs to the progression of aggressive prostate tumour and to helping tumours cleverely find alternative route for malignant progression (Littlepage et al., 2010). Further, these fluorogenic MMP substrates can directly assess the efficacy of MPIs (MMP inhibitors) on MMP activity in intact tumors *in vivo*. Bremer and colleagues show for the first time that the effect of MMP inhibition can be directly imaged within hours after the initiation of treatment using the potent MMP inhibitor, prinomastat (Bremer et al., 2001).

Inhibitors of MMPs have been tested in various animal models of acute and chronic inflammation, as well as in invasive cancer because of their potential in therapeutic approaches. Several lines of study pointed to models used to study the pathophysiology of MMP9. Many inflammatory and vascular animal models were developed for human diseases and the effects of inhibitors have been tested by using MMP9 inhibitors (Hu et al., 2007).

Matrix metalloproteinases (MMPs) degrade all of the extracellular matrix components and may play a role in abnormal alveolar permeability in IPF. MMP1, MMP2 and MMP7 are the most highly expressed genes in IPF (Zuo et al., 2002). Most of these enzymes are localized in epithelial cells, some of them in fibroblast foci. MMP1 is expressed by epithelial cells and it is not present in fibroblasts. MMP2 and MMP9 are strongly localized in fibroblast foci and involved in the disruption of epithelial basement

membrane. The increased level of MMP9 is found in the bronchoalveolar lavage of patients suffering from IPF and is attributed to severe clinical phenotype (García-Alvarez et al., 2006). Additionally, in patients with IPF, impaired balance between MMPs and TIMPs (tissue inhibitor of matrix metalloproteinases) is affected by oxygen species. A profibrotic environment is promoted by reactive oxygen species that induce the imbalance between MMPs and tissue inhibitors of metalloproteinases (TIMP) and activate TGF-β (Kinnula et al., 2005).

Several studies have suggested that there is an increase in MMPs, rather than a loss of MMPs, in IPF (McKeown et al., 2009). In this context, the total pulmonary MMP activity was examined using fluorescence molecular tomographic (FMT) imaging, a state-of-art *in vivo* imaging technology. To monitor the metalloproteinase (MMP) activity by fluorescence molecular tomography (FMT) in the response to the 17-DMAG treatment *in vivo*, a MMP activable probe (MMP680Sense) was introduced. The fluorescence signal that reflected MMP activity was elevated in mice administrated with bleomycin The treatment with the lower dose of 17-DMAG slightly decreases the activity of enzyme, whereas the high dose markedly reduces the activity of MMPs These data showed that the treatment with 17-DMAG diminishes the activity of MMPs in bleomycin- induced fibrosis.

### 5.9. Links of idiopathic pulmonary fibrosis to cancer biology

It has been recently hypothesized that IPF might be considered as a neoproliferative disorder of the lung because it exhibits several pathogenic similarities to cancer. Epigenetic and genetic abnormalities, altered cell-cell communication, uncontrolled proliferation and tissue invasion are fundamental biological hallmarks characterizing both IPF and cancer. Such vision can help to identify new pathogenic mechanisms borrowed from cancer biology, leading to new and more effective approaches (Vancheri, 2012).

# 6. CONCLUSIONS

Based on the current study, the mechanism by which HSP90 promotes pulmonary fibrosis, is presented in the schematic diagram presented in Figure 31. Excessive TGF-β1, a highly pro-fibrotic cytokine, binds to TGF-βRII and forms a complex together with TGF-βRI, which is stabilized by HSP90 interaction. The activated TGF-βRI kinase phosphorylates Smad2/3, which subsequently recruits Smad4, and translocates into nucleus to initiate expression of fibrotic genes.

On the other hand, HSP90 inhibitor (eg. 17-AAG or 17-DMAG) blocks HSP90 and prevents the formation of HSP90/TGF-βRs complex, thus promotes degradation of TGFβRs in proteasomes. This terminates the TGF-β signaling pathway and blocks transdifferentiation of myofibroblasts from fibroblasts or epithelial cells in the lung.

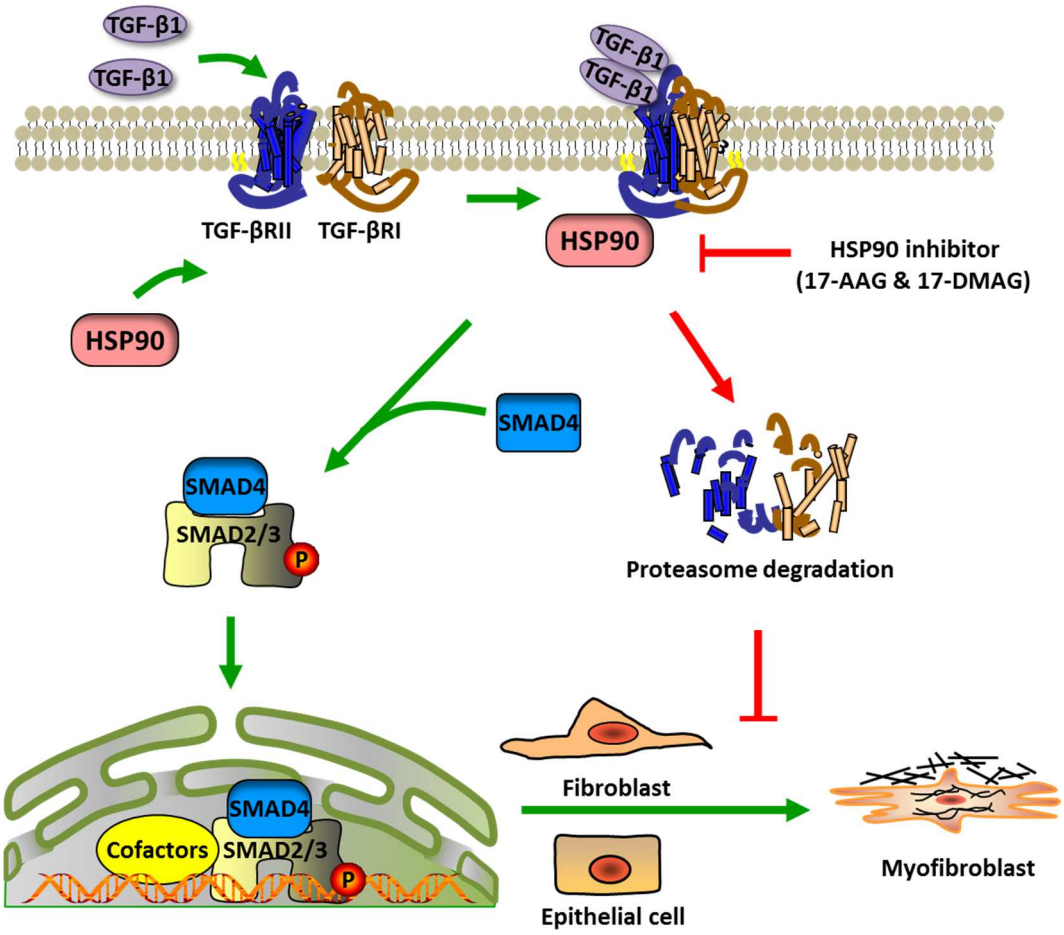


**Figure 31. Schematic diagram for the proposed mechanism by which HSP90 promotes pulmonary fibrosis.** HSP90 (heat shock protein 90); TGF-β R: transforming growth factor receptor; TGF-β:

transforming growth factor; 17-DMAG: 17-(Dimethylaminoethylamino - 17 -demethoxygeldanamycin; 17-AAG: 17-Allylamino-17-demethoxygeldanamycin.

In conclusion, for the first time a pathogenic role of HSP90 was demonstrated in pulmonary fibrosis by manipulating TGF-β-Smad2/3 signaling *in vitro* and *in vivo*. The clinical implications of the findings are profound, because the profibrotic phenotype features are sensitized through HSP90 machinery in pulmonary fibrosis, which may present therapeutic advantages of HSP90 inhibitors in treating IPF.

# 7. PROSPECTIVES

The role of TGF-β in the pathogenesis of IPF has been well characterized. TGF-β is actively involved in initiation and progression of the pulmonary fibrosis (Leask and Abraham, 2004); (Fernandez and Eickelberg, 2012b). More comprehensive study with TGF-β receptors overexpressing mice are clearly required in the future. The gain-of-function experiments seem to be helpful to elucidate the association between TGF-β receptors and HSP90 in pulmonary fibrosis. Tomcik and colleagues demonstrated in replication-deficient adeno-associated virus encoding constitutively active TGF-β receptor I, that 17-AAG reduced dermal thickening, collagen deposition and reduced number of myofibroblast in dermal fibrosis (Tomcik et al., 2014).

In this study only TGF-β receptor I and II were investigated as a client protein for HSP90. It may also be necessary to introduce new profibrotic clients, with the emphasis on those which can be used in the animal model. Haupt and colleagues have been able to classify 64 kinases as true HSP90 clients with the strong representation of pathways associated with tumour progression like the BMP, MAPK and TGF-β signaling cascades. It is of interest to discover new HSP90 clients, which could provide new opportunities for the treatment of pulmonary fibrosis and diagnostic applications (Haupt et al., 2012).

# 8. LIMITATIONS OF THE STUDY

There were limitations to this study. First, the *in vivo* experiment were designed in the model of bleomycin-induced fibrosis. Although this model is used the most frequently, it has been known to have some disadvantages. The lung fibrosis is resolved after 28 days when bleomycin is delivered by intratracheal route. Further, the inflammatory phase occurs within first week, therefore to study the effects of antifibrotic agents, the therapy should be introduced after this phase (B. Moore et al., 2013). In contrast to human lung fibrosis, this model does not reveal a prominence of hyperplastic AECs lining the areas of fibrosis which is the characteristic of usual interstitial pneumonia (UIP) (Degryse et al., 2010).

Second, the effect of HSP90 inhibitor on rescuing epithelial cells from apoptosis have been not investigated in this study. Many lines of evidence prove that lung fibrosis is associated with alveolar epithelial cell death and excessive lung fibroblast proliferation (King Jr et al., 2011; Todd et al., 2012).

Third, in this study canonical TGF-β signaling pathways was only the focus of atention. In the non-canonical pathways, the activated TGF-β receptor complex transmits a signal through other factors such as: p38 MAPK, RHO, PI3K-AKT, ERK, JNK, NF-κB (Akhurst and Hata, 2012). Noh and colleagues elucidated that the treatment with 17-AAG inhibited the phosphorylation of SMAD2, AKT, GSK-3β and ERK in a time-dependent manner (Noh et al., 2012). Their findings suggest that 17-AAG may act via different mechanism to block TGF-β1- induced signaling.

Fourth, the gain-of-function experiments were not carried out. The study of the HSP90 overexpression might elucidate its impact on migration and collagen deposition as well as the change of profibrotic markers such as collagen I, fibronectin, pSMADs and TGF-β 1 receptors.

Fifth, it was not possible to carry out *in vivo* experiments with HSP90 KO due to lack of HSP90 knockout mice. Unfortunately, mammalian Hsp90 is encoded by two genes, Hsp90α and Hsp90β, which are thought to be functionally similar and redundant. The Hsp90β knockout mouse exhibits early embryonic lethality, whereas Hsp90α-deficient mice occurs in adult males which exhibit a failure of spermatogenesis (Grad et al., 2010; Sanchez, 2012).

# 9. SUMMARY

Idiopathic pulmonary fibrosis (IPF) is a progressive, chronic and usually lethal lung disease of unknown causes with limited therapeutic options. Active myofibroblasts in the intestinal and fibroblast foci are responsible for excessive tissue remodeling in response to recurrent alveolar epithelial micro-injuries. Although the underlying mechanisms of IPF are not fully understood, transforming growth factor beta 1 (TGF-β1) is recognized as the key player in disease progression. HSP90 is a highly conserved chaperone protein and is essential for stabilization or degradation of many signaling proteins. HSP90 is centrally involved in the pathobiology of cancer and HSP90 inhibitors have been widely investigated in preclinical and clinical studies against cancer. Recent evidence shows that HSP90 promotes epithelial-mesenchymal transition (EMT) of cancer cells and TGF-β1 signaling via the stabilizing of the TGF-β receptors, however little is known about the role of HSP90 in IPF.

The purpose of the present study is to discover the role of HSP90 in lung fibroblast activation, particularly with regard to TGF-β1-induced profibrotic phenotype, and to determine the effects of HSP90 inhibitor on bleomycin-induced pulmonary fibrosis in mice.

Immunohistochemistry demonstrated intensive immunoreactivity of HSP90 in activated pulmonary fibroblasts in lungs from IPF patients. Moreover, the expression profiling using western blot showed a significant upregulation of HSP90α and HSP90β in lungs as well as primary interstitial lung fibroblasts (ILFBs) derived from IPF patients when compared with donors. Those finding directed the study at effects of HSP90 inhibition on lung fibroblast activation and fibrotic response *in vitro*.

Both resident fibroblasts and alveolar epithelial cells are sources of lung myofibroblasts via cytokine-induced transdifferentiation. TGF-β1, as such a crucial cytokine promoting fibrosis, was used to induce fibroblast activation and EMT of A549 cells in the *in vitro* study. 17-AGG, a selective HSP90 inhibitor, blocked ILFBs activation and collagen production induced by TGF-β1, as demonstrated by western blot of α-SMA expression and Sircol Soluble Collagen assay, respectively. In addition, transwell assay showed that 17-AAG inhibited ILFBs migration induced by serum. Interestingly, 17-AAG also prevented EMT of A549 cells induced by TGF-β1, revealed by western blot and immunofluorescence staining of mesenchymal and epithelial markers.

Furthermore, the diminished protein level of TGF-β RI and/or TGF-β RII was observed, along with less Smad2 phosphorylation after treatment with 17-AAG in both ILFBs and A549 cells stimulated with TGF-β1. In addition, co-immunoprecipitation confirmed a direct interaction between TGF-β RII and HSP90β in ILFBs, which implies that TGF-β receptors are clients of HSP90 and are stabilized by HSP90. And the result with MG-132, a proteasome inhibitor, indicates that the compromised interaction of HSP90 and TGF-βRs leads to proteasomal degradation of TGF-βRs.

In light of the promising *in vitro* effects, the *in vivo* effects of the highly selective HSP90 inhibitor (17-DMAG) was evaluated in attenuation of pulmonary fibrosis, using the established bleomycin-induced pulmonary fibrosis mouse model. Western blot showed increased expression of HSP90 in ILFBs from bleomycin-challenged mice as compared to sham control. Treatment with 17-DMAG (10 or 25 mg/kg) for 14 days was carried out 7 days after bleomycin challenge. 17-DMAG rescued the bodyweight loss and improved the lung compliance. Pulmonary inflammation induced by bleomycin was attenuated by 17-DMAG treatment, indicated by inflammatory cell composition from bronchoalveolar lavage fluid (BALF) and less active matrix metalloproteases (MMPs) measured by *in vivo* fluorescence molecular tomography (FMT) in combined with micro-computed tomography (μCT). Histological assessment including Ashcroft fibrosis scoring and collagen deposition all suggested that 17-DMAG ameliorates bleomycin-induced pulmonary fibrosis.

Taken together, this study supports a central role of HSP90 in progressive pulmonary fibrosis by manipulating TGF-β/Smad signaling and suggests a therapeutic potential of HSP90 inhibitors against IPF.

# 10. ZUSAMMENFASSUNG

Die idiopathische pulmonale Fibrose (IPF) ist eine fortschreitende, chronische und meist tödlich verlaufende Erkrankung mit unbekannter Ursache und wenigen Therapieoptionen. Aktivierte Myofibroblasten in fibrotischen Zentren sind für die exzessiven Gefäßveränderungen verantwortlich, welche in Folge von sogenannten Mikro-Verletzungen im alveolaren Epithel stattfinden. Obwohl die grundlegenden Mechanismen der IPF noch nicht vollständig aufgeklärt sind, wurde das Zytokin TGF-β1 (*Transforming growth factor beta 1*) bereits als ein wichtiges Schlüsselprotein in der Entstehung der Lungenfibrose identifiziert.

Hsp90 (*heat shock protein 90*) ist ein hoch konserviertes *Chaperone*-Protein und trägt zur Regulation der Stabilisierung und Degradation von vielen Signalproteinen bei. Hsp90 spielt des Weiteren in der Pathobiologie von Tumoren eine entscheidende Rolle und entsprechende Hsp90-Inhibitoren werden zurzeit in klinischen Studien in der Krebstherapie untersucht. Neueste Erkenntnisse zeigen, dass Hsp90 die zelluläre Umwandlung von Tumorzellen vom epithelialen zum mesenchymalen Phänotyp (*EMT: epithelial-to-mesenchymal transition*) durch eine Stabilisierung der TGF-β-Rezeptor-Proteine und damit die Aktivierung des nachgeschalteten TGF-β1-Signalweges unterstützt. Ob Hsp90 im Falle der IPF den TGF-β1 Signalweges auf die gleiche Weise reguliert, ist allerdings noch unklar.

Ziel der hier vorgelegten Doktorarbeit ist es, die Rolle von Hsp90 in der Aktivierung der pulmonalen Fibroblasten zu untersuchen. Dabei ist besonders der TGF-β1-induzierte pro-fibrotische Phänotype von Interesse. Des Weiteren soll ein Hsp90-inhibitor im Mausmodell der Bleomycin-induzierten Lungenfibrose auf seine therapeutische Effektivität getestet werden.

Die immunhistochemische Analyse von Lungen von IPF-Patienten zeigte eine deutliche Immunoreaktivität von spezifischen anti-Hsp90-Antikörpern in aktivierten pulmonalen Fibroblasten. Mittels Western-Blot-Verfahren konnte eine signifikante Erhöhung der Proteinexpression der beiden Hsp90-Isoformen, Hsp90α und Hsp90β, in Lungenhomogenisaten und primären, interstitiellen Lungenfibroblasten (*ILFB: interstitial lung fibroblasts*) von IPF-Patienten im Vergleich zu gesunden Donoren festgestellt werden. Die Daten dienten als Ausgangpunkt für die Untersuchungen von

Hsp90-Inhibitoren auf die Aktivierung von Lungenfibroblasten und dessen pro-fibrotische Reaktion in Zellkulturversuchen *in vitro*.
Sowohl gewebsständige Fibroblasten als auch alveolare Epithelzellen können sich über Zytokin-induzierte Transdifferenzierung zu pulmonalen Myofibroblasten entwickeln. Das pro-fibrotische Zytokin TGF-β1 wurde in den *in vitro*-Studien verwendete, um diese Fibroblasten-Aktivierung und die EMT von A549-Zellen (abgeleitet aus einem Adenokarzinom von humanem alveolaren Basal-Epithelzellen) auszulösen. Der selektive Hsp90-Inhibitor, 17-AAG, blockierte die TGF-β1-abhängige ILFB-Aktivierung und Kollagen-Synthese, was in Western-Blot-Analysen auf Myofibroblast-Markerproteine und einem Sircol-Kollagen-Test gezeigt werden konnte. Zusätzlich konnte in einem Transwell-Migrationstest die 17-AAG-vermittelte Inhibition der Serum-induzierten ILFB-Migration nachgewiesen werden. Auch die TGF-β1-induzierte EMT von A549-Zellen ließ sich durch die Zugabe von 17-AAG hemmen. Als Techniken kamen hier das Western-Blot-Verfahren und eine Immunfluoreszenz auf spezifische mesenchymale und epitheliale Marker zur Anwendung.

Zusätzlich konnte eine Abnahme der Expression des TGF-β1-Rezeptor I und/oder II in Kombination mit einer reduzierten Smad2-Phosphorylierung nach der Verabreichung von 17-AAG in beiden Zellsystemen, ILFB und A549, *in vitro* beobachtet werden. Eine Ko-Immunpräzipitation bestätigte eine direkte Protein-Protein-Interaktion des TGF-β1-Rezeptor II mit dem Chaperone Hsp90 in ILFB, was zu der Vermutung führte, dass der Rezeptor ein sogenanntes Substrat-Protein (*client*) für das Chaperone Hsp90 ist und dass der TGF-β1-Rezeptor II durch diese proteinbiochemische Bindung stabilisiert bzw. vor einer Degradation geschützt wird. Versuche mit dem Proteasom-Inhibitor MG-132 konnten zeigen, dass es sich um eine proteasomale Degradation der TGF-β1-Rezeptoren nach ihrer erfolgten Bindung an Hsp90 handelt.

Aufgrund der vielversprechenden *in vitro* Daten wurde der 17-AAG-verwandte Hsp90-inhibitor, 17-DMAG, im etablierten Mausmodell der Bleomycin-induzierten IPF auf sein therapeutisches Potential hin untersucht. Die Western-Blot-Analyse der ILFB zeigte einen deutlichen Anstieg der Hsp90-Expression in Bleomycin-verabreichten Mäusen im Vergleich zu gesunden Tieren. Die Behandlung mit 17-DMAG (mit 10 bzw. 25 mg/kg Körpergewicht) erfolgte ab dem 7. Tag nach Bleomycin-Gabe für die folgenden 14 Tage. Dabei konnte eine Gewichtsreduktion, wie sie üblicherweise unter Bleomycin-Verabreichung zu beobachten ist, verhindert und ein wesentlicher Parameter für die

Lungenfunktion, d.h. die Lungen-Dehnbarkeit (*Compliance*) verbessert werden. Die Analyse der broncho-alveolaren Spülflüssigkeit (*BALF: bronchoalveolar lavage fluid*) zeigte eine verminderte Präsenz von inflammatorischen Zellen in den Tieren, denen neben Bleomycin gleichzeitig auch 17-DMAG verabreicht wurde. Mittels einer Echtzeit-FMT-µCT-Messung (*fluorescence molecular tomography combined with micro-computed tomography*) konnte in diesen Tieren ebenfalls eine reduzierte Aktivität der Matrix-Metalloproteasen *in vivo* gemessen werden. Diese Ergebnisse deuteten darauf hin, dass eine 17-DMAG-Behandlung die durch Bleomycin-ausgelöste sInflammationsreaktion abgeschwächt hat. Eine histologische Untersuchung inklusive der Einstufung auf der Ashcroft-Fibrose-Skala und die Bestimmung der Kollagen-Deposition ließen vermuten, dass der Hsp90-Inhibitor, 17-DMAG, die Entstehung der Bleomycin-induzierten pulmonalen Fibrose verhindern bzw. verzögern kann.

Zusammengefasst lässt sich sagen, dass die hier vorgestellten Ergebnisse zum einen unzweifelhaft eine zentrale Rolle von Hsp90 in der fehlgeleiteten Regulation des TGF-β1/Smad-Signalweges in der pulmonalen Fibrose demonstrieren. Zum anderen wird das therapeutische Potential einer entsprechenden Hsp90-Inhibition, wie z.B. durch 17-DMAG, in der Behandlung der IPF am Beispiel des murinen Bleomycin-Modells aufgezeigt.

# 11. ABBREVIATIONS

**17-AAG** - 17-Allylamino-17-demethoxygeldanamycin

**17-DMAG** - 17-(Dimethylaminoethylamino)-17-demethoxygeldanamycin

**AD** - Alzheimer's disease

**AEC** - alveolar epithelial cell

**AHA1** - activator of HSP90 ATPase 1

**ALKs** - activing- receptor-like kinase

**AP** - Alkaline phosphatase

**APS** - ammonium persulfate

**ATF6** - activating transcription factor 6

**ATP** - adenosine triphosphate

**BAL** - bronchoalveolar lavage

**bFGF** - basic fibroblast growth factor

**BMP** - bone morphogenetic protein

**BS3** - bis(sulfosuccinimidyl)suberate

**BSA** - bovine serum albumin

**CC10** - Clara cell 10

**CDC37** - cycle 37 homologue

**cDNA** - complementary deoxyribonucleic acid

**CHOP** - CCAAT/enhancer-binding protein (C/EBP) homologous protein

**COD** - coefficient of determination

**co-SMADs** - common partner SMADs

**Ct** - threshold cycle

**CTD** - c-terminal domain

**CTGF** - connective tissue growth factor

**CXCL10** - chemokine (c-x-c) motif ligand 10

**CXCR4** - C-X-C chemokine receptor 4

**Da** - dalton

**DAPI** - 4',6-diamidino-2-phenylindole

**DLCO** - diffusing capacity of the lung for carbon monoxide

**DPLD** - diffuse parenchymal lung disease

**DT** - diphtheria toxin

**DTT** - dithiothreitol

**EBV** - Epstein-Barr virus

**ECL** - enhanced chemiluminescence

**EDTA** - ethylenediaminetetraacetic acid

**EGF** - human epidermal growth factor

**EMT** - epithelial - mesenchymal transition

**eNOS** - endothelial nitric-oxide synthase

**ER stress** - endoplasmic reticulum stress

**et al.** - et alii (and others)

**FITC** - fluorescein isothiocyanate

**FMT**- fluorescence molecular tomography

**FOT** - forces oscillation technique

**FVC** - forced vital capacity

**FXa** - factor Xa

**g** - gram

**GER** - gastroesophageal reflux

**GM** - benzoquinone ansamycin geldanamycin

**GRP94** - glucose-regulated protein 94

**HIF** - hypoxia inducible factor

**hILFBs**- human interstitial lung fibroblasts

**HRP** - horse radish peroxidase

**HSP90α A1**- hsp90α class a1

**HSP90α B1**- hsp90α class b1

**HX** - histiocytosis x

**IFN-γ** - interferon-γ

**IIP** - idiopathic interstitial pneumonia

**IL** - interleukin

**IPF** - idiopathic pulmonary fibrosis

**IRE1α** - inositol requiring enzyme 1α

**i-SMADs** - inhibitory SMADs

**kb** - kilo base pairs

**KCl** - potassium chloride

**kDa** - kilo dalton

**$KH_2PO_4$** - monopotassium phosphate

**LAM** - lymphangioleiomyomatosis

**LAP** - latency associated peptide

**lLB** - luria broth

**LTBP** - latent TGF-β-binding proteins

**LTGF-β** - latent precursor molecules of TGF- β

**M** - molar (mole/litre)

**MAPK** - mitogen-activated protein kinase

**MD** - middle-domain

**mg** - milligram

**min** - minute(s)

**miRNA** - microRNA

**ml** - milliliter

**mM** - millimolar

**MMP** - matrix metalloproteinase

**MUC5B** - mucin 5B

**$NA_2HPO_4$ x $H_2O$** - disodium phosphate dihydrate

**NaCl** - sodium chloride

**NADPH** - nicotinamide adenine dinucleotide phosphate-oxidase

**NALP3** - NACHT and LRR, PYD domains-containing protein 3

**nm** - nanometer

**nM** - nanomolar

**NO** - nitric oxide

**NQO1** - NADPH quinone oxidoreductase 1

**NTD** - n-terminal domain

**$PaO_2$** - partial pressure of oxygen in arterial blood

**PBS** - phosphate-buffered saline

**PCR** - polymerase chain reaction

**PDGF**- platelet-derived growth factor

**PERK** - protein kinase RNA-like ER kinase

**PFA** - paraformaldehyde

**PGE2** - prostaglandin E2

**qRT-PCR** - quantitive realtime- polymerase chain reaction

**RD** - macrolactone radicicol

**ROS** - reactive oxygen species

**RPM** - revolution per minute

**RT** - room temperature

**SARA** - anchor for receptor activation

**SDS-PAGE** - SDS-polyacrylamide gel electrophoresis

**SP-C** - surfactant protein C

**TBST** - Tris-buffered saline and Tween 20

**TEMED** - tetramethylethylenediamine

**TERC** - telomerase RNA template component

**TERT** - reverse transcriptase component

**TF** - tissue factor

**TGF-β receptor** - transforming growth factor receptor

**TIMP** - tissue inhibitor of metalloproteinases

**TNF** - tumor necrosis factor

**TRAP1** - tumour necrosis factor receptor-associated protein 1

**UIP** - usual interstitial pneumonia

**UPR** - unfolded protein response

**V** - volt

**VCAM-1 -** vascular cell adhesion molecule-1

**VEGF** - vascular endothelial growth factor

**VEGFR2** - vascular endothelial growth factor receptor 2

**α-SMA** - alpha smooth muscle actin

**μCT** - micro computed tomography

**μg** - microgram

**μl** - microliter

**μm** - micrometer

**μM** - micromolar

# 12. LIST OF FIGURES

# 13. LIST OF TABLES

# 14. BIBLIOGRAPHY

**1.** Agostini, C., and Gurrieri, C. (2006). Chemokine/Cytokine Cocktail in Idiopathic Pulmonary Fibrosis. Proc. Am. Thorac. Soc. *3*, 357–363.

**2.** Akhmetshina, A., Palumbo, K., Dees, C., Bergmann, C., Venalis, P., Zerr, P., Horn, A., Kireva, T., Beyer, C., Zwerina, J., et al. (2012). Activation of canonical Wnt signalling is required for TGF-β-mediated fibrosis. Nat. Commun. *3*, 735.

**3.** Akhurst, R.J., and Hata, A. (2012). Targeting the TGFβ signalling pathway in disease. Nat. Rev. Drug Discov. *11*, 790–811.

**4.** Ambade, A., Catalano, D., Lim, A., and Mandrekar, P. (2012). Inhibition of hsp90 attenuates pro-inflammatory cytokines and prevents LPS induced liver injury. Hepatol. Baltim. Md *55*, 1585–1595.

**5.** Annamalai, B., Liu, X., Gopal, U., and Isaacs, J. (2009). Hsp90 is an essential regulator of EphA2 receptor stability and signaling: Implications for cancer cell migration and metastasis. Mol. Cancer Res. MCR *7*, 1021–1032.

**6.** Annes, J.P., Munger, J.S., and Rifkin, D.B. (2003). Making sense of latent TGFbeta activation. J. Cell Sci. *116*, 217–224.

**7.** Antoniou, K.M., Margaritopoulos, G.A., and Siafakas, N.M. (2013). Pharmacological treatment of idiopathic pulmonary fibrosis: from the past to the future. Eur. Respir. Rev. *22*, 281–291.

**8.** Aoyagi-Ikeda, K., Maeno, T., Matsui, H., Ueno, M., Hara, K., Aoki, Y., Aoki, F., Shimizu, T., Doi, H., Kawai-Kowase, K., et al. (2011). Notch Induces Myofibroblast Differentiation of Alveolar Epithelial Cells via Transforming Growth Factor–β–Smad3 Pathway. Am. J. Respir. Cell Mol. Biol. *45*, 136–144.

**9.** Ashcroft, T., Simpson, J.M., and Timbrell, V. (1988). Simple method of estimating severity of pulmonary fibrosis on a numerical scale. J. Clin. Pathol. *41*, 467–470.

**10.** ATS, and ERS (2000). Idiopathic Pulmonary Fibrosis: Diagnosis and Treatment. Am. J. Respir. Crit. Care Med. *161*, 646–664.

**11.** ATS, and ERS (2002). American Thoracic Society/European Respiratory Society International Multidisciplinary Consensus Classification of the Idiopathic Interstitial Pneumonias. Am. J. Respir. Crit. Care Med. *165*, 277–304.

**12.** Balanis, N., Wendt, M.K., Schiemann, B.J., Wang, Z., Schiemann, W.P., and Carlin, C.R. (2013). Epithelial-to-Mesenchymal Transition Promotes Breast Cancer Progression via a Fibronectin-Dependent Stat3 Signaling Pathway. J. Biol. Chem. jbc.M113.475277.

**13.** Baumgartner, K.B., Samet, J.M., Stidley, C.A., Colby, T.V., and Waldron, J.A. (1997). Cigarette smoking: a risk factor for idiopathic pulmonary fibrosis. Am. J. Respir. Crit. Care Med. *155*, 242–248.

**14.** Blagosklonny, M.V., Toretsky, J., Bohen, S., and Neckers, L. (1996). Mutant conformation of p53 translated in vitro or in vivo requires functional HSP90. Proc. Natl. Acad. Sci. U. S. A. *93*, 8379–8383.

**15.** Bonner, J.C. (2004). Regulation of PDGF and its receptors in fibrotic diseases. Cytokine Growth Factor Rev. *15*, 255–273.

**16.** Bonniaud, P., Margetts, P.J., Kolb, M., Schroeder, J.A., Kapoun, A.M., Damm, D., Murphy, A., Chakravarty, S., Dugar, S., Higgins, L., et al. (2005). Progressive Transforming Growth Factor β1–induced Lung Fibrosis Is Blocked by an Orally Active ALK5 Kinase Inhibitor. Am. J. Respir. Crit. Care Med. *171*, 889–898.

**17.** Borthwick, L.A., Wynn, T.A., and Fisher, A.J. (2013). Cytokine mediated tissue fibrosis. Biochim. Biophys. Acta BBA - Mol. Basis Dis. *1832*, 1049–1060.

**18.** Boulon, S., Marmier-Gourrier, N., Pradet-Balade, B., Wurth, L., Verheggen, C., Jády, B.E., Rothé, B., Pescia, C., Robert, M.-C., Kiss, T., et al. (2008). The Hsp90 chaperone controls the biogenesis of L7Ae RNPs through conserved machinery. J. Cell Biol. *180*, 579–595.

**19.** Brady, C.A., and Attardi, L.D. (2010). p53 at a glance. J. Cell Sci. *123*, 2527–2532.

**20.** Caraci, F., Gili, E., Calafiore, M., Failla, M., La Rosa, C., Crimi, N., Sortino, M.A., Nicoletti, F., Copani, A., and Vancheri, C. (2008). TGF-β1 targets the GSK-3β/β-catenin pathway via ERK activation in the transition of human lung fibroblasts into myofibroblasts. Pharmacol. Res. *57*, 274–282.

**21.** Cassel, S.L., Eisenbarth, S.C., Iyer, S.S., Sadler, J.J., Colegio, O.R., Tephly, L.A., Carter, A.B., Rothman, P.B., Flavell, R.A., and Sutterwala, F.S. (2008). The Nalp3 inflammasome is essential for the development of silicosis. Proc. Natl. Acad. Sci. U. S. A. *105*, 9035–9040.

**22.** Cheresh, P., Kim, S.-J., Tulasiram, S., and Kamp, D.W. (2013). Oxidative stress and pulmonary fibrosis. Biochim. Biophys. Acta BBA - Mol. Basis Dis. *1832*, 1028–1040.

**23.** Citri, A., Skaria, K.B., and Yarden, Y. (2003). The deaf and the dumb: the biology of ErbB-2 and ErbB-3. Exp. Cell Res. *284*, 54–65.

**24.** Clarke, D.L., Carruthers, A.M., Mustelin, T., and Murray, L.A. (2013). Matrix regulation of idiopathic pulmonary fibrosis: the role of enzymes. Fibrogenesis Tissue Repair *6*, 20.

**25.** Dancer, R.C.A., Wood, A.M., and Thickett, D.R. (2011). Metalloproteinases in idiopathic pulmonary fibrosis. Eur. Respir. J. *38*, 1461–1467.

**26.** Daniels, C.E., Lasky, J.A., Limper, A.H., Mieras, K., Gabor, E., and Schroeder, D.R. (2010). Imatinib Treatment for Idiopathic Pulmonary Fibrosis. Am. J. Respir. Crit. Care Med. *181*, 604–610.

**27.** Davis, G.S., Leslie, K.O., and Hemenway, D.R. (1998). Silicosis in mice: effects of dose, time, and genetic strain. J. Environ. Pathol. Toxicol. Oncol. Off. Organ Int. Soc. Environ. Toxicol. Cancer *17*, 81–97.

**28.** Degryse, A.L., and Lawson, W.E. (2011). PROGRESS TOWARD IMPROVING ANIMAL MODELS FOR IPF. Am. J. Med. Sci. *341*, 444–449.

**29.** Degryse, A.L., Tanjore, H., Xu, X.C., Polosukhin, V.V., Jones, B.R., McMahon, F.B., Gleaves, L.A., Blackwell, T.S., and Lawson, W.E. (2010). Repetitive intratracheal bleomycin models several features of idiopathic pulmonary fibrosis. Am. J. Physiol. - Lung Cell. Mol. Physiol. *299*, L442–L452.

**30.** DeZwaan, D.C., Toogun, O.A., Echtenkamp, F.J., and Freeman, B.C. (2009). The Hsp82 molecular chaperone promotes a switch between unextendable and extendable telomere states. Nat. Struct. Mol. Biol. *16*, 711–716.

**31.** Dickey, C.A., Kamal, A., Lundgren, K., Klosak, N., Bailey, R.M., Dunmore, J., Ash, P., Shoraka, S., Zlatkovic, J., Eckman, C.B., et al. (2007). The high-affinity HSP90-CHIP complex recognizes and selectively degrades phosphorylated tau client proteins. J. Clin. Invest. *117*, 648–658.

**32.** Ten Dijke, P., and Hill, C.S. (2004). New insights into TGF-beta-Smad signalling. Trends Biochem. Sci. *29*, 265–273.

**33.** Dollins, D.E., Warren, J.J., Immormino, R.M., and Gewirth, D.T. (2007). Structures of GRP94-nucleotide complexes reveal mechanistic differences between the hsp90 chaperones. Mol. Cell *28*, 41–56.

**34.** Dörthe M Katschinski, L.L. (2004). Interaction of the PAS B domain with HSP90 accelerates hypoxia-inducible factor-1 alpha stabilization. Cell. Physiol. Biochem. Int. J. Exp. Cell. Physiol. Biochem. Pharmacol. *14*, 351–360.

**35.** Eckl, J.M., and Richter, K. (2013). Functions of the Hsp90 chaperone system: lifting client proteins to new heights. Int. J. Biochem. Mol. Biol. *4*, 157–165.

**36.** Egorin, M.J., Rosen, D.M., Wolff, J.H., Callery, P.S., Musser, S.M., and Eiseman, J.L. (1998). Metabolism of 17-(allylamino)-17-demethoxygeldanamycin (NSC 330507) by murine and human hepatic preparations. Cancer Res. *58*, 2385–2396.

**37.** Faner, R., Rojas, M., MacNee, W., and Agustí, A. (2012). Abnormal Lung Aging in Chronic Obstructive Pulmonary Disease and Idiopathic Pulmonary Fibrosis. Am. J. Respir. Crit. Care Med. *186*, 306–313.

**38.** Feng, X.-H., and Derynck, R. (2005). SPECIFICITY AND VERSATILITY IN TGF-β SIGNALING THROUGH SMADS. Annu. Rev. Cell Dev. Biol. *21*, 659–693.

**39.** Fernandez, I.E., and Eickelberg, O. (2012a). New cellular and molecular mechanisms of lung injury and fibrosis in idiopathic pulmonary fibrosis. The Lancet *380*, 680–688.

**40.** Fernandez, I.E., and Eickelberg, O. (2012b). The Impact of TGF-β on Lung Fibrosis: From Targeting to Biomarkers. Proc. Am. Thorac. Soc. *9*, 111–116.

**41.** Flaherty, K.R., King, T.E., Raghu, G., Lynch, J.P., Colby, T.V., Travis, W.D., Gross, B.H., Kazerooni, E.A., Toews, G.B., Long, Q., et al. (2004). Idiopathic Interstitial Pneumonia. Am. J. Respir. Crit. Care Med. *170*, 904–910.

**42.** Fortugno, P., Beltrami, E., Plescia, J., Fontana, J., Pradhan, D., Marchisio, P.C., Sessa, W.C., and Altieri, D.C. (2003). Regulation of survivin function by Hsp90. Proc. Natl. Acad. Sci. *100*, 13791–13796.

**43.** Fukuda, M., Ikuta, K., Yanagihara, K., Tajima, M., Kuratsune, H., Kurata, T., and Sairenji, T. (2001). Effect of Transforming Growth Factor-β1 on the Cell Growth and Epstein–Barr Virus Reactivation in EBV-Infected Epithelial Cell Lines. Virology *288*, 109–118.

**44.** Fulkerson, P.C., Fischetti, C.A., and Rothenberg, M.E. (2006). Eosinophils and CCR3 Regulate Interleukin-13 Transgene-Induced Pulmonary Remodeling. Am. J. Pathol. *169*, 2117–2126.

**45.** García-Alvarez, J., Ramirez, R., Sampieri, C.L., Nuttall, R.K., Edwards, D.R., Selman, M., and Pardo, A. (2006). Membrane type-matrix metalloproteinases in idiopathic pulmonary fibrosis. Sarcoidosis Vasc. Diffuse Lung Dis. Off. J. WASOG World Assoc. Sarcoidosis Granulomatous Disord. *23*, 13–21.

**46.** Gaspar, N., Sharp, S.Y., Pacey, S., Jones, C., Walton, M., Vassal, G., Eccles, S., Pearson, A., and Workman, P. (2009). Acquired Resistance to 17-Allylamino-17-Demethoxygeldanamycin (17-AAG, Tanespimycin) in Glioblastoma Cells. Cancer Res. *69*, 1966–1975.

**47.** Geller, R., Vignuzzi, M., Andino, R., and Frydman, J. (2007). Evolutionary constraints on chaperone-mediated folding provide an antiviral approach refractory to development of drug resistance. Genes Dev. *21*, 195–205.

**48.** Geller, R., Andino, R., and Frydman, J. (2013). Hsp90 Inhibitors Exhibit Resistance-Free Antiviral Activity against Respiratory Syncytial Virus. PLoS ONE *8*, e56762.

**49.** Gong, L., Li, X., Wang, H., Zhang, L., Chen, F., Cai, Y., Qi, X., Liu, L., Liu, Y., Wu, X., et al. (2005). Effect of Feitai on bleomycin-induced pulmonary fibrosis in rats. J. Ethnopharmacol. *96*, 537–544.

**50.** Grad, I., Cederroth, C.R., Walicki, J., Grey, C., Barluenga, S., Winssinger, N., De Massy, B., Nef, S., and Picard, D. (2010). The molecular chaperone Hsp90α is required for meiotic progression of spermatocytes beyond pachytene in the mouse. PloS One *5*, e15770.

**51.** Günther, A., Mosavi, P., Ruppert, C., Heinemann, S., Temmesfeld, B., Velcovsky, H.G., 1, H.M., Grimminger, F., Walmrath, D., and Seeger, W. (2000). Enhanced Tissue Factor Pathway Activity and Fibrin Turnover in the Alveolar Compartment of Patients with Interstitial Lung Disease. Thromb Haemost *83*, 853–860.

**52.** Haupt, A., Joberty, G., Bantscheff, M., Fröhlich, H., Stehr, H., Schweiger, M.R., Fischer, A., Kerick, M., Boerno, S.T., Dahl, A., et al. (2012). Hsp90 inhibition differentially destabilises MAP kinase and TGF-beta signalling components in cancer cells revealed by kinase-targeted chemoproteomics. BMC Cancer *12*, 38.

**53.** Hecker, L., Vittal, R., Jones, T., Jagirdar, R., Luckhardt, T.R., Horowitz, J.C., Pennathur, S., Martinez, F.J., and Thannickal, V.J. (2009). NADPH Oxidase-4

Mediates Myofibroblast Activation and Fibrogenic Responses to Lung Injury. Nat. Med. *15*, 1077–1081.

**54.** Homer, R.J., Elias, J.A., Lee, C.G., and Herzog, E. (2011). Modern Concepts on the Role of Inflammation in Pulmonary Fibrosis. Arch. Pathol. Lab. Med. *135*, 780–788.

**55.** http://www.perkinelmer.com/catalog/category/id/in vivo imaging In Vivo Imaging & Analysis | PerkinElmer.

**56.** Hu, J., Van den Steen, P.E., Sang, Q.-X.A., and Opdenakker, G. (2007). Matrix metalloproteinase inhibitors as therapy for inflammatory and vascular diseases. Nat. Rev. Drug Discov. *6*, 480–498.

**57.** Imokawa, S., Sato, A., Hayakawa, H., Kotani, M., Urano, T., and Takada, A. (1997). Tissue Factor Expression and Fibrin Deposition in the Lungs of Patients with Idiopathic Pulmonary Fibrosis and Systemic Sclerosis. Am. J. Respir. Crit. Care Med. *156*, 631–636.

**58.** Iwai, K., Mori, T., Yamada, N., Yamaguchi, M., and Hosoda, Y. (1994). Idiopathic pulmonary fibrosis. Epidemiologic approaches to occupational exposure. Am. J. Respir. Crit. Care Med. *150*, 670–675.

**59.** Jablonska, E., Markart, P., Zakrzewicz, D., Preissner, K.T., and Wygrecka, M. (2010). Transforming Growth Factor-β1 Induces Expression of Human Coagulation Factor XII via Smad3 and JNK Signaling Pathways in Human Lung Fibroblasts. J. Biol. Chem. *285*, 11638–11651.

**60.** Jokinen, J., Dadu, E., Nykvist, P., Käpylä, J., White, D.J., Ivaska, J., Vehviläinen, P., Reunanen, H., Larjava, H., Häkkinen, L., et al. (2004). Integrin-mediated Cell Adhesion to Type I Collagen Fibrils. J. Biol. Chem. *279*, 31956–31963.

**61.** Kamal, A., Thao, L., Sensintaffar, J., Zhang, L., Boehm, M.F., Fritz, L.C., and Burrows, F.J. (2003). A high-affinity conformation of Hsp90 confers tumour selectivity on Hsp90 inhibitors. Nature *425*, 407–410.

**62.** Khalil, N., O'Connor, R.N., Flanders, K.C., and Unruh, H. (1996). TGF-beta 1, but not TGF-beta 2 or TGF-beta 3, is differentially present in epithelial cells of advanced pulmonary fibrosis: an immunohistochemical study. Am. J. Respir. Cell Mol. Biol. *14*, 131–138.

**63.** Kilshaw, P.J. (1999). Alpha E beta 7. Mol. Pathol. *52*, 203–207.

**64.** Kim, S.N., Lee, J., Yang, H.-S., Cho, J.-W., Kwon, S., Kim, Y.-B., Her, J.-D., Cho, K.-H., Song, C.-W., and Lee, K. (2010). Dose-response Effects of Bleomycin on Inflammation and Pulmonary Fibrosis in Mice. Toxicol. Res. *26*, 217–222.

**65.** King, T.E., Brown, K.K., Raghu, G., du Bois, R.M., Lynch, D.A., Martinez, F., Valeyre, D., Leconte, I., Morganti, A., Roux, S., et al. (2011). BUILD-3: A Randomized, Controlled Trial of Bosentan in Idiopathic Pulmonary Fibrosis. Am. J. Respir. Crit. Care Med. *184*, 92–99.

**66.** King Jr, T.E., Albera, C., Bradford, W.Z., Costabel, U., Hormel, P., Lancaster, L., Noble, P.W., Sahn, S.A., Szwarcberg, J., Thomeer, M., et al. (2009). Effect of

interferon gamma-1b on survival in patients with idiopathic pulmonary fibrosis (INSPIRE): a multicentre, randomised, placebo-controlled trial. The Lancet *374*, 222–228.

**67.** King Jr, T.E., Pardo, A., and Selman, M. (2011). Idiopathic pulmonary fibrosis. The Lancet *378*, 1949–1961.

**68.** Kinnula, V.L., Fattman, C.L., Tan, R.J., and Oury, T.D. (2005). Oxidative Stress in Pulmonary Fibrosis. Am. J. Respir. Crit. Care Med. *172*, 417–422.

**69.** Königshoff, M., Kramer, M., Balsara, N., Wilhelm, J., Amarie, O.V., Jahn, A., Rose, F., Fink, L., Seeger, W., Schaefer, L., et al. (2009). WNT1-inducible signaling protein–1 mediates pulmonary fibrosis in mice and is upregulated in humans with idiopathic pulmonary fibrosis. J. Clin. Invest. *119*, 772–787.

**70.** Korfei, M., Ruppert, C., Mahavadi, P., Henneke, I., Markart, P., Koch, M., Lang, G., Fink, L., Bohle, R.-M., Seeger, W., et al. (2008). Epithelial Endoplasmic Reticulum Stress and Apoptosis in Sporadic Idiopathic Pulmonary Fibrosis. Am. J. Respir. Crit. Care Med. *178*, 838–846.

**71.** Korfei, M., Beck, D. von der, Henneke, I., Markart, P., Ruppert, C., Mahavadi, P., Ghanim, B., Klepetko, W., Fink, L., Meiners, S., et al. (2013). Comparative proteome analysis of lung tissue from patients with idiopathic pulmonary fibrosis (IPF), non-specific interstitial pneumonia (NSIP) and organ donors. J. Proteomics *Complete*, 109–128.

**72.** Kotani, I., Sato, A., Hayakawa, H., Urano, T., Takada, Y., and Takada, A. (1995). Increased procoagulant and antifibrinolytic activities in the lungs with idiopathic pulmonary fibrosis. Thromb. Res. *77*, 493–504.

**73.** Lakatos, H.F., Burgess, H.A., Thatcher, T.H., Redonnet, M.R., Hernady, E., Williams, J.P., and Sime, P.J. (2006). Oropharyngeal aspiration of a silica suspension produces a superior model of silicosis in the mouse when compared to intratracheal instillation. Exp. Lung Res. *32*, 181–199.

**74.** Lamouille, S., Xu, J., and Derynck, R. (2014). Molecular mechanisms of epithelial–mesenchymal transition. Nat. Rev. Mol. Cell Biol. *15*, 178–196.

**75.** Lasithiotaki, I., Antoniou, K.M., Vlahava, V.-M., Karagiannis, K., Spandidos, D.A., Siafakas, N.M., and Sourvinos, G. (2011). Detection of Herpes Simplex Virus Type-1 in Patients with Fibrotic Lung Diseases. PLoS ONE *6*.

**76.** Lawson, W.E., Crossno, P.F., Polosukhin, V.V., Roldan, J., Cheng, D.-S., Lane, K.B., Blackwell, T.R., Xu, C., Markin, C., Ware, L.B., et al. (2008). Endoplasmic reticulum stress in alveolar epithelial cells is prominent in IPF: association with altered surfactant protein processing and herpesvirus infection. Am. J. Physiol. - Lung Cell. Mol. Physiol. *294*, L1119–L1126.

**77.** Leask, A., and Abraham, D.J. (2004). TGF-β signaling and the fibrotic response. FASEB J. *18*, 816–827.

**78.** Lee, C.G., Cho, S.J., Kang, M.J., Chapoval, S.P., Lee, P.J., Noble, P.W., Yehualaeshet, T., Lu, B., Flavell, R.A., Milbrandt, J., et al. (2004). Early Growth

Response Gene 1–mediated Apoptosis Is Essential for Transforming Growth Factor β1–induced Pulmonary Fibrosis. J. Exp. Med. *200*, 377–389.

**79.** Lee, V.Y., Schroedl, C., Brunelle, J.K., Buccellato, L.J., Akinci, O.I., Kaneto, H., Snyder, C., Eisenbart, J., Budinger, G.R.S., and Chandel, N.S. (2005). Bleomycin induces alveolar epithelial cell death through JNK-dependent activation of the mitochondrial death pathway. Am. J. Physiol. - Lung Cell. Mol. Physiol. *289*, L521–L528.

**80.** Ley, B., Collard, H.R., and King, T.E. (2011). Clinical Course and Prediction of Survival in Idiopathic Pulmonary Fibrosis. Am. J. Respir. Crit. Care Med. *183*, 431–440.

**81.** Li, Y., Zhang, T., Schwartz, S.J., and Sun, D. (2009). New developments in Hsp90 inhibitors as anti-cancer therapeutics: Mechanisms, clinical perspective and more potential. Drug Resist. Updat. *12*, 17–27.

**82.** Lilja, A., Weeden, C.E., McArthur, K., Nguyen, T., Donald, A., Wong, Z.X., Dousha, L., Bozinovski, S., Vlahos, R., Burns, C.J., et al. (2015). HSP90 Inhibition Suppresses Lipopolysaccharide-Induced Lung Inflammation In Vivo. PLoS ONE *10*.

**83.** Lin, K., Rockliffe, N., Johnson, G.G., Sherrington, P.D., and Pettitt, A.R. (2008). Hsp90 inhibition has opposing effects on wild-type and mutant p53 and induces p21 expression and cytotoxicity irrespective of p53/ATM status in chronic lymphocytic leukaemia cells. Oncogene *27*, 2445–2455.

**84.** Lipson, K.E., Wong, C., Teng, Y., and Spong, S. (2012). CTGF is a central mediator of tissue remodeling and fibrosis and its inhibition can reverse the process of fibrosis. Fibrogenesis Tissue Repair *5*, S24.

**85.** Littlepage, L.E., Sternlicht, M.D., Rougier, N., Phillips, J., Gallo, E., Yu, Y., Williams, K., Brenot, A., Gordon, J.I., and Werb, Z. (2010). Matrix Metalloproteinases Contribute Distinct Roles in Neuroendocrine Prostate Carcinogenesis, Metastasis, and Angiogenesis Progression. Cancer Res. *70*, 2224–2234.

**86.** Maher, T.M., Wells, A.U., and Laurent, G.J. (2007). Idiopathic pulmonary fibrosis: multiple causes and multiple mechanisms? Eur. Respir. J. *30*, 835–839.

**87.** Maitra, M., Wang, Y., Gerard, R.D., Mendelson, C.R., and Garcia, C.K. (2010). Surfactant Protein A2 Mutations Associated with Pulmonary Fibrosis Lead to Protein Instability and Endoplasmic Reticulum Stress. J. Biol. Chem. *285*, 22103–22113.

**88.** Marcelo Ehrlich, O.G. (2012). Oligomeric interactions of TGF-β and BMP receptors. FEBS Lett. *586*, 1885–1896.

**89.** Matthews, S.B., Vielhauer, G.A., Manthe, C.A., Chaguturu, V.K., Szabla, K., Matts, R.L., Donnelly, A.C., Blagg, B.S.J., and Holzbeierlein, J.M. (2010). Characterization of a novel novobiocin analogue as a putative C-terminal inhibitor of heat shock protein 90 in prostate cancer cells. The Prostate *70*, 27–36.

**90.** Mayor-López, L., Tristante, E., Carballo-Santana, M., Carrasco-García, E., Grasso, S., García-Morales, P., Saceda, M., Luján, J., García-Solano, J., Carballo, F., et al. (2014). Comparative Study of 17-AAG and NVP-AUY922 in Pancreatic and Colorectal

Cancer Cells: Are There Common Determinants of Sensitivity? Transl. Oncol. *7*, 590–604.

**91.** McGovern, T.K., Robichaud, A., Fereydoonzad, L., Schuessler, T.F., and Martin, J.G. (2013). Evaluation of respiratory system mechanics in mice using the forced oscillation technique. J. Vis. Exp. JoVE e50172.

**92.** McKeown, S., Richter, A.G., O'Kane, C., McAuley, D.F., and Thickett, D.R. (2009). MMP expression and abnormal lung permeability are important determinants of outcome in IPF. Eur. Respir. J. *33*, 77–84.

**93.** Milkiewicz, M., Doyle, J.L., Fudalewski, T., Ispanovic, E., Aghasi, M., and Haas, T.L. (2007). HIF-1alpha and HIF-2alpha play a central role in stretch-induced but not shear-stress-induced angiogenesis in rat skeletal muscle. J. Physiol. *583*, 753–766.

**94.** Miyata, Y., Nakamoto, H., and Neckers, L. (2012). The Therapeutic Target Hsp90 and Cancer Hallmarks. Curr. Pharm. Des. *19*, 347–365.

**95.** Miyazono, K. (2000). Positive and negative regulation of TGF-beta signaling. J. Cell Sci. *113 ( Pt 7)*, 1101–1109.

**96.** Moeller, A., Ask, K., Warburton, D., Gauldie, J., and Kolb, M. (2008). The bleomycin animal model: A useful tool to investigate treatment options for idiopathic pulmonary fibrosis? Int. J. Biochem. Cell Biol. *40*, 362–382.

**97.** Molina-Molina, M., Pereda, J., and Xaubet, A. (2007). Experimental Models for the Study of Pulmonary Fibrosis: Current Usefulness and Future Promise. Arch. Bronconeumol. Engl. Ed. *43*, 501–507.

**98.** B. Moore, B., Lawson, W.E., Oury, T.D., Sisson, T.H., Raghavendran, K., and Hogaboam, C.M. (2013). Animal Models of Fibrotic Lung Disease. Am. J. Respir. Cell Mol. Biol. *49*, 167–179.

**99.** Van Moorsel, C.H.M., van Oosterhout, M.F.M., Barlo, N.P., de Jong, P.A., van der Vis, J.J., Ruven, H.J.T., van Es, H.W., van den Bosch, J.M.M., and Grutters, J.C. (2010). Surfactant Protein C Mutations Are the Basis of a Significant Portion of Adult Familial Pulmonary Fibrosis in a Dutch Cohort. Am. J. Respir. Crit. Care Med. *182*, 1419–1425.

**100.** Munje, C., Shervington, L., Khan, Z., and Shervington, A. (2014). Could Upregulated Hsp70 Protein Compensate for the Hsp90-Silence-Induced Cell Death in Glioma Cells? Int. J. Brain Sci. *2014*, e652643.

**101.** Murray, L.A., Argentieri, R.L., Farrell, F.X., Bracht, M., Sheng, H., Whitaker, B., Beck, H., Tsui, P., Cochlin, K., Evanoff, H.L., et al. (2008). Hyper-responsiveness of IPF/UIP fibroblasts: Interplay between TGFβ1, IL-13 and CCL2. Int. J. Biochem. Cell Biol. *40*, 2174–2182.

**102.** Myung, S.J., Yoon, J.-H., Kim, B.H., Lee, J.-H., Jung, E.U., and Lee, H.-S. (2009). Heat Shock Protein 90 Inhibitor Induces Apoptosis and Attenuates Activation of Hepatic Stellate Cells. J. Pharmacol. Exp. Ther. *330*, 276–282.

**103.** Nagaraju, G.P., Long, T.-E., Park, W., Landry, J.C., Taliaferro-Smith, L., Farris, A.B., Diaz, R., and El-Rayes, B.F. (2014). Heat shock protein 90 promotes epithelial to mesenchymal transition, invasion, and migration in colorectal cancer. Mol. Carcinog. n/a – n/a.

**104.** Nagata, Y., Anan, T., Yoshida, T., Mizukami, T., Taya, Y., Fujiwara, T., Kato, H., Saya, H., and Nakao, M. (1999). The stabilization mechanism of mutant-type p53 by impaired ubiquitination: the loss of wild-type p53 function and the hsp90 association. Oncogene *18*, 6037–6049.

**105.** Nalysnyk, L., Cid-Ruzafa, J., Rotella, P., and Esser, D. (2012). Incidence and prevalence of idiopathic pulmonary fibrosis: review of the literature. Eur. Respir. Rev. *21*, 355–361.

**106.** Noh, H., Kim, H.J., Yu, M.R., Kim, W.-Y., Kim, J., Ryu, J.H., Kwon, S.H., Jeon, J.S., Han, D.C., and Ziyadeh, F. (2012). Heat shock protein 90 inhibitor attenuates renal fibrosis through degradation of transforming growth factor-β type II receptor. Lab. Invest. *92*, 1583–1596.

**107.** Noth, I., Anstrom, K.J., Calvert, S.B., de Andrade, J., Flaherty, K.R., Glazer, C., Kaner, R.J., and Olman, M.A. (2012). A Placebo-Controlled Randomized Trial of Warfarin in Idiopathic Pulmonary Fibrosis. Am. J. Respir. Crit. Care Med. *186*, 88–95.

**108.** Oberdorster, G. (1996). Significance of particle parameters in the evaluation of exposure-dose-response relationships of inhaled particles. Inhal. Toxicol. *8 Suppl*, 73–89.

**109.** Oku, H., Shimizu, T., Kawabata, T., Nagira, M., Hikita, I., Ueyama, A., Matsushima, S., Torii, M., and Arimura, A. (2008). Antifibrotic action of pirfenidone and prednisolone: Different effects on pulmonary cytokines and growth factors in bleomycin-induced murine pulmonary fibrosis. Eur. J. Pharmacol. *590*, 400–408.

**110.** Otaka, M., Yamamoto, S., Ogasawara, K., Takaoka, Y., Noguchi, S., Miyazaki, T., Nakai, A., Odashima, M., Matsuhashi, T., Watanabe, S., et al. (2007). The induction mechanism of the molecular chaperone HSP70 in the gastric mucosa by Geranylgeranylacetone (HSP-inducer). Biochem. Biophys. Res. Commun. *353*, 399–404.

**111.** Ou, X.-M., Li, W.-C., Liu, D.-S., Li, Y.-P., Wen, F.-Q., Feng, Y.-L., Zhang, S.-F., Huang, X.-Y., Wang, T., Wang, K., et al. (2009). VEGFR-2 antagonist SU5416 attenuates bleomycin-induced pulmonary fibrosis in mice. Int. Immunopharmacol. *9*, 70–79.

**112.** Pacey, S., Wilson, R.H., Walton, M., Eatock, M.M., Hardcastle, A., Zetterlund, A., Arkenau, H.-T., Moreno-Farre, J., Banerji, U., Roels, B., et al. (2011). A Phase I Study of the Heat Shock Protein 90 Inhibitor Alvespimycin (17-DMAG) Given Intravenously to Patients with Advanced Solid Tumors. Clin. Cancer Res. *17*, 1561–1570.

**113.** Pérez, E.R.F., Daniels, C.E., Schroeder, D.R., St. Sauver, J., Hartman, T.E., Bartholmai, B.J., Yi, E.S., and Ryu, J.H. (2010). Incidence, prevalence, and clinical course of idiopathic pulmonary fibrosis: A population-based study. Chest *137*, 129–137.

**114.** Pulichino, A.-M., Wang, I.-M., Caron, A., Mortimer, J., Auger, A., Boie, Y., Elias, J.A., Kartono, A., Xu, L., Menetski, J., et al. (2008). Identification of Transforming Growth Factor β1–Driven Genetic Programs of Acute Lung Fibrosis. Am. J. Respir. Cell Mol. Biol. *39*, 324–336.

**115.** Raghu, Weill Cornell, Kevin J. Anstrom, and Talmadge E. King, Jr (2014). Randomized Trial of Acetylcysteine in Idiopathic Pulmonary Fibrosis. N. Engl. J. Med. *370*, 2093–2101.

**116.** Raghu, G., Freudenberger, T.D., Yang, S., Curtis, J.R., Spada, C., Hayes, J., Sillery, J.K., Pope, C.E., and Pellegrini, C.A. (2006). High prevalence of abnormal acid gastro-oesophageal reflux in idiopathic pulmonary fibrosis. Eur. Respir. J. *27*, 136–142.

**117.** Raghu, G., Collard, H.R., Egan, J.J., Martinez, F.J., Behr, J., Brown, K.K., Colby, T.V., Cordier, J.-F., Flaherty, K.R., Lasky, J.A., et al. (2011). An Official ATS/ERS/JRS/ALAT Statement: Idiopathic Pulmonary Fibrosis: Evidence-based Guidelines for Diagnosis and Management. Am. J. Respir. Crit. Care Med. *183*, 788–824.

**118.** Raghu, G., Behr, J., Brown, K.K., Egan, J.J., Kawut, S.M., Flaherty, K.R., Martinez, F.J., Nathan, S.D., Wells, A.U., Collard, H.R., et al. (2013). Treatment of Idiopathic Pulmonary Fibrosis With AmbrisentanA Parallel, Randomized Trial. Ann. Intern. Med. *158*, 641–649.

**119.** Ramalingam, T.R., Pesce, J.T., Sheikh, F., Cheever, A.W., Mentink-Kane, M.M., Wilson, M.S., Stevens, S., Valenzuela, D.M., Murphy, A.J., Yancopoulos, G.D., et al. (2008). Unique functions of the type II interleukin 4 receptor identified in mice lacking the interleukin 13 receptor α1 chain. Nat. Immunol. *9*, 25–33.

**120.** Rankin, E., and Giaccia, A. (2008). The role of hypoxia-inducible factors in tumorigenesis. Cell Death Differ. *15*, 678–685.

**121.** Reynolds, H.Y. (2005). Lung Inflammation and Fibrosis. Am. J. Respir. Crit. Care Med. *171*, 98–102.

**122.** Roberts, A.B. (1998). Molecular and cell biology of TGF-beta. Miner. Electrolyte Metab. *24*, 111–119.

**123.** Sanchez, E.R. (2012). Chaperoning steroidal physiology: Lessons from mouse genetic models of Hsp90 and its cochaperones. Biochim. Biophys. Acta BBA - Mol. Cell Res. *1823*, 722–729.

**124.** Sawai, A., Chandarlapaty, S., Greulich, H., Gonen, M., Ye, Q., Arteaga, C.L., Sellers, W., Rosen, N., and Solit, D.B. (2008). Inhibition of Hsp90 Down-regulates Mutant Epidermal Growth Factor Receptor (EGFR) Expression and Sensitizes EGFR Mutant Tumors to Paclitaxel. Cancer Res. *68*, 589–596.

**125.** Scotton, C.J., and Chambers, R.C. (2010). Bleomycin revisited: towards a more representative model of IPF? Am. J. Physiol. Lung Cell. Mol. Physiol. *299*, L439–L441.

**126.** Seibold, M.A., Wise, A.L., Speer, M.C., Steele, M.P., Brown, K.K., Loyd, J.E., Fingerlin, T.E., Zhang, W., Gudmundsson, G., Groshong, S.D., et al. (2011). A

Common MUC5B Promoter Polymorphism and Pulmonary Fibrosis. N. Engl. J. Med. *364*, 1503–1512.

**127.** Selman, M., King, J., Talmadge E., and Pardo, A. (2001). Idiopathic Pulmonary Fibrosis: Prevailing and Evolving Hypotheses about Its Pathogenesis and Implications for Therapy. Ann. Intern. Med. *134*, 136–151.

**128.** Selman, M., Carrillo, G., Estrada, A., Mejia, M., Becerril, C., Cisneros, J., Gaxiola, M., Pérez-Padilla, R., Navarro, C., Richards, T., et al. (2007). Accelerated Variant of Idiopathic Pulmonary Fibrosis: Clinical Behavior and Gene Expression Pattern. PLoS ONE *2*.

**129.** Shelton, S.N., Shawgo, M.E., Matthews, S.B., Lu, Y., Donnelly, A.C., Szabla, K., Tanol, M., Vielhauer, G.A., Rajewski, R.A., Matts, R.L., et al. (2009). KU135, a Novel Novobiocin-Derived C-Terminal Inhibitor of the 90-kDa Heat Shock Protein, Exerts Potent Antiproliferative Effects in Human Leukemic Cells. Mol. Pharmacol. *76*, 1314–1322.

**130.** Shi, Y., and Massagué, J. (2003). Mechanisms of TGF-β Signaling from Cell Membrane to the Nucleus. Cell *113*, 685–700.

**131.** Sidera, K., Gaitanou, M., Stellas, D., Matsas, R., and Patsavoudi, E. (2008). A Critical Role for HSP90 in Cancer Cell Invasion Involves Interaction with the Extracellular Domain of HER-2. J. Biol. Chem. *283*, 2031–2041.

**132.** Sime, P.J., Xing, Z., Graham, F.L., Csaky, K.G., and Gauldie, J. (1997). Adenovector-mediated gene transfer of active transforming growth factor-beta1 induces prolonged severe fibrosis in rat lung. J. Clin. Invest. *100*, 768–776.

**133.** Smith, J.R., and Workman, P. (2009). Targeting CDC37: An alternative, kinase-directed strategy for disruption of oncogenic chaperoning. Cell Cycle *8*, 362–372.

**134.** Sousa, A.M., Liu, T., Guevara, O., Stevens, J., Fanburg, B.L., Gaestel, M., Toksoz, D., and Kayyali, U.S. (2007). Smooth Muscle α-Actin Expression and Myofibroblast Differentiation by TGFβ are Dependent Upon MK2. J. Cell. Biochem. *100*, 1581.

**135.** Spagnolo, P., Luppi, F., Cerri, S., and Richeldi, L. (2012). Genetic testing in diffuse parenchymal lung disease. Orphanet J. Rare Dis. *7*, 79.

**136.** Suemasu, S., Tanaka, K.-I., Namba, T., Ishihara, T., Katsu, T., Fujimoto, M., Adachi, H., Sobue, G., Takeuchi, K., Nakai, A., et al. (2009). A Role for HSP70 in Protecting against Indomethacin-induced Gastric Lesions. J. Biol. Chem. *284*, 19705–19715.

**137.** Taipale, M., Jarosz, D.F., and Lindquist, S. (2010). HSP90 at the hub of protein homeostasis: emerging mechanistic insights. Nat. Rev. Mol. Cell Biol. *11*, 515–528.

**138.** Tanaka, K.-I., Tanaka, Y., Namba, T., Azuma, A., and Mizushima, T. (2010). Heat shock protein 70 protects against bleomycin-induced pulmonary fibrosis in mice. Biochem. Pharmacol. *80*, 920–931.

**139.** Tanjore, H., Xu, X.C., Polosukhin, V.V., Degryse, A.L., Li, B., Han, W., Sherrill, T.P., Plieth, D., Neilson, E.G., Blackwell, T.S., et al. (2009). Contribution of epithelial-derived fibroblasts to bleomycin-induced lung fibrosis. Am. J. Respir. Crit. Care Med. *180*, 657–665.

**140.** Tanjore, H., Lawson, W.E., and Blackwell, T.S. (2013). Endoplasmic reticulum stress as a pro-fibrotic stimulus. Biochim. Biophys. Acta *1832*, 940–947.

**141.** The European Medicines Agency (2010). European Medicines Agency. CHMP Pirfenidone is the first approved drug for IPF by EMA (European Medicines Agency) in 2010 /WC500103073.pdf.

**142.** The U.S. Food and Drug Administration (2014a). Press Announcements - FDA approves Esbriet to treat idiopathic pulmonary fibrosis.

**143.** The U.S. Food and Drug Administration (2014b). Press Announcements - FDA approves Ofev to treat idiopathic pulmonary fibrosis.

**144.** Todd, N.W., Luzina, I.G., and Atamas, S.P. (2012). Molecular and cellular mechanisms of pulmonary fibrosis. Fibrogenesis Tissue Repair *5*, 11.

**145.** Tomcik, M., Zerr, P., Pitkowski, J., Palumbo-Zerr, K., Avouac, J., Distler, O., Becvar, R., Senolt, L., Schett, G., and Distler, J.H. (2014). Heat shock protein 90 (Hsp90) inhibition targets canonical TGF-β signalling to prevent fibrosis. Ann. Rheum. Dis. *73*, 1215–1222.

**146.** Travis, W.D., Costabel, U., Hansell, D.M., King, T.E., Lynch, D.A., Nicholson, A.G., Ryerson, C.J., Ryu, J.H., Selman, M., Wells, A.U., et al. (2013). An Official American Thoracic Society/European Respiratory Society Statement: Update of the International Multidisciplinary Classification of the Idiopathic Interstitial Pneumonias. Am. J. Respir. Crit. Care Med. *188*, 733–748.

**147.** Trepel, J., Mollapour, M., Giaccone, G., and Neckers, L. (2010). Targeting the dynamic HSP90 complex in cancer. Nat. Rev. Cancer *10*, 537–549.

**148.** Tsukamoto, K., Hayakawa, H., Sato, A., Chida, K., Nakamura, H., and Miura, K. (2000). Involvement of Epstein-Barr virus latent membrane protein 1 in disease progression in patients with idiopathic pulmonary fibrosis. Thorax *55*, 958–961.

**149.** Vancheri, C. (2012). Idiopathic Pulmonary Fibrosis. Proc. Am. Thorac. Soc. *9*, 153–157.

**150.** Vancheri, C. (2013). Common pathways in idiopathic pulmonary fibrosis and cancer. Eur. Respir. Rev. *22*, 265–272.

**151.** Vancheri, C., Failla, M., Crimi, N., and Raghu, G. (2010). Idiopathic pulmonary fibrosis: a disease with similarities and links to cancer biology. Eur. Respir. J. *35*, 496–504.

**152.** Verrecchia, F., and Mauviel, A. (2007). Transforming growth factor-β and fibrosis. World J. Gastroenterol. WJG *13*, 3056–3062.

**153.** Waghray, M., Cui, Z., Horowitz, J.C., Subramanian, I.M., Martinez, F.J., Toews, G.B., and Thannickal, V.J. (2005). Hydrogen peroxide is a diffusible paracrine signal for the induction of epithelial cell death by activated myofibroblasts. FASEB J.

**154.** Wandinger, S.K., Richter, K., and Buchner, J. (2008). The Hsp90 Chaperone Machinery. J. Biol. Chem. *283*, 18473–18477.

**155.** Wayne, N., and Bolon, D.N. (2007). Dimerization of Hsp90 Is Required for in Vivo Function DESIGN AND ANALYSIS OF MONOMERS AND DIMERS. J. Biol. Chem. *282*, 35386–35395.

**156.** Wells, A.U., Cullinan, P., Hansell, D.M., Rubens, M.B., Black, C.M., Newman-Taylor, A.J., and Du Bois, R.M. (1994). Fibrosing alveolitis associated with systemic sclerosis has a better prognosis than lone cryptogenic fibrosing alveolitis. Am. J. Respir. Crit. Care Med. *149*, 1583–1590.

**157.** Wettstein, G., Bellaye, P.-S., Kolb, M., Hammann, A., Crestani, B., Soler, P., Marchal-Somme, J., Hazoume, A., Gauldie, J., Gunther, A., et al. (2013). Inhibition of HSP27 blocks fibrosis development and EMT features by promoting Snail degradation. FASEB J. *27*, 1549–1560.

**158.** Whitesell, L., and Lindquist, S. (2005). HSP90 and the chaperoning of cancer. Nat. Rev. Cancer *5*, 761–772.

**159.** Willis, B.C., Liebler, J.M., Luby-Phelps, K., Nicholson, A.G., Crandall, E.D., du Bois, R.M., and Borok, Z. (2005). Induction of Epithelial-Mesenchymal Transition in Alveolar Epithelial Cells by Transforming Growth Factor-β1: Potential Role in Idiopathic Pulmonary Fibrosis. Am. J. Pathol. *166*, 1321–1332.

**160.** Willis, B.C., duBois, R.M., and Borok, Z. (2006). Epithelial Origin of Myofibroblasts during Fibrosis in the Lung. Proc. Am. Thorac. Soc. *3*, 377–382.

**161.** Wollin, L., Wex, E., Pautsch, A., Schnapp, G., Hostettler, K.E., Stowasser, S., and Kolb, M. (2015). Mode of action of nintedanib in the treatment of idiopathic pulmonary fibrosis. Eur. Respir. J. ERJ – 01749–02014.

**162.** Wolters, P.J., Collard, H.R., and Jones, K.D. (2014). Pathogenesis of Idiopathic Pulmonary Fibrosis. Annu. Rev. Pathol. Mech. Dis. *9*, 157–179.

**163.** Wrighton, K.H., Lin, X., and Feng, X.-H. (2008). Critical regulation of TGFβ signaling by Hsp90. Proc. Natl. Acad. Sci. U. S. A. *105*, 9244–9249.

**164.** Wuyts, W.A., Agostini, C., Antoniou, K.M., Bouros, D., Chambers, R.C., Cottin, V., Egan, J.J., Lambrecht, B.N., Lories, R., Parfrey, H., et al. (2013). The pathogenesis of pulmonary fibrosis: a moving target. Eur. Respir. J. *41*, 1207–1218.

**165.** Wygrecka, M., Kwapiszewska, G., Jablonska, E., von Gerlach, S., Henneke, I., Zakrzewicz, D., Guenther, A., Preissner, K.T., and Markart, P. (2011). Role of protease-activated receptor-2 in idiopathic pulmonary fibrosis. Am. J. Respir. Crit. Care Med. *183*, 1703–1714.

**166.** Wynn, T.A. (2011). Integrating mechanisms of pulmonary fibrosis. J. Exp. Med. *208*, 1339–1350.

**167.** Wynn, T.A., and Barron, L. (2010). Macrophages: Master Regulators of Inflammation and Fibrosis. Semin. Liver Dis. *30*, 245–257.

**168.** Xiao, D., and He, J. (2011). Epithelial mesenchymal transition and lung cancer. J. Thorac. Dis. *2*, 154–159.

**169.** Xu, W., Marcu, M., Yuan, X., Mimnaugh, E., Patterson, C., and Neckers, L. (2002). Chaperone-dependent E3 ubiquitin ligase CHIP mediates a degradative pathway for c-ErbB2/Neu. Proc. Natl. Acad. Sci. U. S. A. *99*, 12847–12852.

**170.** Yang, H., Huang, Y., Chen, X., Liu, J., Lu, Y., Bu, L., Xia, L., Xiao, W., Chen, M., Nie, Q., et al. (2010). The role of CTGF in the diabetic rat retina and its relationship with VEGF and TGF-β2, elucidated by treatment with CTGFsiRNA. Acta Ophthalmol. (Copenh.) *88*, 652–659.

**171.** Zhang, K., Lu, Y., Yang, P., Li, C., Sun, H., Tao, D., Liu, Y., Zhang, S., and Ma, Y. (2012). HILI Inhibits TGF-β Signaling by Interacting with Hsp90 and Promoting TβR Degradation. PLoS ONE *7*.

**172.** Zhang, T., Hamza, A., Cao, X., Wang, B., Yu, S., Zhan, C.-G., and Sun, D. (2008). A novel Hsp90 inhibitor to disrupt Hsp90/Cdc37 complex against pancreatic cancer cells. Mol. Cancer Ther. *7*, 162–170.

**173.** Zhao, R., and et al. (2005). Hsp90: a chaperone for protein folding and gene regulation. Biochem. Cell Biol. *83*, 703–710.

**174.** Zhao, R., Davey, M., Hsu, Y.-C., Kaplanek, P., Tong, A., Parsons, A.B., Krogan, N., Cagney, G., Mai, D., Greenblatt, J., et al. (2005). Navigating the Chaperone Network: An Integrative Map of Physical and Genetic Interactions Mediated by the Hsp90 Chaperone. Cell *120*, 715–727.

**175.** Zhou, P., Fernandes, N., Dodge, I.L., Reddi, A.L., Rao, N., Safran, H., DiPetrillo, T.A., Wazer, D.E., Band, V., and Band, H. (2003). ErbB2 Degradation Mediated by the Co-chaperone Protein CHIP. J. Biol. Chem. *278*, 13829–13837.

**176.** Zhuo, Y., Zhang, J., Laboy, M., and Lasky, J.A. (2004). Modulation of PDGF-C and PDGF-D expression during bleomycin-induced lung fibrosis. Am. J. Physiol. - Lung Cell. Mol. Physiol. *286*, L182–L188.

**177.** Zisman, D., Schwarz, M., Anstrom, K.J., and Collard, H.R. (2010). A Controlled Trial of Sildenafil in Advanced Idiopathic Pulmonary Fibrosis. N. Engl. J. Med. *363*, 620–628.

**178.** Zuo, F., Kaminski, N., Eugui, E., Allard, J., Yakhini, Z., Ben-Dor, A., Lollini, L., Morris, D., Kim, Y., DeLustro, B., et al. (2002). Gene expression analysis reveals matrilysin as a key regulator of pulmonary fibrosis in mice and humans. Proc. Natl. Acad. Sci. *99*, 6292–6297.

# 15. ORAL AND POSTER PRESENTATIONS

**Oral presentations:**

- June 2013- Annual Retreat of International Graduate Programme Molecular Biology and Medicine of the Lung, Rauischholzhausen, Germany; 'Role of HSP90 in pulmonary fibrosis'.
- July 2014- Annual Retreat of International Graduate Programme Molecular Biology and Medicine of the Lung, Rauischholzhausen, Germany; 'Inhibition of HSP90 ameliorates pulmonary fibrosis by preventing TGF-β-induced fibroblast activation and epithelial-mesenchymal transition'.

**Poster presentations:**

- August 2012- Annual Retreat of International Graduate Programme Molecular Biology and Medicine of the Lung, Rauischholzhausen, Germany; 'Identifying a New Anti-fibrotic Target for Pulmonary Fibrosis'.
- January 2014- DZL Annual Meeting in Heidelberg, Germany; 'HSP90 inhibition prevents lung fibroblast activation and epithelial- mesenchymal transition'.
- May 2014- ATC International Conference, San Diego, USA, 'HSP90 inhibitor 17-AAG prevents lung fibroblast activation and epithelial- mesenchymal transition by regulating profibrotic proteins'.
- June 2015- ECCPS Retreat, Bad Neuheim, Germany; 'Amplified canonical TGF-β signaling via heat shock protein in pulmonary fibrosis'.

# 16. DECLARATION

„Ich erkläre: Ich habe die vorgelegte Dissertation selbständig, ohne unerlaubte fremde Hilfe und nur mit den Hilfen angefertigt, die ich in der Dissertation angegeben habe.
Alle Textstellen, die wörtlich oder sinngemäß aus veröffentlichten Schriften entnommen sind, und alle Angaben, die auf mündlichen Auskünften beruhen, sind als solche kenntlich gemacht.
Bei den von mir durchgeführten und in der Dissertation erwähnten Untersuchungen habe ich die Grundsätze guter wissenschaftlicher Praxis, wie sie in der „Satzung der Justus-Liebig-Universität Gießen zur Sicherung guter wissenschaftlicher Praxis“ niedergelegt sind, eingehalten.“

Gießen, Juli 2015

_____

Zaneta Sibinska

# 17. ACKNOWLEDGEMENTS

I would like to take this opportunity to thank all the people, without whom this dissertation would not have existed.

Foremost, I would like to express my sincere gratitude to my supervisor, Prof. Dr. rer. nat. Ralph Schermuly for his immense knowledge, constructive ideas, discussion and support.

I would like to thank Prof. Dr. rer. nat. Michael Martin for insightful comments on my thesis.

I would like to express gratitude to Dr. Xia Tian for her initiation of this project, helpful comments and many experimental suggestions. It was nice time to work with her.

I would like to thank Christina Vroom for her big effort on animal experiment and Stephie Viehmann on organizing everyday lab work. With their help, kindness and generosity my work was enjoyable. They are the best technician in the world!

I sincerely thank Dr. Rory Morty for his teaching talent and excellent tutoring in the Molecular Biology and Medicine of the Lung graduate program.

I would to give a special thanks to Prof. Dr. Werner Seeger, who provides all possible conditions for research.

My thanks also extend to Prof. Dr. Andreas Günther, Prof. Dr. Friedrich Grimminger, Dr. Ardeschir Ghofrani and Dr. Norbert Weissmann for the cooperative support.

I would like to take this opportunity to thank the Universities of Giessen and Marburg Lung Center (UGMLC) for the financial support.

I would like to express gratitude to Ewa Bieniek for discussions about histology and life; Dr. phil. nat. Astrid Weiß for translation of summary here in the thesis and also for many experimental suggestions; Dr. Martina Korfei for the help with immunohistochemistry, Kerstin Goth for the help with various protocols, Dr. Janina Kolb for the help with the lung compliance, Dr. Baktybek Kojonazarov for the help with FMT

and Ingrid Breitenborn-Müller for help with many hundred small things in my daily laboratory work.

I would like to thank all my wonderful colleagues: Gayathri Viswanathan, Boyhung Lee, Anuar Kalymbetov, Changwu Lee, Dr. Stanka Mihaylova, Dr. rer. nat. Joachim Berk, Caroline Merkel, Nadine Presser and Elsa Götz for offering experimental tips, the nice working atmosphere they have created and all those enjoyable moments outside the work.

I would like to thank Aneta Drewnicz for her friendship, support and delicious homemade food we have prepared and enjoyed together.

Most importantly, I would like to thank my beloved sister Natalia, her husband Krzysiek and my beautiful niece Lena for all wonderful moments we have spent together. I will always remember our weekend trips and common coffe & cake. I am so lucky to have you so close in Germany.

Last but not least, I thank my beloved parents Halina and Stefan, for their unconditional love and support through all my live. Without them, I would not have a chance to be at this stage of my life. You are far away but always present in my heart.